Analytical Wave Codes for predicting surface waves in a laboratory basin

ISBN 90-365-1763-x

University of Twente, Enschede, The Netherlands
Printed by PrintPartners Ipskamp B. V., Enschede, The Netherlands

ANALYTICAL WAVE CODES FOR PREDICTING SURFACE WAVES IN A LABORATORY BASIN

PROEFSCHRIFT

ter verkrijging van
de graad van doctor aan de Universiteit Twente,
op gezag van de rector magnificus,
prof. dr. F. A. van Vught,
volgens besluit van het College voor Promoties
in het openbaar te verdedigen
op donderdag 13 juni te 15:00 uur

door

Edi Cahyono
geboren op 15 juli 1968
te Malang, Indonesië

Dit proefschrift is goedgekeurd door de promotor
prof. dr. E. van Groesen

en de assistent-promotor
Dr. Andonowati

to the memory of my father

Abstract

This thesis concerns predicting wave evolutions in a laboratory basin. These predictions provide useful information for predicting prescribed wave profiles. These wave generations are motivated by the need for hydrodynamic laboratories. The waves are used to test models of ships and offshore structures in operational conditions before the real ships and structures are constructed and operated. Therefore, the waves to be generated should resemble the wave conditions in seas and oceans, where the ships and structures will be operated.

To generate desired waves as stated above is not easy. This is mainly because the dispersive and nonlinear properties of the waves. For example, in the laboratories some waves may give completely different profiles when they are measured at different positions along the basin. A simple experiment for a bichromatic wave in a long basin confirm this. After propagating 160 m downstream from the wave generator, the wave height is about twice the height of that at a position close to the wave generator.

The wave evolutions are studied using a simple model, a KdV type of equation (mKdV) that has dispersion properties which is also accurate for relatively short waves. This model is considered, on the one hand, since the laboratories are interested in short waves. On the other hand, the model is chosen for its simplicity to understand the wave phenomena.

An exact solution of mKdV equation is difficult to obtain analytically. Therefore, approximate solutions are considered, which are sought by applying two perturbation techniques: a direct perturbation method and the Lindstedt-Poincaré method.

The approximate solutions of mKdV model obtained using the perturbation techniques above are compared to direct numerical simulations and experiments from the literature. The numerical simulations using Finite Element/Finite Difference Methods are done for the basic equations for surface waves. The direct perturbation method is not accurate, since it yields the (linear) dispersion relation which is not accurate in predicting the phase velocity. Moreover, it does not show large envelope deformation as the numerical simulations and experiments do for some type of bichromatic waves. This inaccuracy is too large for spatial and temporal dimensions considered in the long basins.

The Lindstedt-Poincaré method leads to the nonlinear dispersion relation, which significantly reduces the error of propagation speed. However, second order approximation does not reveal large envelope deformations. These deformations arise from the third order side band interactions. The presence of the third order free waves that travel with different velocities than the bound waves determine the recurrence length of the envelope change, and is found to agree with the numerical results.

Analytical Wave Codes (AWC's) based on the perturbation techniques above are constructed. These AWC's, implemented in Matlab, are used to predict wave evolutions obtained from experiments and numerical computations, also for irregular waves. To compute wave elevation at any position there is no need for time and space-stepping, which makes these AWC's very efficient.

Preface

This is the result of work during my PhD project, which was mainly supported by PGSM-project, Jakarta, Indonesia. I would like to express my gratitude to Pak Simbolon, Pak Benny Karyadi and Ibu Faizah from PGSM, and also to Pak Sembiring for the arrangement of this sponsorship.

I would like to thank my promotor Brenny van Groesen very much for many of things, especially his patience to answer my questions and explain things again and again, and to listen and discuss my ideas has resulted in this thesis. I appreciate very much his effort to provide sponsorship that enable me to finish writing this thesis. Thanks to my co-promotor Andonowati for the nice discussion, advices and the tips how to deal with some mathematical problems and also with different cultures.

The mathematical results of this work will be much less useful, from practical point of view, without comparisons with numerical simulations and experiments. I would like to thank Jaap-Harm and René Huijsmans for the numerical and experimental data that make the comparisons possible.

I would like to thank Gert Klopman, Agus and Pearu for the fruitful discussion, Wilbert for helping me with programming during the first and second years of my project. I thank Timco very, very much for helping to solve computer problems, sharing the peaceful office and especially for preparing cofee and tea, and together with Ardhasena for being my paranimfen. I really have a very nice time to have lunch together and sometimes *groep uitje* with Barbera, Debby, Hadi, Helena, Kiran, Manfred, Marielle, Mike, Monica, Nathanael. For Stephan, thanks for helping to find sponsorship for printing this thesis, for Frits I apologise for breaking the light of the bike you lent me during my visit in 1995/96.

Part of this project has been done at ITB, Bandung. I thank Pak Edy Soewono and Toto for the nice discussions, to Math S 3 students for the nice conversation during lunch break.

Outside the university Herman & Silvia, Oom Stan & Tante Hadi, Ko Han & Cik Inge, Family Schukken, thanks for the friendship that makes me feel at home. Vishy is appreciated for taking care of the kitchen we share. To my mother, brother and sisters, thanks for everything. To Silvy, I appreciate very

much your patience and understanding during the difficult time, moreover, your help with the cover of this thesis.

Contents

List of Figures

List of Tables

Chapter 1

Introduction

This chapter is intended to give an overview of the thesis to general readers. Therefore, there will not be any formulas, if so they are very basic and can be neglected without losing the main ideas. It will be started with a brief discussion of general perspective, the contributions of the study in real applications. Before we continue with a short discussion of a hydrodynamic laboratory, we will present the main research problem that we want to answer in this study, which is motivated by wave generations in hydrodynamic laboratories. These wave generations become more intricate because some classes of waves show large 'envelope' deformations during the evolutions. An example of such deformations will be discussed in the section about wave phenomena. Finally, this chapter will be ended with an outline of the thesis.

1.1 General perspective

Human activities in seas and oceans are so many and there is a tendency to increase further. Some of those activities are intended for the exploration and exploitation of plenty natural resources which lie in the seas and oceans, above and under the bottom. Oil drilling and fisheries are among those activities. For such activities, maritime structures, ships, ferries, oil rigs, etc. with several standard requirements, for example safety and comfort, are needed.

In order to achieve those requirements, several tests for the designs of the structures are required. The tests are often done in wave tanks of hydrodynamic laboratories. For the testing in the laboratories, conditions that resemble the conditions in seas and oceans such as waves, currents and wind, should be reconstructed, since the real structures will be operated in those seas and oceans. In this thesis we merely study the wave reconstruction.

Wave evolutions in laboratories have widely been studied in several different ways: experimentally, numerically as well as analytically. Direct numerical

simulations based on the basic equations for surface waves have been done (see for example [12, 25, 58]). A simplified model for surface elevation, a KdV (Korteweg-de Vries) type of equation that will be called modified KdV (mKdV), will be rederived. This mKdV equation has been applied to study surface wave evolutions in several articles, see for examples [8, 19, 20, 21]. From this equation we will derive a complex amplitude equation: based on the narrow-banded spectrum assumption we obtain the modified NonLinear Schrödinger (mNLS) equation. We will show that this mNLS equation is more general than the NLS equation presented by Boyd and Chen [6].

The main concern of this thesis is the development of an Analytical Wave Code (AWC) to predict uni-directional surface wave evolutions from given information of the waves, represented by prescribed signals of one point measurements. This will be discussed in the next section. The AWC is based on an approximate analytical solutions of the mKdV equation by applying a perturbation technique that takes the so-called third order side band contributions into account. Finally, the performance of the AWC in predicting waves is studied by comparing the predictions with direct numerical simulations as well as experiments for two types of waves: bichromatic and irregular waves. We note that for some cases, even a bichromatic wave is not easy to predict, especially when it shows large envelope deformations. For comparisons, we use the direct numerical simulations done by Westhuis [58], and the experiments conducted at MARIN by Westhuis and Huijsmans [56].

Figure 1.1 shows the general perspective of the study in this thesis. The Analytical Wave Code is the main concern of the work. The dark arrows connecting two rectangles show the contents of the work. On the other hand, the light arrows represent work that is not discussed in detail, even though the experiments and direct numerical simulations are very important for the comparisons with the predictions using the Analytical Wave Code.

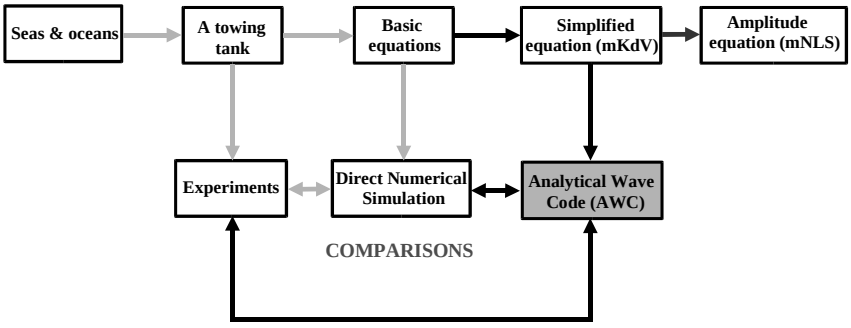

Figure 1.1: The general perspective of the thesis.

1.2 The main interest

Figure 1.2 is a schematic plot of a two dimensional wave tank in a hydrodynamic laboratory. We consider a very big tank, with dimensions of 5 m deep and approximately 200 m long. At one side of the tank a wave generator is installed to produce waves by pulling and pushing the generator. In that way, the generated waves travel to the other side (here to the right), and at the end of the tank there is a 'beach' that acts like a wave absorber. Hence, the presence of reflecting waves running to the left is prevented, or at least minimised, such that the waves traveling to the right are the only significant ones.

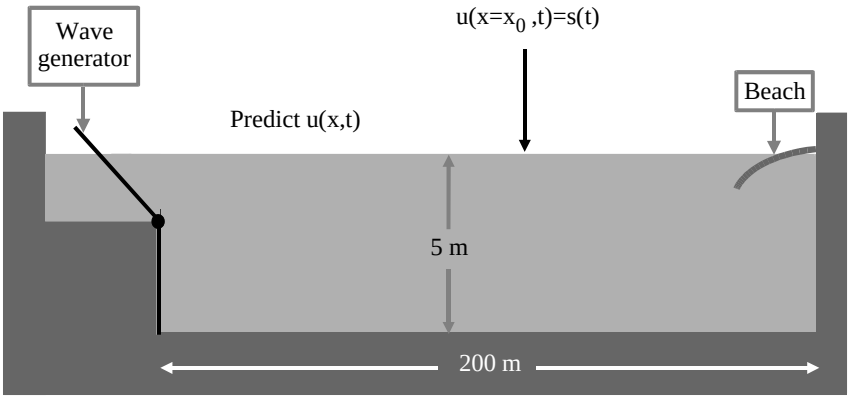

Figure 1.2: Schematic plot of a wave tank.

The main interest of this thesis is to predict how waves evolve if at one point (say at $x = x_0$) in the tank, but away from the wave generator, the waves give a prescribed signal $s(t)$, see Figure 1.2. Hence, we deal with the signaling problem. The prescribed signal resembles the signal measured from wave conditions in seas or oceans on a laboratory scale. For practical purposes, a model of a maritime structure is positioned for testing in the presence of waves.

The prediction of the right traveling waves becomes intricate due to the presence of so-called dispersion and nonlinearity. Their presence exhibits some phenomena of wave evolutions, one of them is a large envelope deformation that will be discussed in the next section. A measured signal of a wave at a point close to the wave generator may be completely different from a signal taken at a point far away from the wave generator. Knowledge of such wave properties is very important for dealing with the signaling problem above. A good prediction of the surface elevation, including at the point where the wave generator is, will provide very useful information for generating specified wave profiles.

This topic has been part of the LABMATH project between two hydrodynamic

laboratories, Maritime Research Institute Netherlands (MARIN) and Indonesian Hydrodynamic Laboratory (IHL), and the Applied Analysis & Mathematical Physics group at the University of Twente and the Center of Mathematics at Institut Teknologi Bandung (P4M-ITB). This project is intended to give scientific support to the daily practice of generating waves in the laboratories.

1.3 A hydrodynamic laboratory

It is already mentioned that new designs of maritime structures such as ships, ferries and oil rigs need to be tested, usually on model scales, in a hydrodynamic laboratory before the actual structures are constructed and operated. The tests are intended to get precise information about the hydrodynamic properties and performance of the designs, with respect to safety, comfort and optimisation of the construction cost of the actual structures.

For such tests a hydrodynamic laboratory usually has several facilities. Each facility is used for specific testing purposes, therefore in general, these facilities have different dimensions, and are equipped differently as well. Take as an example MARIN that is located in Wageningen, the Netherlands [64]. This laboratory has several facilities such as a sea keeping and manoeuvring basin (SMB), a deep water basin, a shallow water basin, an offshore basin and a high speed basin. The SMB is used to study seakeeping and manoeuvring properties of ships. This basin has dimension 170 m $\times$ 40 m $\times$ 5 m. It is equipped with 330 individually controlled wave maker segments on two sides of the basin and adjustable beaches on the opposing sides. This facility also has a carriage, a device to tow a ship model and/or to facilitate measurements during a test, with a maximum speed 6 m/s.

The dimension of the offshore basin is 45 m x 36 m x 10.5 m. This basin has systems for generating waves, current and wind. Current profiles over large water depths, even opposite current at different water depths can be generated. The bottom is adjustable such that the water depth can be varied up to a maximum of 10.5 m. This enables for testing in shallow and deep water conditions. In addition, this basin has a pit with a diameter of 5 meter that gives the opportunity to perform tests at 30 meters water depth. This makes the basin dedicated to Deep Water mooring tests up to 3,000 m.

The Deep Water Towing Tank is equipped with a carriage that has speed up to 9 m/s. This 250 m x 10.5 m x 5.5 m tank is dedicated for resistance and self-propulsion tests, flow observations and various measurements of hydrodynamic forces. For testing performance of a ship in this tank, waves are generated while the ship is kept at fixed position or sails through the tank. In the situation that the ship sails through the tank, it may be towed by the carriage or it may sail by self propulsion.

In chapter 5 we use experimental results that have been conducted in the SMB for some comparisons with predictions of the AWC's. For these needs, uni-

directional waves have been generated in this three-dimensional tank in which the side walls are present. However, we may assume that the generated waves are uni-directional waves, see [56], because of the following. First, the wave elevations along the cross section of the tank do not vary. Second, the reflected waves have been minimised by the wave absorber(s), therefore they are not substantial.

1.4 Wave phenomena in laboratory basins

Surface wave evolutions in laboratory basins have been extensively studied, see [31, 32, 39, 53]. In this section we present some wave phenomena observed in the laboratory. We start with a simple example of waves, a cosine wave with amplitude a

$$u(x,t) = a\cos(kx - \omega t).$$

At time $t = 0$ this wave is shown in Figure 1.3. The wave number k and the (angular) frequency ω are related by the so-called dispersion relation. This relation determines the wave velocity, two waves with different frequencies travel with different velocities. Waves with this property are called *dispersive*. For water waves, shorter waves travel slower.

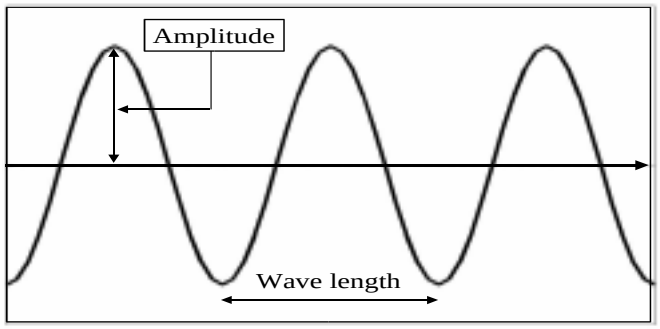

Figure 1.3: A cosine wave at $t = 0$.

Another wave property is nonlinearity. In a very simple case, nonlinearity modifies the wave profile from the cosine form as shown in Figure 1.4. For water waves, the wave profile due to nonlinearity is flatter in the trough and steeper in the crest, called *cnoidal* form.

In practical situations the dispersion and nonlinearity develop much more complex wave phenomena, such as large envelope deformations and breaking. Some reviews on water waves can be found in [26, 61, 62] or more recently in [14]. Recent observations of wave group evolution in wave tanks were reported in

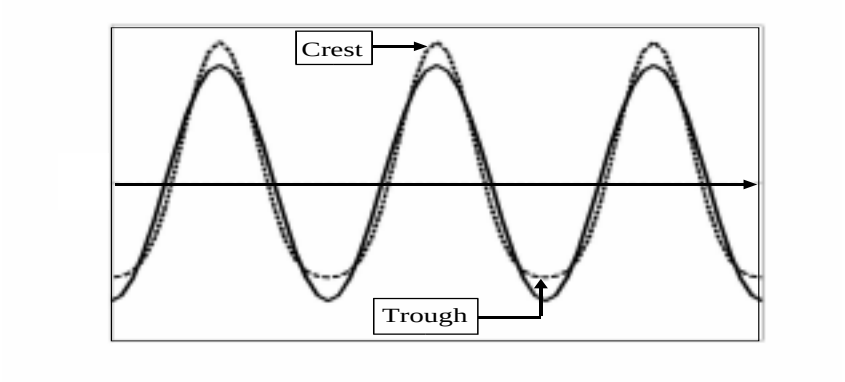

Figure 1.4: Wave profile due to nonlinearity. The solid line is a cosine form, and the dotted line has a cnoidal form.

[53] and in [56] for the case of bichromatic waves. In the following subsections we will present the evolutions of small and large amplitude bichromatic waves. These examples are computed numerically by Westhuis, see [58]. However, these have been proved to be in a good agreement with experiments. In a laboratory a bichromatic wave is usually generated as a superposition of two cosine waves with different frequencies, even though one can also take nonlinear properties of the wave at this point, see [47]. Note that in this section the position $x = 0$ refers to the position of the wave generator. For simplicity of the mathematical computation in chapter 4 and 5, however, we will use $x = 0$ for any point in the tank where the prescribed signal is given.

1.4.1 Small amplitude wave evolutions

In the laboratory, waves are often measured at a fixed point. Hence, we get a wave signal for an interval of time. Figure 1.5 shows signals of a bichromatic wave recorded at several positions. The wave amplitude is up to 8 cm in a tank of 5 m deep, which is considered as a small amplitude wave, and the wave length is 7 m.

Some observations can be made from this figure. The wave amplitude varies from 0 up to 8 cm. This is due to the destructive and constructive interferences of the cosine waves that compose this bichromatic wave. There are 9 waves between two subsequent 0 amplitude waves, which are called a wave group. During the evolution the envelope of the wave group, an imaginary curve connecting the crests of the waves, does not reveal large deformations. This is completely different from an example that we will discuss below.

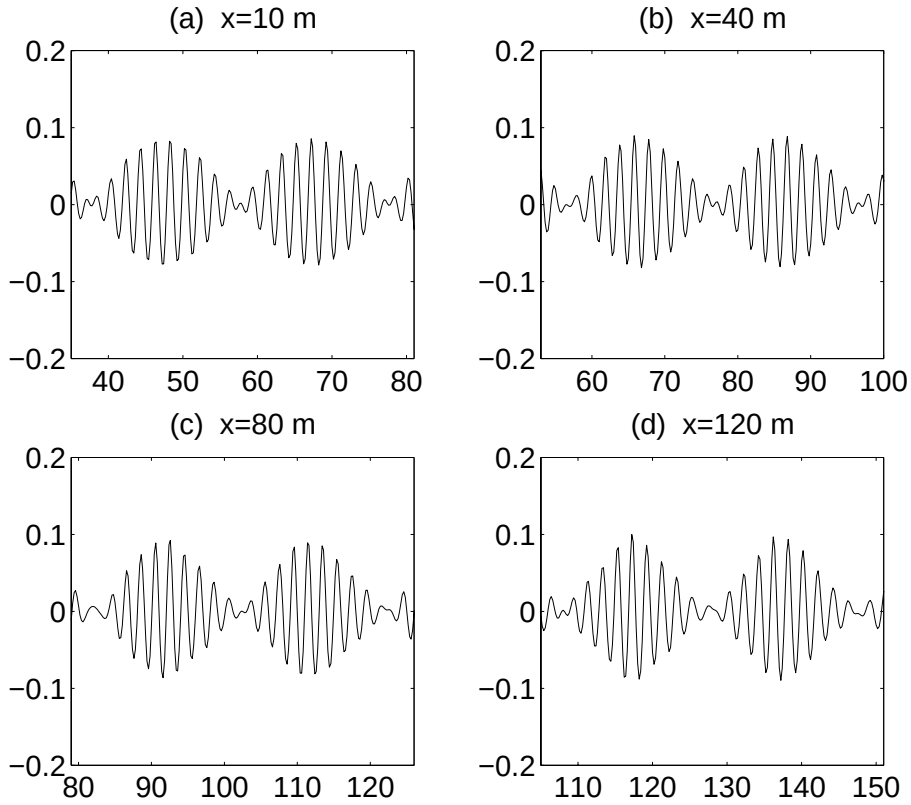

Figure 1.5: Record samples from small amplitude bichromatic wave at positions $x = 10$, 40, 80 and 120 m from the wave maker. For this numerical results, the horizontal and vertical axes are time in sec and elevation in m, respectively.

1.4.2 Large amplitude wave evolutions

In the previous section, we have stated that completely different signals may be obtained from the same waves when they are measured at different positions along the tank. In the following we present a 'simple' example of this phenomenon, i.e. a large envelope deformation of a bichromatic wave. Such evolution has been observed experimentally by Stansberg [49] and Westhuis & Huijsmans [56], and numerically by Westhuis [58]. However, the investigation of the envelope deformations, modulation-demodulation, has been started more than three decades ago by Benjamin and Feir [5]

Figure 1.6 shows a record example of a bichromatic wave measured at several positions which reveal large envelope deformations. At $x = 10$ m (see Figure 1.6 (a)) the wave amplitudes are up to 16 cm (the wave height is up to 32 cm) in a wave tank of 5 m deep. We consider this as a large amplitude wave. As

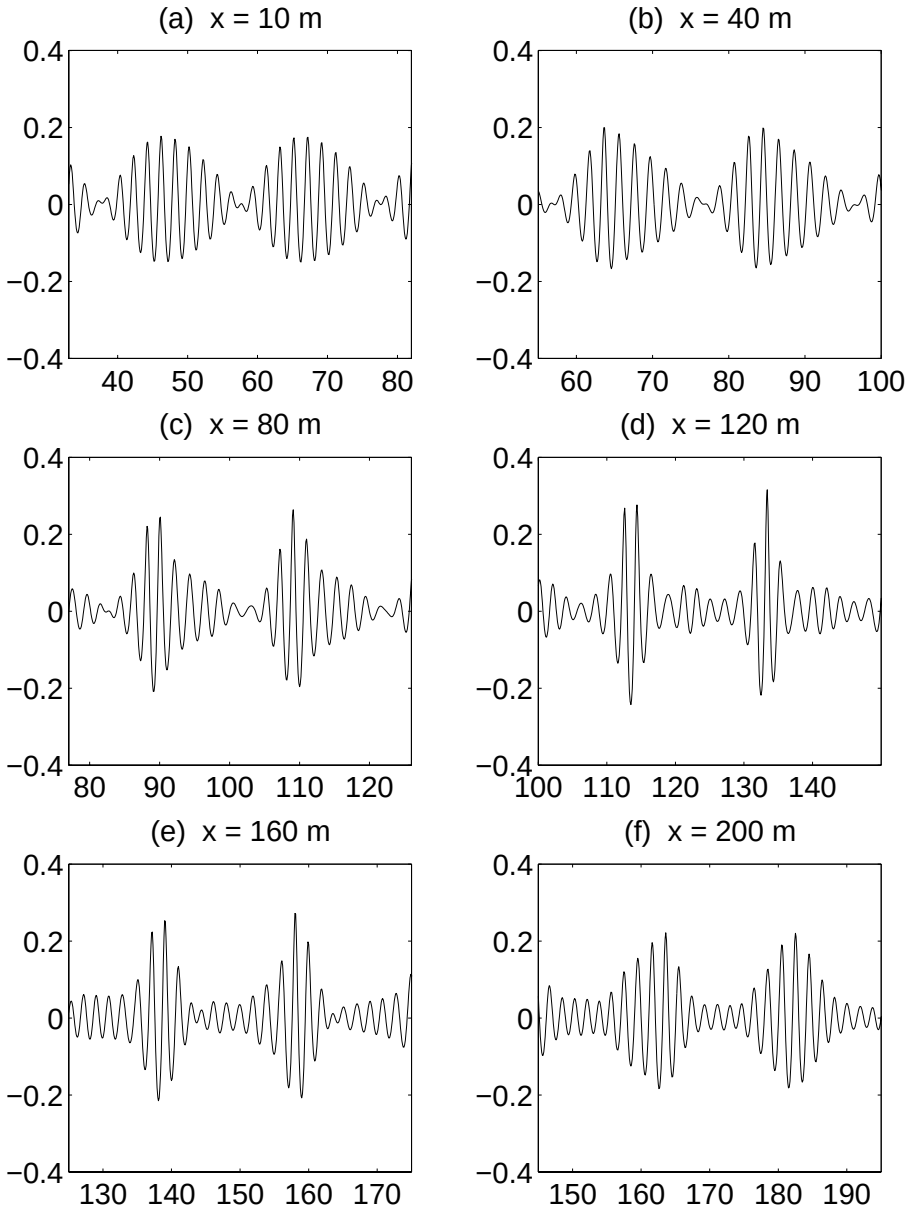

Figure 1.6: Record samples from large amplitude bichromatic wave at positions $x = 10$, 40, 80, 120, 160 and 200 m from the wave maker.

the previous example, the wave length is 7 m, and there are 9 waves within a group.

While traveling downstream from the wave generator, the wave deviates as observed in Figure 1.6 (b) - (f), showing a large envelope deformation phenomenon. This phenomenon starts with a purely bichromatic wave at a point close to the wave maker. Then the wave height increases as observed at $x = 40$ m and 80 m. The asymmetry of the wave group is clearly observed, each group tends to lean forward. At $x = 120$ m the wave group becomes steep, and the wave height is almost twice of the original one. At this point the asymmetry of the wave group is hardly noticed. The opposite occurrence is observed at $x = 160$ and 200 m, the wave height decreases, and each group tends to lean backward. Analysing the spectrum of this wave, it is observed that new side band frequencies appear.

This example shows that predicting wave evolutions is not easy, although it is possible as we will show in chapters 4 and 5. A Bichromatic wave is just a simple example, since at a point close to the wave maker this wave is merely composed of two cosine waves. However, it already shows a phenomenon that is not easy to reconstruct analytically. In practical situations, we will deal with more complex waves than just a bichromatic wave. Irregular waves, laboratory terminology for waves composed of many modes as observed in seas and oceans, show more complex phenomena, even when these are small amplitude waves.

1.5 Outline of the thesis

The thesis consists of six chapters. Although they are relatively independent, in chapter 3 we discuss perturbation methods for ordinary differential equations which facilitate a better understanding of the theory that will be used in chapter 4 and chapter 5. Below is a summary of each chapter.

Chapter 2

Some surface wave models are presented in this chapter. The main interest is to find a model for uni-directional waves with exact dispersion properties. We start with the discussion of the basic equations for surface waves, and then, a derivation of Boussinesq type of equations. These Boussinesq equations have the exact dispersion relation as the basic equations. Finally, from these Boussinesq equations we derive mKdV, a model for uni-directional waves with exact dispersion properties, using uni-directionalisation procedure.

Chapter 3

Asymptotic methods to find approximate solutions of nonlinear differential equations are discussed. We will restrict the analysis to ordinary differential equations. The methods and ideas, however, are equally useful for the perturbation

analysis of partial differential equations. As a classical example we take a nonlinear extention of the harmonic oscillator equation. First, we apply a naive perturbation technique, by approximating the solution with a series expansion in small amplitude. This approximate solution gives a good approximation for small period of time. We observe that this nonlinear harmonic oscillator equation yields bounded solutions as long as the amplitude is small. However, the approximate solution linearly grows in time, therefore it is not a good approximation for a large time period. Since we consider a large time period, we need to improve the method above. In this improved method both the approximate solution and its frequency are expressed as series expansions in the amplitude. This method is known as the Lindstedt-Poincaré technique, which prevents the linear growth of the approximate solution.

Chapter 4

Some numerical and experimental bichromatic waves reveal large envelope deformations during the evolutions. In this chapter we investigate this envelope deformation phenomenon analytically. To do that, we apply mKdV model, and perturbation techniques to find its approximate solutions. A naive perturbation and the Lindstedt-Poincaré methods are applied. The direct second order approximation obtained from the naive method is found to underestimate the wave propagation speed, which is improved by applying the nonlinear dispersion relation obtained in the Lindstedt-Poincaré method. The large envelope deformations, however, can not be explained from the second order theory, but from third order. We show that third order side band contributions quadratically depend on the quotient of amplitude and wave number (or frequency) difference, and become essential if this quotient is large. However, if this quotient is too large, the perturbation techniques above break down. Hence, the wave number (or frequency) difference is an additional perturbation parameter that needs to be taken into account.

Chapter 5

This chapter is the main part of the thesis, the construction of Analytical Wave Codes that will be used to predict waves based on a given signal from one point measurement, say at $x = 0$. This signal is only given for a finite time-interval T. The prescribed signal is assumed to be periodic with the period T. Hence, this signal can be expressed in a Fourier series.

The same perturbation methods as in chapter 4 are applied to find an approximate solution of mKdV equation. The difference is that we now consider waves with 'many' frequencies, instead of two. The amplitude spectrum of the lowest order contribution (of the solution) should be determined such that at $x = 0$ the approximations satisfy the prescribed signal up to the relevant orders. Three approximations will be considered: direct second order approximation,

second order approximation with nonlinear dispersion relation and third order side band approximation. Analytical Wave Codes are developed based on these approximations: AWC1, AWC2 and AWC3, respectively. In predicting waves AWC1 underestimates the wave propagation speed, that can be improved by AWC2. Both are not capable to predict large envelop deformations of wave groups. AWC3, which also takes the nonlinear dispersion into account, can predict an envelope deformation, show amplitude increase as the direct numerical results and experiments. Asymmetry of the envelope during the evolution is also observed.

Chapter 2

Surface wave models

This chapter is a discussion of some surface wave models. The main interest is to present a derivation of a uni-directional wave model with exact dispersion properties and a quadratic nonlinearity from the basic equations for surface waves. This uni-directional model will be used in chapter 4 to investigate bichromatic wave evolutions, and in chapter 5 to develop an analytical wave code for predicting (irregular) wave evolutions. This derivation will give a general perspective of the relation between direct numerical results based on the basic equations, as done by Westhuis in [58], and the corresponding analytical solutions obtained from the uni-directional model in this thesis. Moreover, the numerical results have been proved to be in good agreement with experiments, hence we will also compare the analytical approximations with the experiments.

To do that, we start with the Hamiltonian structure of the basic equations for surface waves where most of the discussion is given in [18]. These basic equations are based on assumptions of an inviscid, incompressible and irrotational fluid. Following [4], Boussinesq-type equations are derived after approximating the kinetic energy. These Boussinesq-type equations have the exact dispersion relation as the basic equations. Using uni-directionalisation argument in [18] we derive the uni-directional model which is a KdV-type equation. We finally end this chapter with a derivation of an amplitude (NLS-type) equation. This is more general than the relation between standard KdV and NLS equations that was presented in [6]. We note that the solutions of the NLS equation are restricted to narrow-banded spectra, but the solutions of a KdV-type equation are not. Hence, solutions obtained from the KdV-type equation are more general than solutions found from the NLS equation.

Since the interest is to give a general overview that yields a connection of the experimental and direct numerical results with analytical approximations based on a simplified model, many details are left out. These details, however, can easily be found in the cited references.

2.1 Hamiltonian structure of the basic equations

2.1.1 Basic equations for surface waves

We consider a layer of two-dimensional incompressible fluid (water) over an even bottom, see Figure 2.1. Note that the fluid is assumed to be unbounded in x-direction. We assume that at the free surface there are no over taking waves. This assumption enables us to write the free surface elevation as a function $\eta(x,t)$ measured from the undisturbed level $z=0$.

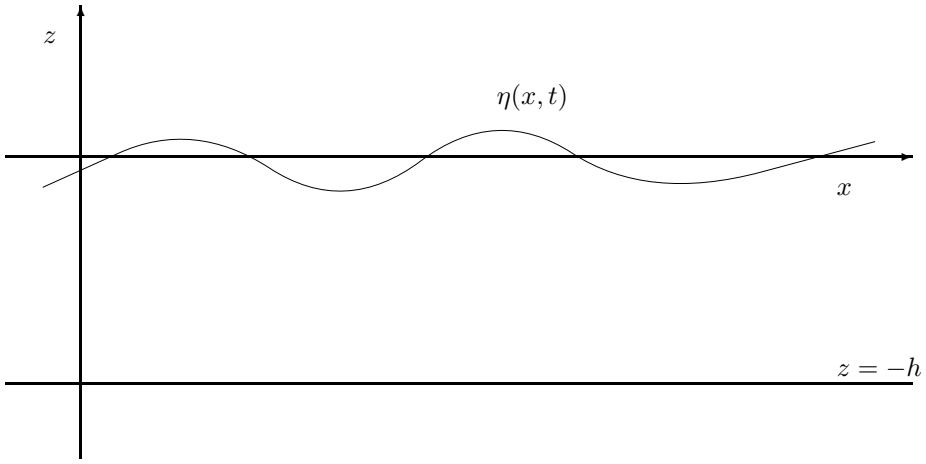

Figure 2.1: The fluid domain $D(\eta)$ above an even bottom $z=-h$. The free surface elevation is described by the graph of a function $z=\eta(x,t)$.

Let $D(\eta)$ denote the domain of the fluid i.e.

$$D(\eta)=\{(x,z):-h<z<\eta(x,t)\}.$$

Assuming that the fluid flow is irrotational at some time $t=t_0$, then it follows that the flow remains irrotational for all time t. Mathematically, this implies that the particle velocity can be expressed as the gradient of velocity potential $\phi(x,z)$, i.e. $\mathbf{u}(x,z)=\nabla\phi(x,z)$. Since the fluid is incompressible, div$\mathbf{u}(x,z)=0$ leads to

$$\Delta\phi=0 \quad \text{in} \quad D(\eta).$$

In the following the density is normalised to 1. We consider an impermeable bottom such that no fluid particles are able to cross the bottom. This means that the normal component of the potential velocity at the (even) bottom is zero. This leads to the condition at the bottom

$$\frac{\partial\phi}{\partial z}=0 \text{ at } z=-h.$$

The momentum equation leads to the *Bernoulli equation*. At the free surface, after neglecting surface tension, this gives the *dynamic boundary condition*

$$\partial_t \phi = -\frac{1}{2}|\nabla\phi|^2 - g\eta \quad \text{at} \quad z = \eta(x,t).$$

Finally, the condition that no fluid flows through the surface leads to the *kinematic boundary condition*:

$$\partial_t \eta = -\frac{\partial\phi}{\partial x}\frac{\partial\eta}{\partial x} + \frac{\partial\phi}{\partial z} \quad \text{at} \quad z = \eta(x,t).$$

Derivations of these equations can be found in standard text books, e.g. [13, 28]. These equations have been extensively studied for direct numerical simulations (see for examples [12, 25, 58]) and analytically ([48, 63]). In chapters 3 and 5 we will use some numerical results given in [58] for comparisons with analytical results obtained from a uni-directional model.

In practical situations both in laboratory or numerical wave tanks, there are some additional boundary conditions. In the laboratories the additional boundary conditions are due to the presence of the side walls, the 'beach' and the wave maker(s). In the numerics this is due to the restriction of the numerical domain that should be finite. Experiments for uni-directional waves, however, show that there is no significant effect of the side walls, see [56]. Measurements along a line perpendicular to the wave propagation give signals that are similar. And, reflecting waves have significantly been minimised by the wave absorber(s). In the direct numerical simulation done by Westhuis [58] the boundary conditions at the wave maker and the beach have been modeled and treated as in the real wave tank.

2.1.2 Hamiltonian formulation

From now on we introduce the notation φ to denote the potential velocity at the free surface $z = \eta(x,t)$, i.e.

$$\varphi(x,t) = \phi(x, z = \eta(x,t), t).$$

We define a Hamiltonian $H(\varphi,\eta)$ as the total energy of the fluid expressed in two variables at the free surface φ and η that is given by

$$H(\varphi,\eta) = P(\eta) + K(\varphi,\eta), \tag{2.1}$$

where $P(\eta)$ and $K(\varphi,\eta)$ are the potential energy and kinetic energy, respectively. Choosing $z = 0$ as reference level and neglecting the surface tension, the potential energy is given by

$$P = \int\int_{z=0}^{\eta(x,t)} gz \;\; dzdx = \frac{1}{2}\int g\eta^2 dx, \tag{2.2}$$

where g is the acceleration due to gravity.

The kinetic energy reads

$$K = \frac{1}{2}\int_D |\nabla\phi|^2 dxdz, \tag{2.3}$$

where ϕ should be found by solving the following boundary value problem

$$\begin{aligned} \Delta\phi &= 0 \text{ in } D \equiv \{(x,z) : -h < z < \eta(x,t)\} && (2.4)\\ \phi &= \varphi \text{ at } z = \eta(x,t) && (2.5)\\ \frac{\partial\phi}{\partial z} &= 0 \text{ at } z = -h. && (2.6) \end{aligned}$$

By solving this boundary value problem, ϕ depends on the given functions φ and η at the free surface. Hence, the kinetic energy can be expressed as a functional of φ and η.

Now it turns out that the basic nonlinear surface equations can be described as a Hamiltonian system with φ and η as canonical variables in Hamiltonian (see [18].):

$$\partial_t \begin{pmatrix} \varphi \\ \eta \end{pmatrix} = \begin{pmatrix} 0 & -1 \\ 1 & 0 \end{pmatrix} \begin{pmatrix} \delta_\varphi H \\ \delta_\eta H \end{pmatrix}. \tag{2.7}$$

2.1.3 Transformation of basic variables

For the discussion later on, we will consider a new variable u different from the surface potential φ, defined by

$$u(x,t) = \partial_x \varphi(x,t), \tag{2.8}$$

and express the Hamiltonian in the variables u and η. The Hamiltonian in this new variable reads

$$\hat{H}(u,\eta) = H(\varphi,\eta). \tag{2.9}$$

Observe that this is well-defined, since the kinetic energy is invariant by adding any constant to φ, $H(\varphi + \text{constant}, \eta) = H(\varphi,\eta)$.

On substituting (2.8) and (2.9) into (2.7), after dropping the hat, we have the following Poisson system

$$\partial_t \begin{pmatrix} u \\ \eta \end{pmatrix} = \begin{pmatrix} 0 & -\partial_x \\ -\partial_x & 0 \end{pmatrix} \begin{pmatrix} \delta_u H \\ \delta_\eta H \end{pmatrix}. \tag{2.10}$$

For the derivation of Boussinesq equation in section 3.3, we will use this Poisson system, instead of the Hamiltonian system (2.7).

2.2 Approximation for the kinetic energy

The Hamiltonian system (2.7) and the Poisson system (2.10) are exact. However, they cannot be expressed explicitly in the form of φ (or u) and η. This is due to the expression of the kinetic energy (2.3). In this section we introduce an approximation for the kinetic energy that enables us to write the Poisson system (2.10) in explicit expressions of the potential velocity at free surface u and the free surface elevation η.

To start with, we note that $|\nabla\phi|^2 = \operatorname{div}(\phi\nabla\phi) - \phi \operatorname{div}(\nabla\phi)$. The second term in the right hand side vanishes, since $\operatorname{div}(\nabla\phi) \equiv \Delta\phi = 0$ in $D(\eta)$. Using Gauss' divergence theorem, the kinetic energy can be written as

$$K = \frac{1}{2}\int_D \operatorname{div}(\phi\nabla\phi)dxdz = \frac{1}{2}\int_{\partial D} \phi\frac{d\phi}{dn}ds. \tag{2.11}$$

Let $\bar{D} = \{(x,z) : -h < z < 0\}$. We use continuation argument by extending the domain of the potential velocity $\phi(x,z)$ from D to $D \cup \bar{D}$. Hence, the kinetic energy can be split into $K_{\bar{D}}$ and $K_{D\bar{D}}$

$$K = K_{\bar{D}} + K_{D\bar{D}}, \tag{2.12}$$

where

$$K_{\bar{D}} = \frac{1}{2}\int_{\partial\bar{D}} \phi\frac{d\phi}{dn}ds, \tag{2.13}$$

$$K_{D\bar{D}} = \frac{1}{2}\int\int_{z=0}^{\eta(x)} |\nabla\phi|^2 dzdx. \tag{2.14}$$

Note that when infinitesimally small waves are considered, the integral (2.14) is small. Neglecting the integral (2.14), the kinetic energy is only given by $K_{\bar{D}}$. This leads to the linear theory of surface water waves.

Before we proceed, let $\hat{\phi}(k,z)$ be the Fourier transform of $\phi(x,z)$ with respect to the variable x:

$$\phi(x,z) = \int \hat{\phi}(k,z)e^{ikx}dk.$$

Since ϕ satisfies Laplace equation in the domain $\bar{D}$ and the condition (2.6) at the bottom, this implies that $\hat{\phi}(k,z)$ should satisfy $\hat{\phi}_{zz} - k^2\hat{\phi} = 0$ and $\hat{\phi}_z|_{z=-h} = 0$. Hence, we have

$$\hat{\phi}(k,z) = \alpha(k)\cosh k(z+h). \tag{2.15}$$

Since we restrict to the real potential velocity ϕ, therefore, α satisfies

$$\alpha(-k) = \alpha^*(k),$$

where the star denotes the complex conjugate.

It is now possible to write this approximate kinetic energy explicitly in u and η. We start with the kinetic energy in the domain $\bar{D}$ that reads

$$\begin{aligned} K_{\bar{D}} &= \frac{1}{2}\int \phi(x,0)\frac{d\phi}{dn}(x,0)dx = \frac{1}{4}\left\{\frac{\partial}{\partial z}\int \phi^2(x,z)dx\right\}\Big|_{z=0} \\ &= \frac{1}{4}\left\{\frac{\partial}{\partial z}\int |\hat{\phi}(k,z)|^2 dk\right\}\Big|_{z=0} = \frac{1}{4}\int |\alpha(k)|^2 \left\{\frac{\partial}{\partial z}\cosh^2 k(z+h)\right\}\Big|_{z=0} dk \\ &= \frac{1}{2}\int |\alpha(k)|^2 k\cosh kh \sinh kh \;\; dk \\ &= \frac{1}{2}\int \hat{u}(k)\cdot \hat{R}^2(k)\cdot \hat{u}^*(k)dk \end{aligned} \tag{2.16}$$

where

$$\hat{R}(k) = \sqrt{\frac{\tanh kh}{k}}$$
$$\hat{u}(k) = \alpha(k)k\sinh(kh).$$

Observe that $\hat{u}$ is the Fourier transform of the potential velocity at the undisturbed surface

$$u(x) = \partial_x \phi(x, z=0, t).$$

Writing (2.16) back in the physical space we have

$$K_{\bar{D}} = \frac{1}{2}\int uR^2 u dx, \tag{2.17}$$

where R is the *pseudo-differential operator* that corresponds to the function $\hat{R}$. The action of the operator R can only be described in Fourier sense: $R(\exp(ikx)) = \hat{R}(k)\exp(ikx)$.

The integral (2.14) will be approximated by neglecting the vertical fluid velocity. In doing so, the kinetic energy $K_{D\bar{D}}$ is easily found to be

$$\begin{aligned} K_{D\bar{D}} &= \frac{1}{2}\int\int_{z=0}^{\eta(x)} \left(\frac{\partial\phi}{\partial x}(x,z)\right)^2 dzdx = \frac{1}{2}\int\int_{z=0}^{\eta(x)} \left(\frac{\partial\phi}{\partial x}(x,0)\right)^2 dzdx \\ &= \frac{1}{2}\int\int_{z=0}^{\eta(x)} u^2(x)dzdx = \frac{1}{2}\int u^2\eta \;\; dx. \end{aligned} \tag{2.18}$$

2.3 Boussinesq equations

The Boussinesq model consists of two equations, and involves two unknowns: a potential velocity and the surface elevation. Although in the following discussion we consider the potential velocity at the free surface, there are actually several options of potential velocities to be considered, e.g. the depth-integrated flux (see in [36, 37, 46]) or the velocity at an arbitrary level (see in [41, 46]). A review of Boussinesq-type of equations for gravity waves can be found in [38].

2.3.1 Linear Boussinesq equations

In this subsection we only consider infinitesimally small waves such that the kinetic energy K can be approximated by $K_{\bar{D}}$. Hence, the Hamiltonian $H(u,\eta)$ is approximated by

$$H_{\text{lin}}(u,\eta) = K_{\bar{D}} + P = \frac{1}{2}\int \{uR^2u + g\eta^2\}dx. \tag{2.19}$$

Using this approximation the Poisson system (2.10) reads

$$\partial_t \begin{pmatrix} u \\ \eta \end{pmatrix} = \begin{pmatrix} 0 & -\partial_x \\ -\partial_x & 0 \end{pmatrix} \begin{pmatrix} \delta_u H_{\text{lin}} \\ \delta_\eta H_{\text{lin}} \end{pmatrix}$$

which are linear Boussinesq-type equations

$$u_t + g\eta_x = 0, \tag{2.20}$$
$$\eta_t + \partial_x R^2 u = 0. \tag{2.21}$$

This is a set of *linear dispersive equations* which has exact dispersion properties. A single equation for surface elevation η can easily be found by eliminating u:

$$\eta_{tt} = g\partial_x^2 R^2 \eta.$$

This equation gives a solution that represents waves running to the right and to the left. Since it is linear, the general solution is given by a superposition of modes

$$\eta(x,t) = \int \left[\alpha(k)\cos\{kx - \omega t\} + \beta(k)\cos\{kx + \omega t\}\right] dk,$$

where k and ω satisfy the exact dispersion, $\omega = \sqrt{gk\tanh(kh)}$, and $\alpha(k)$ and $\beta(k)$ are component amplitudes of wave modes running to the right and to the left, respectively.

2.3.2 Nonlinear Boussinesq equations

The nonlinear Boussinesq-type equations are derived using the approximate kinetic energy presented in the previous section. The Hamiltonian $H(u,\eta)$ reads

$$H(u,\eta) = K_E + P = \frac{1}{2}\int \{uR^2u + u^2\eta + g\eta^2\}dx. \tag{2.22}$$

On substituting this into (2.10) we have

$$u_t + \frac{1}{2}\partial_x u^2 + g\eta_x = 0 \tag{2.23}$$
$$\eta_t + \partial_x(u\eta) + \partial_x R^2 u = 0. \tag{2.24}$$

These are Boussinesq-type equations that have exact dispersion properties and a quadratic nonlinearity.

2.3.3 Transformations to normalised variables

In the following we normalise the Boussinesq-type equations (2.23) and (2.24) by introducing transformations of variables

$$x = h\tilde{x}, \quad z = h\tilde{z}, \quad t = \sqrt{g/h}\ \tilde{t},$$
$$u = \sqrt{gh}\ \tilde{u}, \quad \eta = h\tilde{\eta},$$

and wave parameters; wave length, wave number and frequency

$$\lambda = h\tilde{\lambda}, \quad k = \tilde{k}/h, \quad \omega = \tilde{\omega}\sqrt{g/h}.$$

On substituting this into (2.23) and (2.24), and dropping the tildes, we come to Boussinesq-type equations in normalised form

$$u_t + \frac{1}{2}\partial_x u^2 + \eta_x = 0 \tag{2.25}$$
$$\eta_t + \partial_x(u\eta) + \partial_x R^2 u = 0, \tag{2.26}$$

where R is given by $R(k) = \sqrt{\frac{\tanh k}{k}}$. We note that we use the same notation R for the differential operator and the corresponding function in normalised variables in the sense that $R\exp(ikx) = R(k)\cdot\exp(ikx)$. Suryanto in [50] used (2.25) and (2.26) to study reflection properties of hydrodynamic beaches. In his study the surface elevation, which in fact represents bi-directional waves, are decomposed into incident and reflecting waves.

Replacing R^2 by the Taylor expansion up to second order in k

$$R^2(k) \approx 1 - \frac{1}{3}k^2,$$

we come to the standard Boussinesq equations

$$u_t + \eta_x + \frac{1}{2}\partial_x u^2 = 0 \tag{2.27}$$
$$\eta_t + u_x + \frac{1}{3}u_{xxx} + \partial_x(u\eta) = 0. \tag{2.28}$$

2.4 Uni-directionalisation to a KdV-type equation

In this section we present a derivation of a model equation of waves that mainly propagate to one direction. The model, which has exact dispersion properties and a quadratic nonlinearity, is a variant of KdV equation that is also capable to model relatively short waves.

2.4.1 Transformation to uni-directional variables

We start by introducing a transformation from u and η to new variables r and s given by

$$\begin{pmatrix} r \\ s \end{pmatrix} = A \begin{pmatrix} u \\ \eta \end{pmatrix}, \quad \text{with} \quad A = \begin{pmatrix} \frac{1}{2}R & \frac{1}{2} \\ \frac{1}{2}R & -\frac{1}{2} \end{pmatrix}. \tag{2.29}$$

The variables $r(x,t)$ and $s(x,t)$ are candidates of waves mainly propagate to the right and to the left, respectively, as we see in the following.

We use the notation R^{-1} for the inverse of the operator R, in the sense that

$$R^{-1}\left(\exp(ikx)\right) = \frac{1}{R(k)}\exp(ikx).$$

On substituting transformation (2.29) into (2.25), we have

$$\partial_t \begin{pmatrix} r \\ s \end{pmatrix} = A \begin{pmatrix} 0 & -\partial_x \\ -\partial_x & 0 \end{pmatrix} A^T \begin{pmatrix} \delta_r \bar{H}(r,s) \\ \delta_s \bar{H}(r,s) \end{pmatrix}, \tag{2.30}$$

where the Hamiltonian $\bar{H}(r,s) = H_0(r,s) + H_1(r,s)$. After using

$$\int \left[R^{-1}r)(Rs) + (Rr)(R^{-1}s) - 2rs\right] dx = 0,$$

H_0 and H_1 are given by

$$\bar{H}_0(r,s) = \frac{1}{2}\int \left[2r^2 + 2s^2\right] dx \tag{2.31}$$

and

$$\begin{aligned} \bar{H}_1(r,s) &= \frac{1}{2}\int \left[(R^{-1}r)^2 r - (R^{-1}s)^2 s + 2(R^{-1}r)(R^{-1}s)r \right. \\ &\qquad \left. -2(R^{-1}r)(R^{-1}s)s - (R^{-1}r)^2 s + (R^{-1}s)^2 r\right] dx. \end{aligned} \tag{2.32}$$

Observe that

$$A \begin{pmatrix} 0 & -\partial_x \\ -\partial_x & 0 \end{pmatrix} A^T$$

is skew-symmetric, which implies that the transformation preserves the Hamiltonian structure. This means that the Hamiltonian $\bar{H}(r,s)$, which is the total energy, is conserved. The equation (2.30) now becomes

$$\begin{aligned} \partial_t \begin{pmatrix} r \\ s \end{pmatrix} &= \begin{pmatrix} -\Gamma & 0 \\ 0 & \Gamma \end{pmatrix} \begin{pmatrix} \delta_r \bar{H}(r,s) \\ \delta_s \bar{H}(r,s) \end{pmatrix} \\ &= \begin{pmatrix} -\Gamma & 0 \\ 0 & \Gamma \end{pmatrix} \begin{pmatrix} 2r + \delta_r \bar{H}_1(r,s) \\ 2s + \delta_s \bar{H}_1(r,s) \end{pmatrix} \end{aligned} \tag{2.33}$$

where $\Gamma = \frac{1}{2}\partial_x R$.

2.4.2 Uni-directionalisation

In the lowest order, the equation (2.33) is decomposed into two equations of waves running to the right r, and to the left s:

$$r_t + \partial_x R r = 0,$$

$$s_t - \partial_x R s = 0.$$

Hence, we already have a uni-directional model which has exact dispersion properties, but this model is still linear. To get nonlinear equations for waves mainly propagate to the right (or to the left) is not straightforward, since the contributions of r and s are coupled in the Hamiltonian component $\bar{H}_1(r, s)$. In the following we restrict to the case that contribution of waves run to the left s is small. In hydrodynamic laboratories such restriction is done by generating waves (using wave generators) at one side of the tank that (are forced to) propagate to the other side.

Since the contribution of $s(x, t)$ is small, we can replace $\bar{H}_1(r, s)$ in (2.33) by $\bar{H}_1(r, 0)$. This leads to an equation for r which has the exact dispersion properties as the basic equations and a quadratic nonlinearity:

$$r_t + \partial_x R \left[r + \frac{1}{2} R^{-1} \left(r \cdot (R^{-1} r) \right) + \frac{1}{4} \left(R^{-1} r \right)^2 \right] = 0. \tag{2.34}$$

To observe this equation for the limiting case of long waves, we proceed the following. Consider a long wave $r_1(x, t)$, and write it in the form

$$r_1(x,t) = \int \alpha(k,t) e^{ikx} dk, \quad \text{where} \quad \alpha(k,t) = \frac{1}{2\pi} \int r_1(x,t) e^{-ikx} dx.$$

Since $r_1(x, t)$ is a long wave, there should be a small number K_0 ($0 < K_0 << 1$), such that $\alpha(k, t) = 0$ outside the interval $[-K_0, K_0]$. Therefore, $r_1(x, t)$ becomes

$$r_1(x,t) = \int_{-K_0}^{K_0} \alpha(k,t) e^{ikx} dk.$$

Introduce the notation for the dispersion relation

$$\Omega(k) = k \sqrt{\frac{\tanh k}{k}}. \tag{2.35}$$

For small k this dispersion relation can be approximated by the Taylor expansion

$$\Omega(k) \approx k - \frac{1}{6} k^3 + O(k^5).$$

The differential operator $\partial_x R$ applied to this long wave can be approximated as follows

$$\begin{aligned}\partial_x R\left(r_1(x,t)\right) &= \int_{-K_0}^{K_0} \alpha(k,t)\Omega(k)e^{ikx}dk \\ &= \int_{-K_0}^{K_0} \alpha(k,t)\left[k-\frac{1}{6}k^3\right]e^{ikx}dk \\ &= \left[\partial_x+\frac{1}{6}\partial_x^3\right]r_1(x,t).\end{aligned}$$

On the other hand, applying to $r_1(x,t)$, the nonlinearity has the form

$$\begin{aligned}&\partial_x R\left[\frac{1}{2}R^{-1}\left(r_1\cdot(R^{-1}r_1)\right)+\frac{1}{4}\left(R^{-1}r_1\right)^2\right] \\ &\quad=\int_{-K_0}^{K_0}\int_{-K_0}^{K_0}\alpha(k_1,t)\alpha(k_2,t)\mu(k_1,k_2)e^{i\{k_1+k_2\}x}dk_1dk_2,\end{aligned}$$

where

$$\mu(k_1,k_2)=(k_1+k_2)R(k_1+k_2)\left[\frac{1}{2}\frac{1}{R(k_1)R(k_1+k_2)}+\frac{1}{R(k_1)R(k_2)}\right].$$

Observe that for $|k_1|,\ |k_2| << 1$, $\mu(k_1,k_2)$ can well be approximated by

$$\mu(k_1,k_2)\approx\frac{3}{4}(k_1+k_2).$$

This implies

$$\partial_x R\left[\frac{1}{2}R^{-1}\left(r\cdot(R^{-1}r_1)\right)+\frac{1}{4}\left(R^{-1}r_1\right)^2\right]\approx\frac{3}{4}\partial_x\left(r_1(x,t)\right)^2.$$

Hence, for this limiting case, the equation (2.34) is nothing else, but the standard KdV equation

$$r_t+r_x+\frac{1}{6}r_{xxx}+\frac{3}{4}\partial_x r^2=0. \tag{2.36}$$

In the following we show that up to second order r in equation (2.34) can be replaced by η. In other words, based on the uni-directionalisation the surface elevation η is governed by equation (2.34). To do that, we rewrite (2.34) in the form

$$\partial_t r=-\Gamma\left(2r+\delta_r\bar{H}_1(r,0)\right).$$

That gives

$$\partial_t(r-s)=-\Gamma\left(2(r-s)+\delta_r\bar{H}_1(r,0)\right)-\left[\partial_t s+2\Gamma s\right].$$

Since r and η are the same in the lowest order, this leads to

$$\partial_t\eta=-\Gamma\left(2\eta+\delta_\eta\bar{H}_1(\eta,0)\right)-F,$$

where the forcing F is given by

$$F = \partial_t s + 2\Gamma s.$$

Hence, the surface elevation evolves according to a KdV-type equation with the presence of a force.

The expression of F shows that the force merely contains waves traveling to the left. Before we proceed, observe that the inverse transformation (2.29) reads

$$\begin{aligned} 2r &= \eta + Ru, \\ 2s &= -\eta + Ru. \end{aligned}$$

Restricting on an initial condition $u_0 = u(x,0)$ and $\eta_0 = \eta(x,0)$ which gives $s_0 = s(x,0)$ small compared to η_0, implies that F is also small and remains small for finite time-interval. In this case, the surface elevation η is governed by

$$\eta_t + \partial_x R\left[\eta + \frac{1}{2}R^{-1}\left(\eta \cdot (R^{-1}\eta)\right) + \frac{1}{4}\left(R^{-1}\eta\right)^2\right] = 0.$$

Details for standard KdV equation is given in [17, 18].

In chapter 4 and 5 we will use a KdV-type model that has exact dispersion properties as the basic equations for surface waves and the quadratic nonlinearity given by the standard KdV. In normalised variables, this equation has the form

$$u_t + i\Omega(-i\partial_x)u + \frac{3}{4}\partial_x u^2 = 0. \tag{2.37}$$

From now on, we use the function u for the wave elevation, and we end this section with the following remark.

Remark 2.1 *Throughout our discussions we use the term modified KdV (mKdV) equation that refers to the equation (2.37). In this equation we use the notation Ω for both the differential operator and the dispersion relation, given by (2.35), in the sense that $\Omega(-i\partial_x)\exp(ikx) = \Omega(k)\exp(ikx)$. We use the notation K, defined by $K(\omega) = \Omega^{-1}(\omega)$, the inverse function of Ω. Obviously, we have*

$$\Omega(-k) = -\Omega(k) \quad \textit{and} \quad K(-\omega) = -K(\omega),$$

as shown in Figure 2.2.

2.5 Amplitude equation for mKdV model

The Nonlinear Schrödinger (NLS) and NLS-type equations have extensively been applied to study wave modulations, see in [1, 2, 35, 51]. In this section

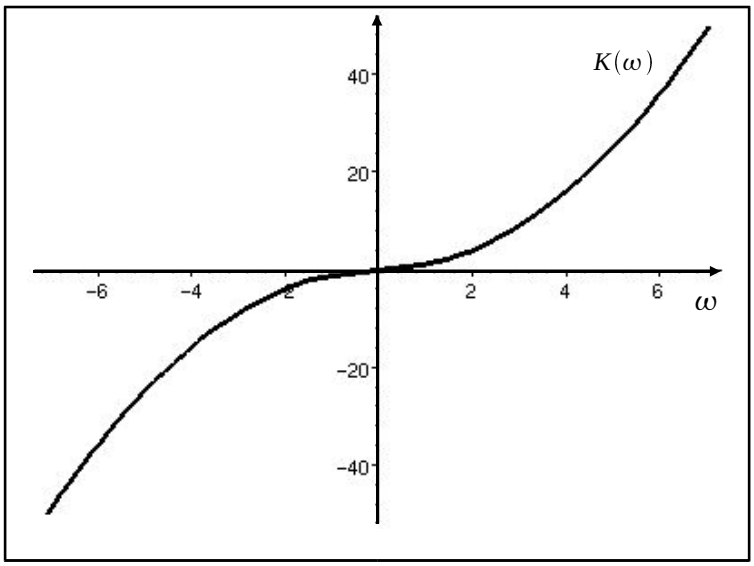

Figure 2.2: Exact dispersion relation.

we present a derivation of a generalised NLS (gNLS) equation from a KdV-type equation. To do that, we consider a KdV-type equation in the form

$$u_t + i\tilde{\Omega}(-i\partial_x)u + auu_x = 0. \tag{2.38}$$

Replacing $\tilde{\Omega}$ with Ω and a with $\frac{3}{2}$, we have mKdV equation (2.37). Brief derivations of NLS and gNLS equations from mKdV equation were given in [20, 22]. Replacing $\tilde{\Omega}$ with $\Omega_{bc} = ck - bk^3$, we have a KdV-type equation in the form

$$u_t + cu_x + bu_{xxx} + auu_x = 0. \tag{2.39}$$

Boyd and Chen have used this equation to study weakly nonlinear wave-packets and presented a derivation of the NLS equation from this equation (see [6]). We will show that the derived NLS-type equation below is more general than the NLS equation given in [6].

2.5.1 Dispersive distortion

We start with the general, but linear solution of the equation (2.38)

$$u(x,t) = \int \alpha(k) e^{i[kx - \tilde{\Omega}(k)t]} dk + \text{c.c.}, \tag{2.40}$$

where α is the spectral function of the field at $t = 0$. Introduce the notation $\Theta(k)$ to denote the phase of mode with wave number k that satisfies the dispersion relation

$$\Theta(k) = kx - \tilde{\Omega}(k)t.$$

The linear solution u in (2.40) can also be written in the form

$$u(x,t) = A(x,t)e^{i\Theta(\bar{k})} + \text{c.c.}, \tag{2.41}$$

where

$$\begin{aligned} A(x,t) &= \int \alpha(k) e^{i[\{k-\bar{k}\}x - \{\tilde{\Omega}(k)-\tilde{\Omega}(\bar{k})\}t]} dk \\ &= \int \alpha(\bar{k}+\kappa) e^{i[\kappa x - \{\tilde{\Omega}(\bar{k}+\kappa)-\tilde{\Omega}(\bar{k})\}t]} d\kappa. \end{aligned} \tag{2.42}$$

Obviously, this complex amplitude $A(x,t)$ satisfies

$$A_t + i[\tilde{\Omega}(\bar{k} - i\partial_x) - \tilde{\Omega}(\bar{k})]A = 0, \tag{2.43}$$

since

$$A_t = -i \int \{\tilde{\Omega}(\bar{k}+\kappa) - \tilde{\Omega}(\bar{k})\}\alpha(\bar{k}+\kappa) e^{i[\kappa x - \{\Omega(\bar{k}+\kappa)-\Omega(\bar{k})\}t]} d\kappa.$$

The notation $\tilde{\Omega}(\bar{k} - i\partial_x) - \tilde{\Omega}(\bar{k})$ should be interpreted as follows:

$$[\tilde{\Omega}(\bar{k} - i\partial_x) - \tilde{\Omega}(\bar{k})] \exp(i\kappa x) = \{\tilde{\Omega}(\bar{k}+\kappa) - \tilde{\Omega}(\bar{k})\} \exp(i\kappa x).$$

Introducing the transformation

$$t = \tau, \quad \zeta = x - \tilde{\Omega}'(\bar{k})t,$$

the equation (2.43) becomes

$$A_\tau + i\tilde{\Omega}_2(-i\partial_\zeta)A = 0, \tag{2.44}$$

where

$$\tilde{\Omega}_2 = \tilde{\Omega}(\bar{k}+\kappa) - \tilde{\Omega}(\bar{k}) - \tilde{\Omega}'(\bar{k}).$$

We note that the linear amplitude equation (2.44) is exact and valid for narrow-banded as well as broad-banded spectra.

2.5.2 Nonlinear effects

To incorporate the nonlinearity in the deformation of the envelope amplitude, the generation of a second order double harmonic bound wave and a variation of the equilibrium level is anticipated:

$$u = A_0 e^{i\Theta(\bar{k})} + Be^{2i\Theta(\bar{k})} + C + \text{c.c.} \tag{2.45}$$

The amplitudes A_0, B and C are allowed to vary slowly in the frame of reference, and B and C are of second order in the amplitude A_0. The slowly varying assumption implies that only narrow-banded spectra are considered. It

is natural to restrict to solutions u which are, either, square integrable in time (decaying at infinity) or are periodic with some period T. In the case $\int u dx = 0$, and the variations in the equilibrium level should satisfy at any time t, we have

$$\int C dx = 0.$$

Before we proceed, we make the following remark:

Remark 2.2 *For $A_0 e^{i\Theta(\bar{k})}$ is given by the first order of the Ansatz (2.45), we have*

$$i\tilde{\Omega}(-i\partial_x)\left(A_0 e^{i\Theta(\bar{k})}\right) = i\left[\tilde{\Omega}(\bar{k} - i\partial_x)\left(A_0\right)\right] e^{i\Theta(\bar{k})}.$$

This notation will be clear for simple examples below.

i) For $\tilde{\Omega}(k) = k^2$

$$\begin{aligned} i(-i\partial_x)^2\left(A_0 e^{i\Theta(\bar{k})}\right) &= -i\partial_x^2\left(A_0 e^{i\Theta(\bar{k})}\right) \\ &= -i\left[\partial_x^2 A_0 + 2i\bar{k}\partial_x A_0 - \bar{k}^2 A_0\right] e^{i\Theta(\bar{k})} \\ &= \left[\tilde{\Omega}(\bar{k} - i\partial_x)\left(A_0\right)\right] e^{i\Theta(\bar{k})}, \end{aligned}$$

ii) For $\tilde{\Omega}(k) = k^3$

$$\begin{aligned} i(-i\partial_x)^3\left(A_0 e^{i\Theta(\bar{k})}\right) &= -\partial_x^3\left(A_0 e^{i\Theta(\bar{k})}\right) \\ &= -i\left[\partial_x^3 A_0 + 3i\bar{k}\partial_x^2 A_0 - \bar{k}^2\partial_x A_0 - i\bar{k}^3 A_0\right] e^{i\Theta(\bar{k})} \\ &= \left[\tilde{\Omega}(\bar{k} - i\partial_x)\left(A_0\right)\right] e^{i\Theta(\bar{k})}. \end{aligned}$$

Inserting the Ansatz in the equation gives a residue that has to be made as small as possible. This residue is given by

$$R_{res} + R_2 + \text{h.o.t.}$$

where h.o.t. means higher order terms. The resonant and second order residues read

$$R_{res} = \left[\partial_t A_0 + i\left\{\tilde{\Omega}(\bar{k} - i\partial_x) - \tilde{\Omega}(\bar{k})\right\} A_0 + ai\bar{k}\left\{A_0 C + A_0\bar{C} + \bar{A}_0 B\right\}\right] e^{i\Theta(\bar{k})}$$

and

$$R_2 = i\left[\tilde{\Omega}(2\bar{k})B - 2\tilde{\Omega}(\bar{k})B + a\bar{k}A_0^2\right] e^{2i\Theta(\bar{k})} + \left[C_t + \tilde{\Omega}'(0)C_x + \frac{a}{2}\partial_x A_0\bar{A}_0\right].$$

Before we continue, we introduce the notations

$$\gamma_0 = \frac{1}{\tilde{\Omega}'(\bar{k}) - \tilde{\Omega}'(0)} \text{ and } \gamma_2 = \frac{\bar{k}}{2\tilde{\Omega}(\bar{k}) - \tilde{\Omega}(2\bar{k})}.$$

Making the second order residue $R_2 = 0$ defines the second order coefficients. Obviously, we have

$$B = a\gamma_2 A_0^2, \tag{2.46}$$

and

$$C_t + \Omega'(0)C_x + \frac{a}{2}\partial_x A_0 \bar{A}_0 = 0.$$

The last equation can be written

$$C_\tau - \Omega(\bar{k})C_\zeta + \Omega'(0)C_\zeta + \frac{a}{2}\partial_\zeta A_0 \bar{A}_0 = 0.$$

Assuming that C_τ is of higher order than the other terms, therefore it is neglected here, we have

$$-\Omega(\bar{k})C_\zeta + \Omega'(0)C_\zeta + \frac{a}{2}\partial_\zeta A_0 \bar{A}_0 = 0,$$

which gives an explicit expression for C in the form

$$\text{and } C = \frac{a}{2}\gamma_0[|A_0|^2 - I_0] \text{ with } I_0 = \int |A_0|^2 dx. \tag{2.47}$$

Finally, to avoid resonant terms by making $R_{res} = 0$ and applying (2.46) and (2.47), we have an equation for A_0 that is given by

$$\partial_\tau A_0 + a^2\gamma_0 I_0 \bar{k} A_0 + i\tilde{\Omega}_2(-i\partial_\zeta)A_0 + i\tilde{\gamma}|A_0|^2 A_0 = 0$$

with

$$\tilde{\gamma} = a^2(\gamma_0 + \gamma_2).$$

This result can be simplified by introducing an additional phase in A_0:

$$A_0 = Ae^{a^2 i\gamma_0 I_0 \bar{k}\zeta}$$

leading to

$$\partial_\tau A + i\tilde{\Omega}_2(-i\partial_\zeta)A + i\gamma|A|^2 A = 0. \tag{2.48}$$

Approximating $\tilde{\Omega}_2$ with the Taylor expansion

$$\tilde{\Omega}_2 = \frac{1}{2}\tilde{\Omega}''(\bar{k})\kappa^2 + \frac{1}{6}\tilde{\Omega}'''(\bar{k})\kappa^3 + O(\kappa^4).$$

Let β_2 and β_3 denote

$$\beta_2 = -\frac{1}{2}\tilde{\Omega}''(\bar{k}) \text{ and } \beta_3 = -\frac{1}{6}\tilde{\Omega}'''(\bar{k}).$$

Taking this approximation up to second order in κ leads to the standard Nonlinear Schrödinger (NLS) equation

$$A_\tau + i\beta_2 A_{\zeta\zeta} + i\tilde{\gamma}|A|^2 A = 0. \tag{2.49}$$

In [6] $\tilde{\Omega}(k)$ was replaced by Ω_{bc}, therefore, the NLS equation reads

$$A_\tau + i3bkA_{\zeta\zeta} - i\frac{a^2}{6bk}|A|^2A = 0. \tag{2.50}$$

Comparing the NLS equation (2.50) and the gNLS equation (2.48), the gNLS equation is more general, since the NLS equation (2.50) is obtained after taking the Taylor approximation of $\tilde{\Omega}_2$ up to second order in κ and replacing $\tilde{\Omega}(k)$ by $\Omega_{bc}(k)$.

We note that the NLS equation derived from the KdV equation (2.39) is always the *defocusing* case; envelope solitary waves cannot be found as solutions of such KdV equation. For the wave number larger than a critical value $k \geq k_{crit}$, however, the NLS equation derived from the modified KdV equation (2.37) yields the *focusing* case, where the NLS equation does have a solitary solution, meaning that the mKdV has envelope solitary wave solutions.

For the surface wave problems, we have $\beta_3 \neq 0$. Approximating $\tilde{\Omega}_2$ up to third order in κ leads to

$$A_\tau + i\beta_2 A_{\zeta\zeta} + \beta_3 A_{\zeta\zeta\zeta} + i\tilde{\gamma}|A|^2A = 0.$$

This result is an amplitude equation for broader spectra and known as the Dysthe NLS (dNLS) equation (see [15, 16, 52]).

Chapter 3

Perturbation Methods

In this chapter we consider asymptotic methods to find approximate solutions of nonlinear differential equations. Most part of the discussion is contained in [23]. We will restrict the analysis to ordinary differential equations. The methods and ideas, however, are equally useful for the perturbation analysis of partial differential equations that we will discuss in the next chapters. The perturbation techniques we will present in the following can be found in some standard text books: e.g. [27, 40, 29, 30].

As a classical example to which the ideas can be best illustrated is to find the solution $x(t)$ that satisfies a nonlinear extention of the harmonic oscillator equation

$$\ddot{x} + x + x^2 = 0, \quad \text{for} \quad t > 0, \tag{3.1}$$

with the initial condition

$$x(0) = \epsilon, \ \dot{x}(0) = 0.$$

The dot represents the derivative with respect to the temporal variable t. Neglecting the nonlinearity, the solution is simply the motion of the harmonic oscillator:

$$x_1(t) = \epsilon \cos t.$$

For small ϵ this may well be a good approximation of the nonlinear equation also. We note that for the linear oscillator, all solutions have the same period, 2π, that is independent of amplitude.

Writing $y = \epsilon x$ the initial values are normalised: $y(0) = 1$, $\dot{y}(0) = 0$, but now the 'small' parameter ϵ appears in the equation:

$$\ddot{y} + y + \epsilon y^2 = 0. \tag{3.2}$$

This shows more clearly that the contribution of nonlinearity is 'small' (as long as y remains bounded). The equation (3.2) is often called weakly nonlinear because it is indeed nonlinear but reduces to linear when $\epsilon = 0$.

Before discussing perturbation methods, we will investigate the global properties of the solutions by phase plane analysis. In most cases this is not possible but here we can exploit the standard analysis for Newtonian systems:

$$\ddot{x} = -\frac{\partial V}{\partial x}$$

where V is the potential energy given by

$$V(x) = \frac{1}{2}x^2 + \frac{1}{3}x^3.$$

The plot of this potential energy and the phase portrait of solutions are given in Figure 3.1. From this figure we conclude that for (3.1), all solutions with ϵ smaller than a critical value are periodic. One phenomenon that is not directly visible from the phase plane analysis is that the periods of the periodic motion depend on the amplitude (on ϵ), in contrast to the linear equation for which every solution has period 2π. This can, however, be expected by observing that the equation can be written like

$$\ddot{x} + \omega^2(x)x = 0,$$

with $\omega^2(x) = 1 + x$. Here the period depends on the solution, but it is not known in advance. It can therefore be expected that perturbation methods will also have to be able to vary the frequency with ϵ.

3.1 Naive perturbation method

We consider an approximate solution in the form of series expansion

$$x(\epsilon, t) = \epsilon x_1(t) + \epsilon^2 x_2(t) + \epsilon^3 x_3(t) + \cdots . \tag{3.3}$$

On substituting this into (3.1), this series expansion leads for each $x_k,\ k \geq 1$ to an equation in the form

$$\ddot{x}_k + x_k = F_k$$

where F_k depends on the functions $x_j,\ j \leq k-1$ and is therefore known in a successive solution strategy. The solution of this linear equation can be found explicitly. However, even though the forcing F_k is bounded, the solution does not have to be bounded. When the forcing is periodic with the period as the solution of the homogeneous equation, the phenomenon of resonance appears.

3.1.1 The linear oscillator driven by forces

Before we discuss the naive perturbation method in detail, we will recall some examples. The explicit solution of

$$\ddot{u} + \omega_0^2 u = a\cos\omega t, \quad \omega \neq \omega_0$$

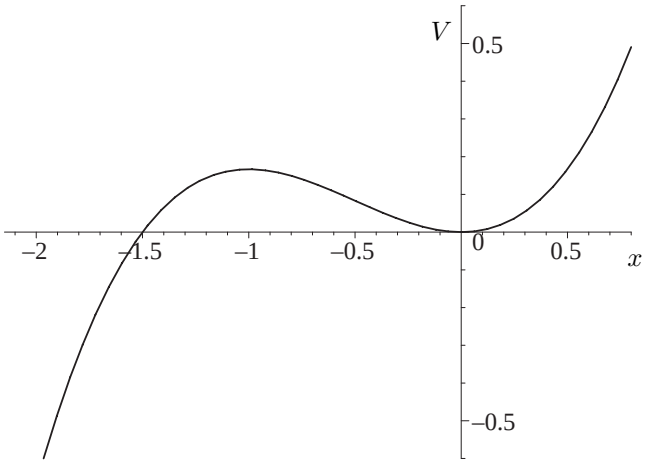

(a) The potential energy V

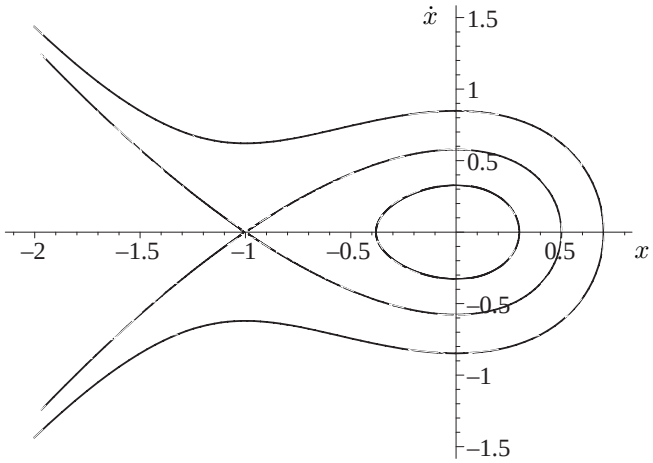

(b) The phase portrait

Figure 3.1: Plots of the potential energy V and the phase portrait of solutions of equation (3.1). The perturbation analysis is for the bounded, periodic solutions.

is given by

$$u(t) = \frac{a}{\omega_0^2 - \omega^2} \cos \omega t.$$

This shows that the solution is bounded, and is forced to be periodic with the same period of the driving force. It is quite different for $\omega = \omega_0$, which gives

$$u(t) = \frac{a}{2\omega_0} t \sin \omega_0 t;$$

that is unbounded, growing linearly in time. The unboundedness is a consequence of the forcing with the same period as the natural frequency ω_0 of the system. This phenomenon is called *resonance*.

Resonance will be essential in the discussion of a nonlinear dispersion relation for water waves in the next chapters. Therefore, it is important to investigate whether the resonance occurs, as an example, in the equation

$$\ddot{u} + \omega_0^2 u = f(t).$$

In other words, can we give conditions on f that guarantee that the solution is uniformly bounded. Consider the following cases:

i) *f is periodic.*
The answer will be clear if f is periodic with period $T_0 = \frac{2n\pi}{\omega_0}$, where n is a positive integer. Hence, f can be expanded as a Fourier series, and the requirement must be that the coefficients in the front of the term with $e^{i\omega_0 t}$ vanish, i.e.

$$\int_0^{T_0} f(t) \cos \omega_0 t \; dt = 0, \quad \text{and} \int_0^{T_0} f(t) \sin \omega_0 t \; dt = 0.$$

These conditions on f are known as *solvability conditions*.

ii) *f is not periodic.*
In the case f is not periodic, but square integrable, Fourier-integral methods can be applied. We now consider the following example with complex notation for simplicity

$$\dot{z} + i\omega_0 z = f(t).$$

Writing

$$f(t) = \int F(\omega) e^{-i\omega t} d\omega; \quad F(\omega) = \frac{1}{2\pi} \int f(t) e^{i\omega t} dt$$

the solution reads

$$z(t) = \int \frac{F(\omega)}{i\omega_0 - i\omega} e^{-i\omega t} d\omega.$$

We now show that $z(t)$ is bounded. The last integral seems to have a singularity at $\omega = \omega_0$. To investigate the behaviour near ω_0, write $\omega = \omega_0 + \sigma$. Hence, we have

$$z(t) = e^{-i\omega_0 t} \int \frac{F(\omega_0 + \sigma)}{-i\sigma} e^{-i\sigma t} d\sigma.$$

Observe that

$$\begin{aligned}\frac{d}{dt}\int \frac{F(\omega_0+\sigma)}{-i\sigma}e^{-i\sigma t}d\sigma &= \int F(\omega_0+\sigma)e^{-i\sigma t}d\sigma \\ &= e^{i\omega_0 t}\int F(\omega)e^{-i\omega t}d\omega = e^{i\omega_0 t}f(t).\end{aligned}$$

The explicit solution reads

$$z(t) = e^{-i\omega_0 t}\int^t e^{i\omega_0 s}f(s)ds$$

known as the *variation of constant formula*. This shows that no resonance will appear: the solution remains uniformly bounded, even though $F(\omega_0) \neq 0$, i.e. even when the fundamental frequency ω_0 is present in the driving force. Of course, when the driving force is periodic, resonance appears as we have already seen above. The equation

$$\dot{z} + i\omega_0 z = Ae^{-i\omega_0 t}$$

gives $z(t) = Ate^{-i\omega_0 t}$ which also follows from the variation of constant formula:

$$z(t) = e^{-i\omega_0 t}\int^t e^{i\omega_0 s}Ae^{-i\omega_0 s}ds = Ate^{-i\omega_0 t}.$$

The explanation of this seemingly discrepancy is the difference in energy-content in the resonant forcing. The energy is finite for square integrable functions, and hence infinitesimally small per unit time, while the energy is infinite for the periodic forcing (finite per unit time). This is also seen from looking at the increase in 'energy' over a time interval T:

$$|z(T)|^2 - |z(0)|^2 = \int_0^T \partial_t|z(t)|^2dt = 2\mathrm{Re}\int_0^T z(t)\overline{f(t)}dt.$$

In practical situations the analysis above leads to some confusions when energy content is not taken into account properly. We will have to deal with this in the analysis for the nonlinear dispersion relation for nonlinear wave equation further on, and therefore make the following remarks.

Remark 3.1 *In practical situation, we are dealing with signals that were measured, 'given' only for a finite time, say*

$$s(t),\ t \in [0,T].$$

Then, in principle there are two ways to continue the mathematical reasoning:

i) Extend the signal by zero outside the given time-interval. This then leads to a square integrable function

$$s_0(t) = \begin{cases} s(t), & t \in [0,T], \\ 0, & t \notin [0,T], \end{cases}$$

where

$$s_0(t) = \int \hat{s}_0(\omega) e^{-i\omega t} d\omega, \quad \hat{s}_0(\omega) = \frac{1}{2\pi} \int s_0(t) e^{i\omega t} dt = \frac{1}{2\pi} \int_0^T s_0(t) e^{i\omega t} dt.$$

Approximating the integrals by Riemann-sum, there results

$$s_0(t) = \sum \hat{s}_0(n \cdot \Delta\omega) e^{-i\Delta\omega \cdot t \cdot n} \Delta\omega.$$

ii) Make a $T-$periodic continuation of the signal, and use Fourier series:

$$s(t) = \sum c_n e^{-i\frac{2\pi}{T} t \cdot n}, \quad c_n = \frac{1}{T} \int_0^T s(t) e^{i\frac{2\pi}{T} t \cdot n} dt.$$

The relation between the methods will be clear now: the choice $\Delta\omega = \frac{2\pi}{T}$ leads to complete agreement, provided that

$$c_n = \hat{s}_0(n \cdot \Delta\omega) \cdot \Delta\omega \quad \textit{for} \quad \Delta\omega = \frac{2\pi}{T},$$

which shows the appearance of the length T of the time interval in the relation between the discrete and continuous spectra.

3.1.2 Direct approximation

We are now back to the discussion of the naive perturbation method and proceed up to third order. On substituting (3.3) into (3.1) and taking into account the initial conditions, we have

$$\ddot{x}_1 + x_1 = 0, \quad x_1(0) = 1, \quad \dot{x}_1(0) = 0, \tag{3.4}$$

$$\ddot{x}_2 + x_2 = -x_1^2, \quad x_2(0) = 0, \quad \dot{x}_2(0) = 0, \tag{3.5}$$

$$\ddot{x}_3 + x_3 = -2x_1x_2, \quad x_3(0) = 0, \quad \dot{x}_3(0) = 0. \tag{3.6}$$

Clearly the solution for x_1 is given by $x_1 = \cos t$. Hence, the forcing of the equation x_2 is given by $x_1^2 = \cos^2 t = \frac{1}{2}(1 + \cos 2t)$. The solution for x_2 can be written as

$$x_2(t) = -\frac{1}{2} + \frac{1}{3}\cos t + \frac{1}{6}\cos 2t.$$

The terms $-\frac{1}{2}$ and $\frac{1}{6}\cos 2t$ of this solution are due to the forcing of the equation. The term $\frac{1}{3}\cos t$ is a solution of the homogeneous equation and taken into account to satisfy the initial conditions. This idea is also considered in the next chapters when *free waves* are taken into account to compensate *bound waves* such that the solutions satisfy the initial signal.

The forcing of the equation x_3 can be expanded (after some straightforward calculation) to

$$-2x_1x_2 = -\frac{1}{3} + \frac{5}{6}\cos t - \frac{1}{3}\cos 2t - \frac{1}{6}\cos 3t. \tag{3.7}$$

The solution can be written down, but the appearance of the source $\frac{5}{6}\cos t$ indicates that resonance will appear:

$$x_3(t) = -\frac{1}{3} + \frac{5}{12}t\sin t + \frac{83}{144}\cos t - \frac{1}{9}\cos 2t - \frac{1}{48}\cos 3t.$$

Hence, up to third order, the solution reads

$$\begin{aligned} x(\epsilon,t) &= \epsilon\cos t + \epsilon^2(-\frac{1}{2} + \frac{1}{3}\cos t + \frac{1}{6}\cos 2t) \\ &\quad +\epsilon^3(-\frac{1}{3} + \frac{5}{12}t\sin t + \frac{83}{144}\cos t - \frac{1}{9}\cos 2t - \frac{1}{48}\cos 3t). \end{aligned}$$

The interpretation of this solution is as follows. For small value of $t > 0$, in fact for t in any interval of length, $t \in [0, T]$, this is a good approximation for ϵ sufficiently small, since the third order term, although increasing linearly in time, is bounded by constant $\epsilon^3 T$, and a same result hold for the other terms. In practice, however, we want to go further and have a solution that is also correct for larger values of time, as an example, in the next chapters we deal with long time wave evolutions in long wave tanks of hydrodynamic laboratories. Since the solution is known to be bounded (for small value of ϵ) for all time (from phase plane analysis), we would even like to have an approximation that holds for all time, also $t \to \infty$; an approximation with this property is called a *uniformly valid* approximation. Clearly the approximation constructed above does not satisfy this criterion, since $\epsilon^3 t$ will explode for $t \to \infty$ at fixed ϵ.

3.2 Improved perturbation method

The naive perturbation method above (series expansion in ϵ) does not give a possibility to prevent the linear growth in time, since this is caused by the resonance phenomenon in the equation for x_3. Moreover, this method does not give any solutions in which their periods depend on the solutions themselves as already predicted using the standard analysis for Newtonian system. All improved perturbation techniques are based on creating more flexibility in the Ansatz for the solution so that this resonance can be prevented. Throughout

this section the initial conditions are neglected. If one needs to take these conditions into account, they simply need to add the corresponding solution(s) of the homogeneous equation as presented in the previous section.

In the following we will present one technique, which will be called the *amplitude-phase method*, for reasons to become clear soon. For the problem discussed above, we take an Ansatz

$$x(\epsilon, t) = \epsilon \cos[(\omega_0 + \epsilon\omega_1 + \epsilon^2\omega_2 + \dots)t] + \epsilon^2\xi_2 + \epsilon^3\xi_3 + \dots .$$

The expansion on the frequency above is known as Lindstedt-Poincaré method. On substituting this Ansatz into the right hand side of (3.1), we have residual

$$Res = A^{(1)}\epsilon + A^{(2)}\epsilon^2 + A^{(3)}\epsilon^3 + O(\epsilon^4),$$

where

$$\begin{aligned} A^{(1)} &= (-\omega_0^2 + 1)\cos[(\omega_0 + \epsilon\omega_1 + \epsilon^2\omega_2 + \dots)t], \\ A^{(2)} &= \ddot{\xi}_2 + \xi_2 + \cos^2[(\omega_0 + \epsilon\omega_1 + \epsilon^2\omega_2 + \dots)t] \\ &\quad -2\omega_1 \cos[(\omega_0 + \epsilon\omega_1 + \epsilon^2\omega_2 + \dots)t], \\ A^{(3)} &= \ddot{\xi}_3 + \xi_3 + 2\xi_2 \cos[(\omega_0 + \epsilon\omega_1 + \epsilon^2\omega_2 + \dots)t] \\ &\quad -(2\omega_2 + \omega_1^2)\cos[(\omega_0 + \epsilon\omega_1 + \epsilon^2\omega_2 + \dots)t]. \end{aligned}$$

The Ansatz will be a good approximation to the solution provided that the residual is small. Particularly, to get an approximation up to third order, the condition $A^{(j)} = 0$ for $j = 1, 2, 3$ should be satisfied. These conditions will yield solutions for ω_j and ξ_j that needs to be computed consecutively as follows. Taking $A^{(1)} = 0$, we find that $\omega_0 = 1$. Next, the resonant and non-resonant terms in $A^{(2)}$ should be taken to be zero separately, which give a condition

$$2\omega_1 \cos[(\omega_0 + \epsilon\omega_1 + \epsilon^2\omega_2 + \dots)t] = 0 \Rightarrow \omega_1 = 0$$

and an equation

$$\ddot{\xi}_2 + \xi_2 + \cos^2[(\omega_0 + \epsilon\omega_1 + \epsilon^2\omega_2 + \dots)t] = 0.$$

Neglecting the initial conditions, the forcing $\cos^2[(\omega_0 + \epsilon\omega_1 + \epsilon^2\omega_2 + \dots)t]$ of the equation ξ_2 gives solution

$$\xi_2 = -\frac{1}{2} + \frac{1}{6}\cos[2(\omega_0 + \epsilon\omega_1 + \epsilon^2\omega_2 + \dots)t].$$

Hence, the term $-2\xi_2 \cos[(\omega_0 + \epsilon\omega_1 + \epsilon^2\omega_2 + \dots)t]$ in $A^{(3)}$ (after some simple calculations) equals to

$$\frac{5}{6}\cos[(\omega_0 + \epsilon\omega_1 + \epsilon^2\omega_2 + \dots)t] - \frac{1}{6}\cos[3(\omega_0 + \epsilon\omega_1 + \epsilon^2\omega_2 + \dots)t].$$

Collecting the resonant and non-resonant terms of $A^{(3)}$ we have

$$(\frac{5}{6} - 2\omega_2)\cos[(\omega_0 + \epsilon\omega_1 + \epsilon^2\omega_2 + \dots)t],$$

and

$$\ddot{\xi}_3 + \xi_3 - \frac{1}{6}\cos[3(\omega_0 + \epsilon\omega_1 + \epsilon^2\omega_2 + \dots)t]$$

respectively. Taking those terms vanish we have

$$\omega_2 = \frac{5}{12}$$

and

$$\ddot{\xi}_3 + \xi_3 = -\frac{1}{6}\cos[3(\omega_0 + \epsilon\omega_1 + \epsilon^2\omega_2 + \dots)t]. \tag{3.8}$$

Solving (3.8) the solution ξ_3 reads

$$\xi_3 = -\frac{1}{48}\cos[3(\omega_0 + \epsilon\omega_1 + \epsilon^2\omega_2 + \dots)t].$$

Hence, up to third order, the approximate solution is given by

$$\begin{aligned} x(\epsilon, t) &= \epsilon\cos[(1 + \frac{5}{12}\epsilon^2)t] + \epsilon^2\left(-\frac{1}{2} + \frac{1}{6}\cos[2(1 + \frac{5}{12}\epsilon^2)t]\right) \\ &\quad -\epsilon^3\frac{1}{48}\cos[3(1 + \frac{5}{12}\epsilon^2)t]. \end{aligned}$$

Immediate observations on this solution are that the solution is bounded (it does not contain resonant term that linearly grows in time), and the period depends on amplitude ϵ. These facts distinguish the improved method from the naive perturbation method.

3.3 Conclusion and discussion

We have presented two perturbation methods: the naive perturbation method and the improved perturbation method. Consider the solutions that are bounded by restricting to small value of ϵ (less than a critical value). For longer time interval the former method is not accurate in predicting the solution: the resonant contribution is present in the third order which linearly grows in time. The latter method, however, has taken care of the resonance by expanding the frequency as a series expansion of amplitude. Taking the resonant terms to vanish, the approximate solution is bounded and the frequency depends on amplitude as already predicted.

We have implemented the improved perturbation method up to third order. If a very long time interval is to be considered, higher order frequency correction may be taken into account. That can simply be done iteratively as follows:

i) Collect the resonant and non-resonant terms of $A^{(j)}$.

ii) Make the resonant terms equal to zero. This determines a condition that leads to the solution for $\omega^{(j)}$.

iii) Make the non-resonant terms to vanish. This leads to an equation for ξ_j without resonant forcing. Solving this equation gives a bounded solution for ξ_j.

So far we applied these methods to a nonlinear ordinary differential equation that leads to a single frequency solution in the lowest order. We have also shown that the expansions of the solution and the frequency only depend on amplitude. The case is very different for partial differential equations. For an example consider the modified KdV equation

$$u_t + i\Omega(-i\partial_x)u + \frac{3}{4}\partial_x u^2 = 0,$$

which in the lowest order gives the solution in the form

$$u^{(1)}(x,t) = \int \alpha(k) \exp i\{kx - \Omega(k)t\} dk.$$

Particularly, for

$$u^{(1)}(x,t) = q \exp i\{k_1 x - \Omega(k_2)t\} + q \exp i\{k_2 x - \Omega(k_2)t\} + \text{c.c.}$$

the expansion will also depend on the difference $k_2 - k_1$. The next chapters will deal with the implementation of the perturbation methods above for the mKdV equation to study wave evolution phenomena.

Chapter 4

Nonlinear evolution of bichromatic wave groups

In this chapter we will discuss the evolution of bichromatic wave groups. This is motivated to understand the appearance of large deformations of bichromatic waves that are of relevance for hydrodynamic laboratories. The deformations are reported for numerical results in [54, 55, 57, 58] and experiments in [49, 56]. Recalling this deformation phenomenon that has been presented in chapter 1, the evolution is started with a pure bichromatic wave at a point (very) close to the wave maker. Then, the amplitude grows, showing asymmetry of the envelope, and each group tends to lean forward. The growing process of the amplitude continues until it reaches its optimum then decreases. Strictly speaking, the initially purely bichromatic wave is modulated and eventually developing into a more complex wave field.

Throughout the discussion we will follow the analysis given in [8, 9, 22] which mainly use the perturbation techniques presented in chapter 3 that will be modified for partial differential equations. Mathematically speaking, we are looking for the solution of $u(x,t)$ that satisfies the 'modified' KdV (mKdV) equation

$$u_t + i\Omega(-i\partial_x)u + \frac{3}{4}\partial_x u^2 = 0, \tag{4.1}$$

with the initial signal

$$u(0,t) = 2q\left[\cos(\omega_{-1}t) + \cos(\omega_{+1}t)\right], \tag{4.2}$$

where $\omega_{\pm 1} = \bar{\omega} \pm \nu$. Writing $u(0,t)$ as

$$u(0,t) = 4q\cos\nu t\cos\bar{\omega}t$$

this initial signal has cosine shaped envelopes, see Figure 4.1. Note that all variables and parameters are in normalised forms. The function $u(x,t)$ represents the wave elevation. In this chapter we take q small, meaning that we only consider wave amplitudes that are small compared to the water depth.

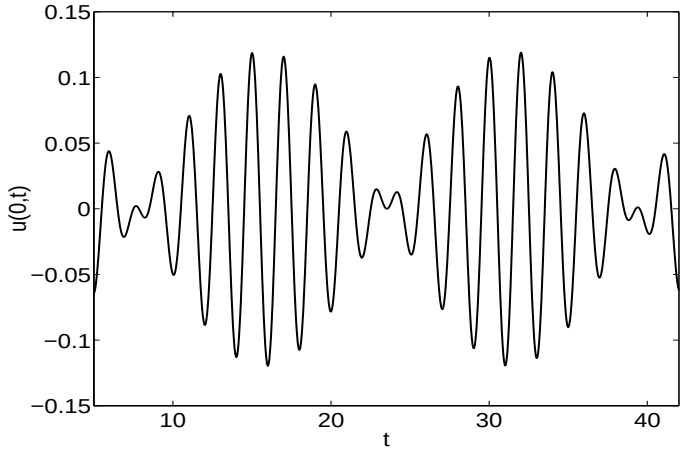

Figure 4.1: Beat pattern of the initial signal $u(0,t)$, for $q = 0.03,\ \bar{\omega} = \pi,\ \nu = 0.2$.

For some comparisons with experiments or direct numerical simulations we rewrite the transformation(s) to the laboratory variables that have been presented in chapter 2. The corresponding laboratory variables (in the right hand sides) are given by the following transformation

$$x^* = hx, \quad t^* = t\sqrt{h/g}, \quad \eta = hu, \tag{4.3}$$

where h is the uniform depth and g is the acceleration due to gravity. The spatial variable x^* denotes the horizontal direction, and t^* is the temporal variable. The transformations of wave parameters such as wave length, wave number and angular frequency, are given by

$$\lambda^* = h\lambda, \quad k^* = k/h, \quad \omega^* = \omega\sqrt{\frac{g}{h}}. \tag{4.4}$$

Observe that these transformations normalise the depth of the layer and the propagation speed of infinitesimal long waves. From now on we use the same notations for normalised and laboratory variables. To distinguish the laboratory variables from the corresponding normalised ones we simply use physical units for those quantities.

For comparisons with direct numerical results that are based on the basic equations for surface waves and experiments in this and the coming chapters, we note the following remark.

Remark 4.1 *The nonlinearity of this mKdV model may not be accurate compared to the Stokes theory for relatively short waves, a theory mostly used for comparison, see for example in [3]. This mKdV model, however, is chosen for its simplicity to understand the theory that we will discuss below, yet it still gives*

a good approximation to the numerics and experiments as we will see in the following discussions. If a better accuracy in the nonlinearity is really needed, one should consider the basic equations for surface waves. However, this introduces much more complexity in the algebraic computations.

4.1 Direct second order approximation

In chapter 3 we presented how a naive perturbation technique can be used to compute an approximate solution of an ordinary differential equation. In this section we apply this technique to find an approximate solution of mKdV (4.1) with the initial signal (4.2) up to second order. Hence, we approximate the solution $u(x,t)$ with a series expansion in the form

$$u = u^{(1)} + u^{(2)} + u^{(3)} + \cdots . \tag{4.5}$$

The superscripts stand for the order in amplitude q, the perturbation parameter. On substituting (4.5) into (4.1) we have equations for $u^{(j)}$, in particular for $j = 1,\ 2,\ 3$

$$u_t^{(1)} + i\Omega(-i\partial_x)u^{(1)} = 0, \qquad u^{(1)}(0,t) = 2q\left[\cos(\omega_{-1}t) + \cos(\omega_{+1}t)\right], \tag{4.6}$$

$$u_t^{(2)} + i\Omega(-i\partial_x)u^{(2)} = -\frac{3}{4}\partial_x\left[u^{(1)}\right]^2, \quad u^{(2)}(0,t) = 0, \tag{4.7}$$

$$u_t^{(3)} + i\Omega(-i\partial_x)u^{(3)} = -\frac{3}{2}\partial_x\left[u^{(1)}u^{(2)}\right], \quad u^{(3)}(0,t) = 0. \tag{4.8}$$

These are linear equations that can be solved easily. In lowest order the driving force to the linear equation is zero, but in second order and third order the driving forces are given by $-\frac{3}{4}\partial_x\left[u^{(1)}\right]^2$ and $-\frac{3}{2}\partial_x\left[u^{(1)}u^{(2)}\right]$, respectively.

Before solving these equations, we will introduce some notations for simplicity. The notation $\Theta(\omega)$ denotes the phase of the mode with frequency ω satisfying the dispersion relation

$$\Theta(\omega) = K(\omega)x - \omega t,$$

and $V_g(K(\omega))$ denotes the group velocity at frequency ω. We will also use the notations

$$\begin{array}{lcl} K_{\pm 1} & = & K(\omega_{\pm 1}), \\ \bar{k} & = & \frac{K_{-1}+K_{+1}}{2} \text{ and} \\ \kappa & = & \frac{K_{+1}-K_{-1}}{2} = \nu K'(\bar{\omega}) + O(\nu^2). \end{array}$$

Observe that for fixed $\bar{\omega}$ and small ν, we have $\kappa \sim \nu$.

Solving the equation (4.6) leads to the lowest order solution $u^{(1)}$ in the form

$$u^{(1)} = 2q\left[\cos\Theta_{-1} + \cos\Theta_{+1}\right], \tag{4.9}$$

where $\Theta_{\pm 1} = \Theta(\omega_{\pm 1})$. For algebraic computation later, it is convenient to write $u^{(1)}$ in the exponential form

$$u^{(1)} = q\left[e^{i\Theta_{-1}} + e^{i\Theta_{+1}}\right] + \text{c.c.},$$

where c.c. denotes the complex conjugate. This is a superposition of two linear dispersive waves. Another interpretation may be given by writing equation (4.9) as

$$u^{(1)} = 4q\cos[\kappa x - \nu t]\cos[\bar{k}x - \bar{\omega}t],$$

which is a carrier wave $\cos[\bar{k}x - \bar{\omega}t]$ modulated by an envelope $4q\cos[\kappa x - \nu t]$. The corresponding second order solution is found by solving (4.7) where $u^{(1)}$ is given by (4.9). This solution reads

$$u^{(2)} = u^{(2)}_{\text{bw}} + u^{(2)}_{\text{free}}, \tag{4.10}$$

where

$$u^{(2)}_{\text{bw}} = \frac{3}{2}q^2 \left[\begin{array}{l} s_{-1}e^{2i\Theta_{-1}} + s_{+1}e^{2i\Theta_{+1}} + 2se^{i[\Theta_{-1}+\Theta_{+1}]} \\ +s_0 e^{i[\Theta_{+1}-\Theta_{-1}]} \end{array} \right] + \text{c.c.} \tag{4.11}$$

and

$$u^{(2)}_{\text{free}} = -\frac{3}{2}q^2 \left[\begin{array}{l} s_{-1}e^{i\Theta(2\omega_{-1})} + s_{+1}e^{i\Theta(2\omega_{+1})} + 2se^{i\Theta(2\bar{\omega})} \\ +s_0 e^{i\Theta(2\nu)} \end{array} \right] + \text{c.c.} \tag{4.12}$$

The coefficients $s,\ s_0,\ s_\pm$ are given by

$$s = \frac{\bar{k}}{2\bar{\omega} - \Omega(2\bar{k})},\ s_{\pm 1} = \frac{K_{\pm 1}}{2\omega_{\pm 1} - \Omega(2K_{\pm 1})},\ s_0 = \frac{2\kappa}{2\nu - \Omega(2\kappa)}.$$

Observe that for $\kappa \to 0$ implies $s_0 \to \sigma_0$ and $s, s_\pm \to \sigma_2$, where

$$\sigma_0 = \frac{1}{V_g(K(\bar{\omega})) - 1},\quad \sigma_2 = \frac{K(\bar{\omega})}{2\bar{\omega} - \Omega(2K(\bar{\omega}))}.$$

Before we continue to investigate the performance of this direct second order theory, we make remarks on this second order solution as follows.

Remark 4.2 *The solution $u^{(2)}$ contains $u^{(2)}_{bw}$ and $u^{(2)}_{\text{free}}$. The solution $u^{(2)}_{bw}$ is due to the forcing $\frac{3}{4}\partial_x\left[u^{(1)}\right]^2$. This contains four components that are called bound waves, since these components do not satisfy the dispersion relation and cannot exist 'individually'.*

Remark 4.3 *The second order forcing function $-\frac{3}{4}\partial_x\left[u^{(1)}\right]^2$ acts as an input to the linear system (4.7) that determines the output $u^{(2)}_{bw}$. Borrowing terminology from signal theory, the coefficients $s,\ s_0,\ s_\pm$ are often called second order transfer functions.*

These contributions of the first and second order solution in the frequency domain can be seen in Figure 4.2. The main frequencies $\omega_\pm$ stimulate second order

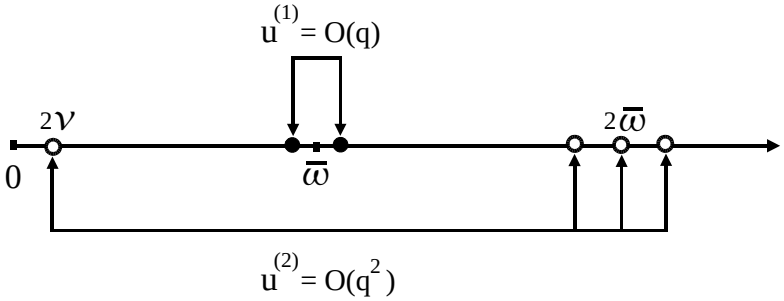

Figure 4.2: Schematic plot of the first and second order contributions in the frequency domain.

interactions in the low frequency 2ν (also called subharmonic interaction) and high frequencies $2\bar{\omega}$, and $2\bar{\omega} \pm 2\nu$ (superharmonic interactions).

The components of the second order solution, $u^{(2)}_{\text{bw}}$ and $u^{(2)}_{\text{free}}$, have different properties. On the one hand, the bound wave components do not satisfy the dispersion relation and propagate with the same velocity as the main waves, the first order solution. On the other hand, the free waves, $u^{(2)}_{\text{free}}$, are solutions of the homogeneous equation and are present such that $u^{(2)}$ satisfies the initial signal. Therefore, $u^{(2)}_{\text{free}}$ satisfies the dispersion relation, and these free waves travel with different velocity than the bound waves. The difference in the phase velocity may cause a complex interference pattern in the wave evolution. Figure 4.3 shows these second order components and the results of the direct second order theory at different positions. Since the presence of the free waves are to compensate the bound waves at $x = 0$, at this position $u^{(2)}_{\text{bw}}$ and $u^{(2)}_{\text{free}}$ are out of phase (see Figure 4.3 (a)) implying $u(0,t) = u^{(1)}(0,t)$ (see Figure 4.3 (c)). At $x = 10$, however, these second order components are no longer out of phase as shown in Figure 4.3 (b). Moreover, the free waves $u^{(2)}_{\text{free}}$, that are composed of four modes, produce a signal with complex pattern. The direct second order approximation as a sum of these first and second order components gives a signal with envelopes that steepen upward (see Figure 4.3 (d)).

In the following we will compare the direct second order approximation

$$u(x,t) = u^{(1)}(x,t) + u^{(2)}(x,t)$$

with direct numerical results for two different bichromatics: namely Bichromatic 1 and Bichromatic 2. The numerical simulation was run in a basin of 5 m depth, using FEM/FD for the basic equations for surface waves developed by Westhuis, see [58]. This numerical simulation has been proved to be a good approximation to experiments. Table 4.1 shows parameters in normalised and laboratory quantities, which are the same for these Bichromatics. The only difference between these bichromatics is the amplitude parameter q; for Bichromatic 1 $q = 0.004$

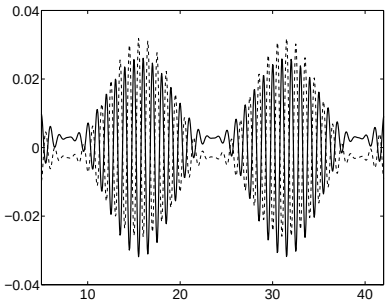

(a) $u^{(2)}_{\mathrm{bw}}(0,t)$ solid line, and $u^{(2)}_{\mathrm{free}}(0,t)$ dashed line.

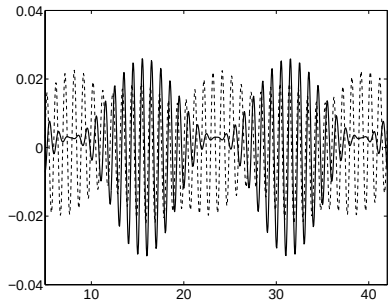

(b) $u^{(2)}_{\mathrm{bw}}(10,t)$ solid line, and $u^{(2)}_{\mathrm{free}}(10,t)$ dashed line.

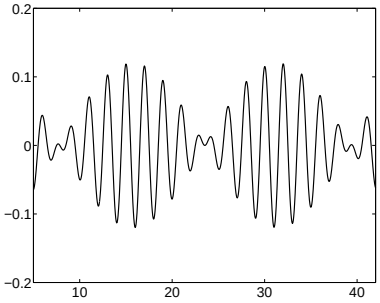

(c) $u(0,t)$

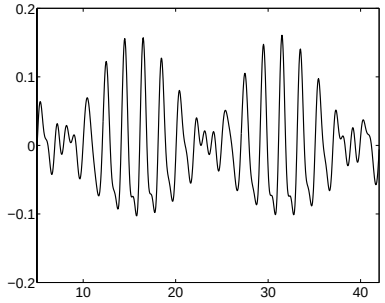

(d) $u(10,t)$

Figure 4.3: The second order components and the results from the direct second order theory at $x = 0$ and 10. For this example, $q = 0.03$, $\bar{\omega} = \pi$, $\nu = 0.2$, the horizontal axis is time, and the vertical axis is elevation.

	Normalized	Laboratory
$\bar{\omega}$	2.2464	3.1450 s^{-1}
k	5.0593	1.0119 m^{-1}
ν	0.1107	0.1550 s^{-1}
κ	0.4970	0.0994 m^{-1}

Table 4.1: Parameter data of Bichromatic 1 and Bichromatic 2 in normalised variables and laboratory variables.

and for Bichromatic 2 $q = 0.008$. In the laboratory variables, the amplitude q of Bichromatic 1 is 0.02 m, and the amplitude of the Bichromatic 2 is 0.04 m. The parameters for Bichromatic 2 are chosen based on the experiments of Stansberg [49], which showed large envelope deformations. To investigate the effects of the amplitude q, direct numerical simulations (see [58]) as well as experiments (see [56]) have been conducted for several values of amplitudes, while keeping the other parameters fixed. For bichromatic wave with amplitude $q = 0.009$ (0.045 m in laboratory variables), breaking waves were observed. Since we are not interested in the breaking phenomenon in this thesis, this is not presented here.

Figure 4.4 shows numerical results and the corresponding direct second order approximations at $x = 10$, 80 and 160 m (from the wave maker). We note that for these comparisons we add phase constants such that at $x = 10$ m our approximations are in phase with the numerical results. At $x = 0$, which refers to the position of the wave maker, the approximations are superpositions of two monochromatic waves only. This is based on the assumption that the wave maker is controlled to produce superpositions of two modes, although in practice it is not possible to do so, see Remark 4.4.

From Figure 4.4 three observations can be made. The first is that the numerical results show that the envelope of Bichromatic 2 spatially deforms, but the envelope of Bichromatic 1 does not. The second observation is that there is a phase shift between the numerical results and the approximations for both Bichromatic 1 and Bichromatic 2. This phase shift depends on the position where the signals are measured, indicating that the direct second order is not accurate in predicting the propagation speed. Take for example Bichromatic 1; at position $x = 160$ m the phase shift is about a half wave length, that corresponds to a distance of about 3 m in the laboratory. The last observation is that the envelope of direct second order approximation does not deform as indicated by the numerical result for the Bichromatic 2.

We end this section with the following remark.

Remark 4.4 *A small discrepancy between numerical and analytical results is observed in the initial waveforms. This discrepancy is due to the following*

i) the fact that the signal is not taken at the wave maker, but at a point away from, but close to the wave maker (10 m downstream from the wave maker),

ii) there is a start-up effect in generating the realistic and numerical waves that disturbs the periodicity; see (4.28) in section 4.4.

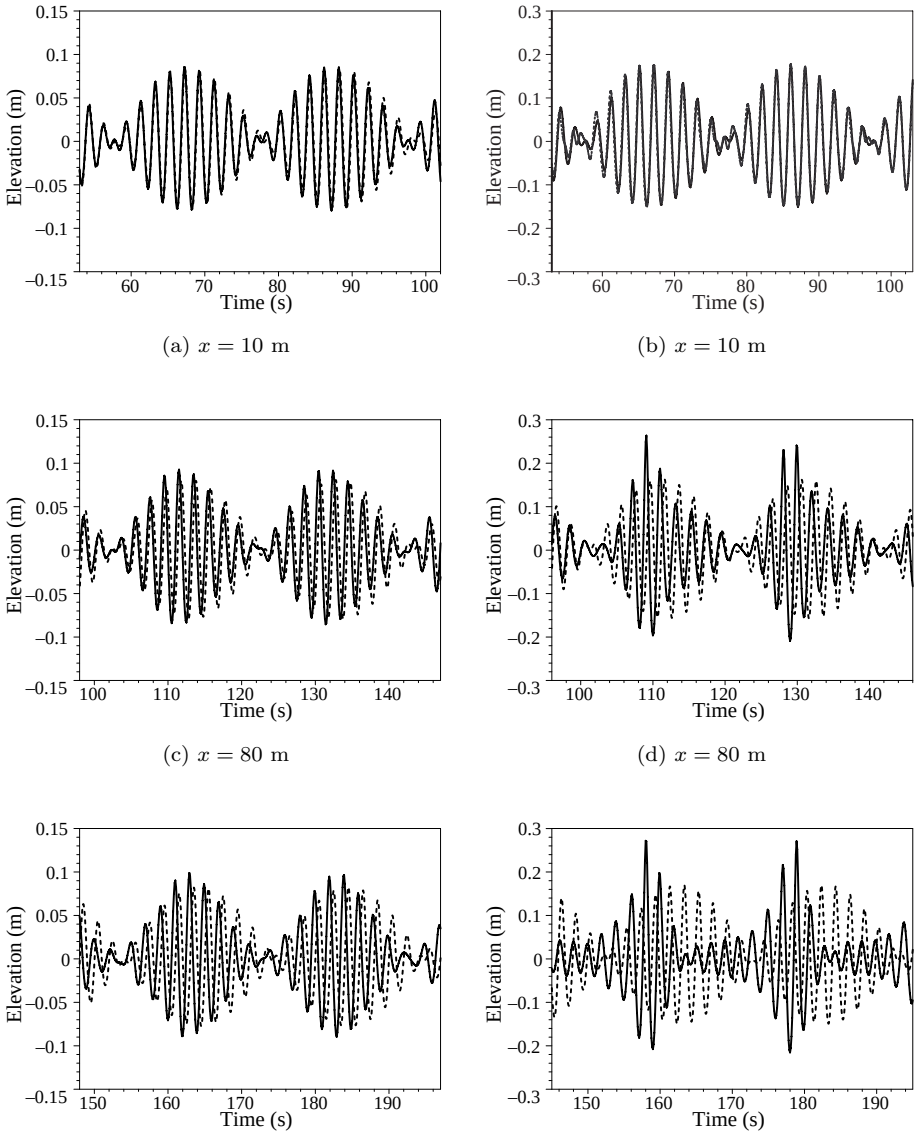

(a) $x = 10$ m (b) $x = 10$ m

(c) $x = 80$ m (d) $x = 80$ m

(e) $x = 160$ m (f) $x = 160$ m

Figure 4.4: Numerical results (solid line) and direct second order approximations (dashed line) for Bichromatic 1 (a), (c), (e) and Bichromatic 2 (b), (d), (f) measured at various positions.

4.2 Nonlinear dispersion relation

The error in propagation speed as observed in the previous section is too large for the relevant distances and times in the laboratories. This error can be explained from the resonance due to nonlinearity in the third order. The forcing $\frac{3}{2}\partial_x\left[u^{(1)}u^{(2)}\right]$ in the equation (4.8) contains a resonant term F_{res} and a non-resonant term F_{nonres},

$$\frac{3}{2}\partial_x\left[u^{(1)}u^{(2)}\right] = F_{\text{res}} + F_{\text{nonres}}.$$

In this section we will deal with this resonant term. The non-resonant term which leads to periodic solutions will be discussed in the next sections. This resonant term reads

$$F_{\text{res}} = \frac{9}{4}q^3K_{-1}(s_0+s_-+2s)e^{i\Theta_-} + \frac{9}{4}q^3K_{+1}(s_0+s_++2s)e^{i\Theta_+} + \text{c.c.}.$$

Solving (4.8) leads to

$$\begin{aligned} u^{(3)} &= -\frac{9}{4}q^3tK_{-1}(s_0+s_-+2s)e^{i\Theta_-} - \frac{9}{4}q^3tK_{+1}(s_0+s_++2s)e^{i\Theta_+} + \text{c.c.} \\ &\quad + \text{Periodic Terms.} \end{aligned}$$

This contribution to the third order linearly grows in time, which then quickly dominates the second order terms.

To prevent the growth of the solution linearly in time, we take care of the resonant term by introducing the following Ansatz

$$\begin{aligned} u(x,t) &= 2q[\cos\theta_- + \cos\theta_+] + u^{(2)} + u^{(3)} + \cdots, \\ &= \left[q\left\{e^{i\theta_-} + e^{i\theta_+}\right\} + \text{c.c}\right] + u^{(2)} + u^{(3)} + \cdots, \end{aligned} \tag{4.13}$$

where

$$\theta_\pm = k_\pm x - \omega_\pm t,$$

with

$$k_\pm = k_\pm^{(0)} + k_\pm^{(1)} + k_\pm^{(2)} + \cdots.$$

The superscripts denote the order in the perturbation parameter q as for $u^{(j)}$. Observe that now the wave number $k_\pm$ is given by a series expansion in the amplitude q. Note that the second order solution $u^{(2)}$ is different than in the previous section that will become clear later.

For the coming discussion we approximate $\Omega(k_\pm)$ with the Taylor expansion about $k_\pm^{(0)}$. This reads

$$\Omega(k_\pm) = \Omega_\pm + k_\pm^{(1)}\Omega'_\pm + \left[k_\pm^{(2)}\Omega'_\pm + \frac{1}{2}\left(k_\pm^{(1)}\right)^2\Omega''_\pm\right] + \cdots.$$

where $\Omega_\pm$ and its derivatives should be evaluated at $k_\pm^{(0)}$.

Substituting the Ansatz (4.13) into (4.1), and collecting first, second and third order terms into $A^{(1)},\ A^{(2)},\ A^{(3)}$ respectively, we have a residual

$$A^{(1)} + A^{(2)} + A^{(3)} + O(q^4),$$

where

$$A^{(1)} = qi[\{-\omega_- + \Omega(k_-^{(0)})\}e^{i\theta_-} + \{-\omega_+ + \Omega(k_+^{(0)})\}e^{i\theta_+}] + \text{c.c.}, \quad (4.14)$$

$$A^{(2)} = u_t^{(2)} + i\Omega(-i\partial_x)u^{(2)} + F^{(2)}, \quad (4.15)$$

$$A^{(3)} = u_t^{(3)} + i\Omega(-i\partial_x)u^{(3)} + F^{(3)}. \quad (4.16)$$

Before we give the expression for $F^{(j)},\ j \geq 2$ for ease of notation we will discuss $A^{(1)}$ first.

The Ansatz is a good approximation to the solution provided that the residue is small. Making the lowest order term from the residual to vanish, $A^{(1)} = 0$, we have

$$\omega_\pm = \Omega(k_\pm^{(0)}).$$

Writing this relation explicitly in the wave number gives

$$k_\pm^{(0)} = K_\pm.$$

The function $F^{(j)}$ contains resonant and non-resonant terms. We will write it in the form

$$F^{(j)} = F_{\text{res}}^{(j)} + F_{\text{nonres}}^{(j)}, \text{ for } j \geq 2.$$

$F_{\text{res}}^{(2)}$ is found by collecting the second order term from $i\Omega(-i\partial_x)u$. This gives

$$F_{\text{res}}^{(2)} = \frac{3}{2}qi\left[k_-^{(1)}\Omega'_- e^{i\theta_-} + k_+^{(1)}\Omega'_+ e^{i\theta_+}\right] + \text{c.c.}$$

The non-resonant term $F_{\text{nonres}}^{(2)}$ is given by the second order terms from the nonlinearity $\frac{3}{4}\partial_x u^2$. This reads

$$F_{\text{nonres}}^{(2)} = \frac{3}{2}qi\left[\begin{array}{l} K_- e^{2i\theta_-} + K_+ e^{2i\theta_+} + \{K_+ + K_-\}e^{i(\theta_+ + \theta_-)} \\ +\{K_+ - K_-\}e^{i(\theta_+ - \theta_-)} \end{array}\right] + \text{c.c.}$$

Observe that $A^{(2)}$ contains the resonant term $F_{\text{res}}^{(2)}$ and the non-resonant term

$$u_t^{(2)} + i\Omega(-i\partial_x)u^{(2)} + F_{\text{nonres}}^{(2)}.$$

To make the Ansatz correct up to second order, the condition $A^{(2)} = 0$ has to be satisfied. Actually a more strict condition has to be satisfied; both the resonant and non-resonant terms have to be equal to zero. This leads to

$$F_{\text{res}}^{(2)} = 0$$

and

$$u_t^{(2)} + i\Omega(-i\partial_x)u^{(2)} = -F_{\text{nonres}}^{(2)}. \quad (4.17)$$

From $F^{(2)}_{\rm res} = 0$, we have

$$k^{(1)}_{\pm} = 0.$$

The second order contribution is to be found by solving the equation (4.17) with the initial signal $u^{(2)}(0,t) = 0$. This leads to the solution $u^{(2)}$ in the form

$$u^{(2)} = u^{(2)}_{\rm bw} + u^{(2)}_{\rm free}, \tag{4.18}$$

where

$$u^{(2)}_{\rm bw} = \frac{3}{2}q^2\left[s_{-1}e^{2i\theta_{-1}} + s_{+1}e^{2i\theta_{+1}} + 2se^{i[\theta_{-1}+\theta_{+1}]} + s_0e^{i[\theta_{+1}-\theta_{-1}]}\right] + \text{c.c.} \tag{4.19}$$

and $u^{(2)}_{\rm free}$ is given in (4.12). Observe that $\Theta_{\pm 1}$ in (4.11) is replaced by $\theta_{\pm 1}$ in (4.19).

The main aim of this section is merely to prevent the growth of the third order contribution by taking care of the resonance. Therefore, we only consider $F^{(3)}_{\rm res}$ and leave $F^{(3)}_{\rm nonres}$ for the next section. After using $k^{(1)}_{\pm} = 0$, we have

$$F^{(3)}_{\rm res} = qi\left[\begin{array}{l}\left\{k^{(2)}_{-}\Omega'_{-} + \frac{9}{4}q^2K_{-}[s_0 + s_{-1} + 2s]\right\}e^{i\theta_{-}} \\ +\left\{k^{(2)}_{+}\Omega'_{+} + \frac{9}{4}q^2K_{+}[s_0 + s_{+1} + 2s]\right\}e^{i\theta_{+}}\end{array}\right] + \text{c.c.}$$

To get the Ansatz correct up to third order, the resonant and non-resonant terms have to be made to vanish. Making the resonant term vanish, we have

$$k^{(2)}_{\pm} = -\frac{9}{4}q^2\frac{K_{\pm 1}}{V_g(K_{\pm 1})}(s_0 + s_{\pm 1} + 2s) = -K_{\rm corr}(\omega_{\pm 1}).$$

This leads to the well-known nonlinear dispersion relation (NDR)

$$k(\omega_{\pm}) = k^{(0)}_{\pm} + k^{(1)}_{\pm} + k^{(2)}_{\pm} = K(\omega_{\pm}) - K_{\rm corr}(\omega_{\pm 1}).$$

Observe that this wave number correction quadratically depends on the amplitude q. In this technique we use a wave number correction, instead of a frequency correction (as mostly found in literature, for an example of monochromatic wave see [59]) for the NDR. The wave number correction is more convenient for the signaling problem.

The first order contribution of the Ansatz (4.13), which will also be written as $u^{(1)}$, is given by

$$\begin{aligned} u^{(1)} &= 2q\left[\cos\theta_{-1} + \cos\theta_{+1}\right] \\ &= 2q\left[\cos\{\Theta_{-1} - xK_{\rm corr}(\omega_{-1})\} + \cos\{\Theta_{+1} - xK_{\rm corr}(\omega_{+1})\}\right]. \end{aligned}$$

It is obvious that even though $K_{\rm corr}(\omega_{\pm})$ is small, for large x ($\sim O\left(\frac{1}{q^2}\right)$) the contribution of this wave number correction is essential. This is already mentioned in [62]. Without taking this correction into account causes the large

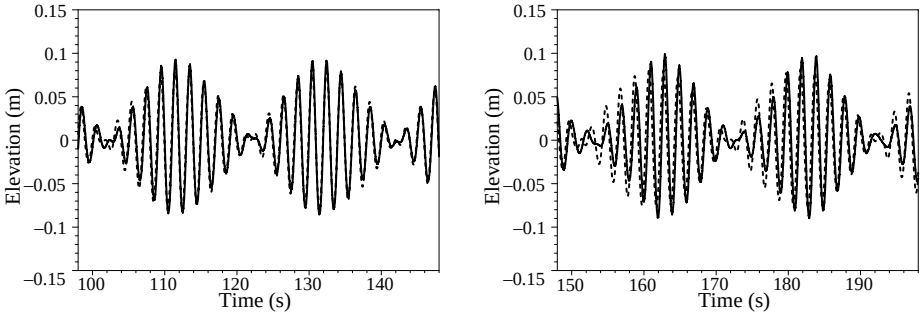

(a) Bichromatic 1 at $x = 80$ m.

(b) Bichromatic 1 at $x = 160$ m.

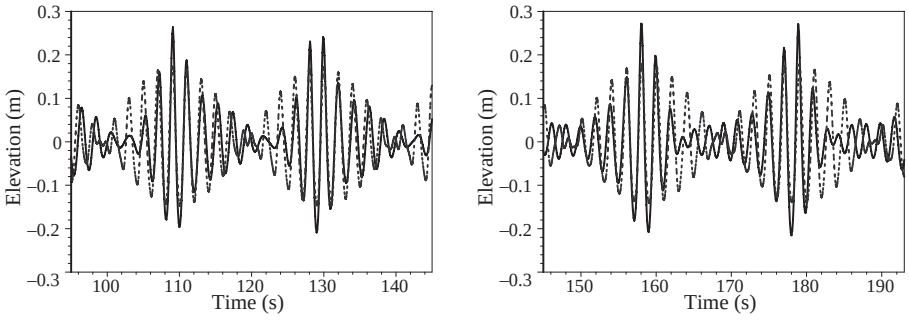

(c) Bichromatic 2 at $x = 80$ m.

(d) Bichromatic 2 at $x = 160$ m.

Figure 4.5: Numerics (solid line) and the second order approximation with NDR (dashed line) for Bichromatic 1 and Bichromatic 2.

phase shift of the carrier waves as observed in Figure 4.4. A review of resonant interactions among surface water waves, both theoretically and experimentally, was given by Hammack and Henderson in [26].

Figure 4.5 shows the numerical results and the second order approximation using the NDR for Bichromatic 1 and Bichromatic 2 evaluated at the same positions as in Figure 4.4. In this figure we observe that the phase shift in Figure 4.4 has been significantly reduced, indicating that the NDR has significantly improved the propagation speed. We also notice that this improved second order approximation is not capable to show large envelope deformations for Bichromatic 2 as indicated by the numerical result.

4.3 Third order side band contributions and large envelope deformations

The numerical results have shown that the envelope of Bichromatic 2 does deform, but our second order approximations do not. Before we proceed, we remark that the simpler amplitude equation, NLS, (see [6, 20, 22] for details of the relation between KdV & NLS) does show the amplitude increase and skew deformation qualitatively as in the numerics and experiments, see [51, 58]. Since the NLS equation is of third order nonlinearity, this becomes a motivation to proceed the analysis up to third order.

In the previous section we have made the resonant term of $A^{(3)}$ to be zero and got the NDR. In this section we include the solution that is forced by the non-resonant terms:

$$u_t^{(3)} + i\Omega(-\partial_x)u^{(3)} = -F^{(3)}_{\text{nonres}}. \tag{4.20}$$

The forcing function $F^{(3)}_{\text{nonres}}$ contains terms of high frequencies $3[\bar{\omega} \pm \nu]$, $3\bar{\omega} \pm 2\nu$ and side band frequencies $\bar{\omega} \pm 3\nu$. These terms are results from the multiplication of the first order and the second order solutions, $\frac{3}{2}\partial_x\left(u^{(1)}u^{(2)}\right)$ which do not give resonance.

In this section we will merely consider the third order contributions that are essential to the growth of the wave height. It will be clear later that these contributions are due to the terms of the forcing $F^{(3)}_{\text{nonres}}$ at the side band frequencies $\bar{\omega} \pm 3\nu$ that are found from the multiplication of the first order solution and the second order bound wave. To do that, we separate $F^{(3)}_{\text{nonres}}$ into two terms

$$F^{(3)}_{\text{nonres}} = F^{(3)}_{\nu} + F^{(3)}_{\text{non}\nu}.$$

where

$$F^{(3)}_{\nu} = q^3 i\left[b_{-3}e^{i(2\theta_+ - \theta_-)} + b_{-3}e^{i(2\theta_- - \theta_+)}\right] + \text{c.c.} \tag{4.21}$$

with

$$b_{\pm 3} = \frac{9}{4}\left(s_0 + s_\pm\right)\cdot\left(K_{\pm 1} \pm 2\kappa\right).$$

Restricting to the forcing function $F^{(3)}_{\nu}$, the third order contributions should be computed from

$$\partial_t u^{(3)}_{\nu} + i\Omega(-\partial_x)u^{(3)}_{\nu} = -F^{(3)}_{\nu}. \tag{4.22}$$

In the following discussion we will show that this equation yields a third order solution that infinitely grows as $\kappa \to 0$. Before proceeding, we make a remark.

Remark 4.5 *The third order contribution due to the forcing $F^{(3)}_{non\nu}$ on the equation*

$$\xi_t + i\Omega(-\partial_x)\xi = -F^{(3)}_{non\nu} \tag{4.23}$$

is of order q^3 and remains bounded as $\kappa \to 0$.

The proof of this remark is actually rather simple, even though it involves many terms that seem complicated. To prove this remark we start with writing $F^{(3)}_{\text{non}\nu}$

$$F^{(3)}_{\text{non}\nu} = \frac{9}{4}q^3 i \left[\begin{array}{l} s_- e^{3i\theta_-} + s_+ e^{3i\theta_+} + [s_- + s]e^{i[2\theta_- + \theta_+]} + [s_+ + s]e^{i[2\theta_+ + \theta_-]} \\ + s_- e^{i[\Theta(2\omega_{-1})+\theta_-]} + s_+ e^{i[\Theta(2\omega_{+1})+\theta_+]} + s_- e^{i[\Theta(2\omega_{-1})+\theta_+]} + \\ s_+ e^{i[\Theta(2\omega_{+1})+\theta_-]} + s e^{i[\Theta(\omega_{-1}+\omega_{+1})+\theta_-]} + s e^{i[\Theta(\omega_{-1}+\omega_{+1})+\theta_+]} \\ + s_- e^{i[\Theta(2\omega_{-1})-\theta_-]} + s_+ e^{i[\Theta(2\omega_{+1})-\theta_+]} + s_- e^{i[\Theta(2\omega_{-1})-\theta_+]} + \\ s_+ e^{i[\Theta(2\omega_{+1})-\theta_-]} + s e^{i[\Theta(\omega_{-1}+\omega_{+1})-\theta_-]} + s e^{i[\Theta(\omega_{-1}+\omega_{+1})-\theta_+]} \\ + s_0 e^{i[\Theta(\omega_{+1}-\omega_{-1})+\theta_-]} + s_0 e^{i[\Theta(\omega_{-1}-\omega_{+1})+\theta_+]} \end{array} \right] + \text{c.c.}$$

The terms contain $e^{i[\Theta(2\omega_{\pm 1})-\theta_\pm]}$ and $e^{i[\Theta(\pm\{\omega_{+1}-\omega_{-1}\})\pm\theta_\pm]}$ seem like resonant terms, but they are not, since they do not satisfy the dispersion relation.

It is already shown in section 4.1 that s_0, s and $s_\pm$ are bounded, even for $\kappa \to 0$. Hence, for this limiting case $F^{(3)}_{\text{non}\nu}$ is also bounded, and moreover, $F^{(3)}_{\text{non}\nu} = O(q^3)$. We now prove that $\xi(x,t)$ that satisfies (4.23) is also bounded and of order q^3. To do so, we take an example for the forcing term

$$\frac{9}{4}q^3 i s e^{i[\Theta(\omega_{-1}+\omega_{+1})-\theta_-]},$$

but leave the rest terms which can be done in a similar way. Consider

$$\zeta_t + i\Omega(-i\partial_x)\zeta = -\frac{9}{4}q^3 i s e^{i[\Theta(\omega_{-1}+\omega_{+1})-\theta_-]}.$$

The solution reads

$$\zeta = \frac{9}{4}q^3 \frac{s}{\omega_{+1} - \Omega(K(\omega_{-1}+\omega_{+1}) - K(\omega_{-1}))} e^{i[\Theta(\omega_{-1}+\omega_{+1})-\theta_-]}.$$

Observe that for $\kappa \to 0$, we have

$$\frac{s}{\omega_{+1} - \Omega(K(\omega_{-1}+\omega_{+1}) - K(\omega_{-1}))} \to \frac{\sigma_2}{\bar{\omega} - \Omega(K(2\bar{\omega}) - K(\bar{\omega}))},$$

and $\bar{\omega} - \Omega(K(2\bar{\omega}) - K(\bar{\omega})) \neq 0$. This will clearly be shown in a schematic plot in k,ω-plane, see Figure 4.6. In this figure it is clearly seen that $K(\bar{\omega}) \neq K(2\bar{\omega}) - K(\bar{\omega})$, since $K(\omega)$ is a convex (or $\Omega(k)$ is a concave) function. Hence, we have shown that ζ is bounded and of order q^3. Applying a similar way to solve (4.23), by considering all terms of $F^{(3)}_{\text{non}\nu}$, will complete the proof of Remark 4.5.

Solving (4.22) with the initial signal $u^{(3)}(0,t) = 0$ leads to the solution

$$u^{(3)}_\nu = u^{(3)}_{\text{sb}} + u^{(3)}_{\text{free}}. \tag{4.24}$$

where

$$\begin{aligned} u^{(3)}_{\text{sb}} &= q^3 \left[a_{+3} e^{i(2\theta_+ - \theta_-)} + a_{-3} e^{i(2\theta_- - \theta_+)} \right] + \text{c.c.} \\ &= 2q^3 \left[a_{+3} \cos(2\theta_+ - \theta_-) + a_{-3} \cos(2\theta_- - \theta_+) \right] \end{aligned} \tag{4.25}$$

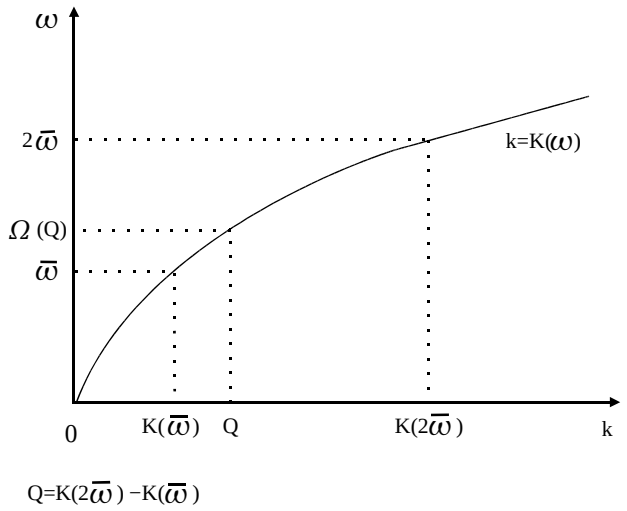

Figure 4.6: Schematic plot of the dispersion relation. Concavity of Ω implies that $\bar{\omega} - \Omega(K(2\bar{\omega}) - K(\bar{\omega})) \neq 0$.

and

$$u_{\text{free}}^{(3)} = -2q^3 \left[a_{+3} \cos\Theta(\bar{\omega} + 3\nu) + a_{-3} \cos\Theta(\bar{\omega} - 3\nu)\right]. \tag{4.26}$$

The third order side band transfer functions $a_\pm$ are given by

$$a_{\pm 3} = \frac{9}{4}(s_0 + s_\pm)\frac{K_{\pm 1} \pm 2\kappa}{\bar{\omega} \pm 3\nu - \Omega(K_{\pm 1} \pm 2\kappa)}.$$

Since for the water wave problem $\Omega'' \neq 0$, we observe that in the limit $\kappa \to 0$, we have

$$a_{\pm 3} \sim \frac{-\gamma}{2\kappa^2\Omega'' \pm \frac{4}{3}\kappa^3\Omega'''},$$

where $\gamma = \frac{9}{4}(\sigma_0 + \sigma_2)$. Obviously, the third order side band transfer functions $a_{\pm 3}$ are unbounded, $O\left(\frac{1}{\kappa^2}\right)$ as $\kappa \to 0$. It is now convenient to introduce $\alpha_{\pm 3} = \kappa^2 a_{\pm 3}$ and $\beta_{\pm 3} = \alpha_{+3} \pm \alpha_{-3}$, hence $\beta_{+3} \sim \frac{-\gamma}{\Omega''}, \beta_{-3} \sim \frac{\gamma\Omega'''}{\Omega''^2}\kappa$, and get

$$\begin{aligned} u_{\text{sb}}^{(3)} &= 2q\left(\frac{q}{\kappa}\right)^2 \left[\alpha_{+3}\cos(2\theta_+ - \theta_-) + \alpha_{-3}\cos(2\theta_- - \theta_+)\right] \\ &= q\left(\frac{q}{\kappa}\right)^2 \left[\beta_{+3}\cos\bar{\theta}\cdot\cos(3\cdot\Delta\theta) + \beta_{-3}\sin\bar{\theta}\cdot\sin(3\cdot\Delta\theta)\right] \end{aligned}$$

where $\bar{\theta} = \frac{\theta_+ + \theta_-}{2}$ and $\Delta\theta = \frac{\theta_+ - \theta_-}{2}$. A schematic plot of the third order side band contributions is presented in Figure 4.7. Note that third order contributions at higher frequencies are neglected here.

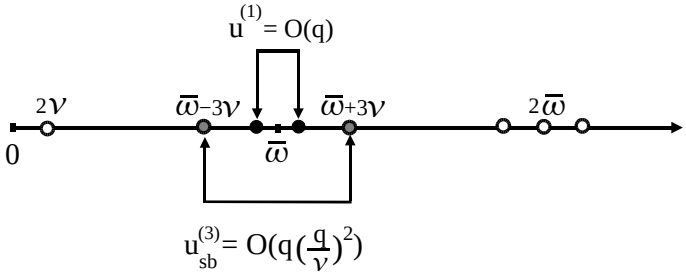

Figure 4.7: Schematic plot of the first order, second order and third order side band contributions in the frequency domain.

Summarising so far, the first order and third order side band contributions together can be written like

$$\begin{aligned} u^{(1)} + u^{(3)}_{\rm sb} &= q\cos\bar{\theta}\left(4\cos\Delta\theta + \left(\frac{q}{\kappa}\right)^2 \beta_{+3}\cos(3\cdot\Delta\theta)\right) \\ &\quad + q\left(\frac{q}{\kappa}\right)^2 \beta_{-3}\sin\bar{\theta}\cdot\sin(3\cdot\Delta\theta). \end{aligned}$$

The effect of the side band contributions is clearly seen:

- the carrier wave $\cos\bar{\theta}$ is modulated by the linear modulation $4\cos\Delta\theta$ and a triple periodic contribution $\left(\frac{q}{\kappa}\right)^2 \beta_{+3}\cos(3\cdot\Delta\theta)$; the amplitude of this last contribution may become substantial for small κ;
- in addition, the signal contains a contribution from the out-of phase carrier wave that is modulated by a same triple periodic function. This last effect, is proportional to $q^2\Omega'''(K(\bar{\omega}))/\kappa$; since (for the surface wave problem) $\Omega'''(\bar{\omega}) \neq 0$ this term will cause skew-symmetric distortions of the envelope.

Figure 4.8 shows the third order side band approximation

$$u(x,t) = u^{(1)} + u^{(2)}_{\rm bw} + u^{(3)}_{\rm sb} + u^{(2)}_{\rm free} + u^{(3)}_{\rm free}, \tag{4.27}$$

and the five components of Bichromatic 2 at $x = 80$ m. We note that all parameters are in laboratory quantities. In Figure 4.8 (b) we observe that the lowest order component $u^{(1)}$ is a sinusoidally shaped wave group with wave height of 32 cm. The contributions of $u^{(2)}_{\rm bw}$ and $u^{(2)}_{\rm free}$ are about 2.5 cm, small compared to $u^{(1)}$. The component $u^{(2)}$ reveals a beat pattern that steepens downward due to the subharmonic bound wave (see Figure 4.8 (c)). The second order free waves $u^{(2)}_{\rm free}$, which are composed of four modes that travel with their

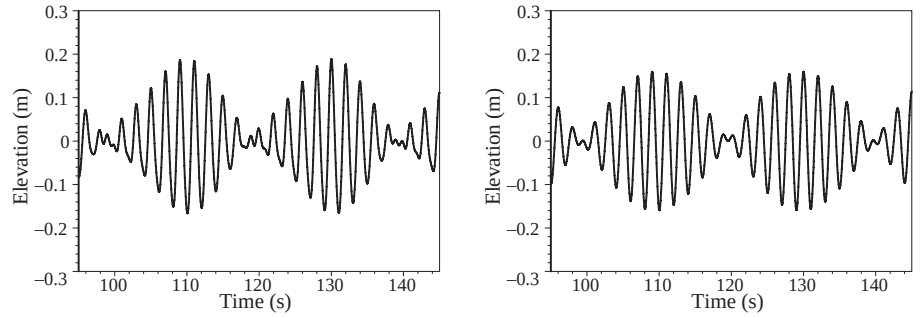

(a) Third order side band solution u

(b) First order contribution $u^{(1)}$

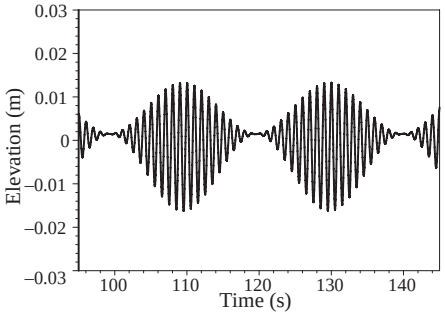

(c) Second order contribution $u^{(2)}$

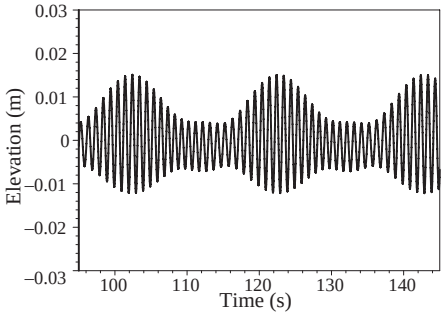

(d) Second order free wave $u^{(2)}_{\text{free}}$

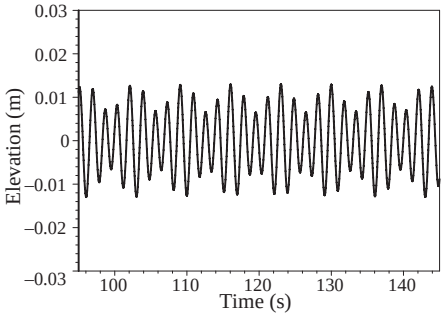

(e) Third order side contribution $u^{(3)}_{\text{sb}}$

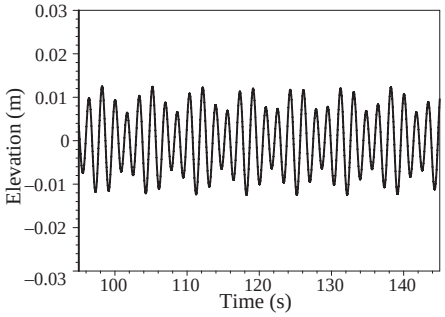

(f) Third order free wave $u^{(3)}_{\text{free}}$

Figure 4.8: The third order side band approximation consisting of the five components: the first order, second order and third order side band contributions. For this case of Bichromatic 2, at the position $x = 80$ m, the axes (in laboratory variables) are elevation in m (vertical) and time in s (horizontal).

own speeds, show a complex interference pattern (Figure 4.8 (d)). The wave height of $u_{\text{sb}}^{(3)}$ and $u_{\text{free}}^{(3)}$ are about 2.5 cm, that is as dominant as the second order solution, see Figure 4.8 (e) and (f). The sum of these five components results in a complex pattern of wave group in 4.8 (a).

In Figure 4.9, we plot the third order side band approximation (4.27) and the numerical result for Bichromatic 2. In this figure we observe that the envelope deforms as a result of the third order side band approximation. The carrier waves of the numerical result and the approximation are in phase for large 'amplitudes', the most important part of this evolution. For small amplitudes, however, the phases differ. An asymmetry of the third order side band approximation during the evolution is observed, even though it is not as strong as the numerical result. The inadequateness in predicting this asymmetry is due to the start-up effect in generating bichromatic waves numerically and experimentally. This start-up effect disturbs the periodicity of the wave groups. Mathematically speaking, this start-up effect modifies the initial signal to be

$$u(0,t) = 2q\left[\cos(\omega_{-1}t) + \cos(\omega_{+1}t)\right] \cdot f(t) \tag{4.28}$$

at the wave generator. In the numerics the function f is given by

$$f(t) = \begin{cases} 0 & \text{for } t \leq 0, \\ t/\tau, & \text{for } 0 < t < \tau, \\ 1, & \text{for } t \geq \tau. \end{cases}$$

An approximate solution composed by 'many' frequencies should be considered to deal with a start-up effect in the initial signal. This will be discussed in the next chapter.

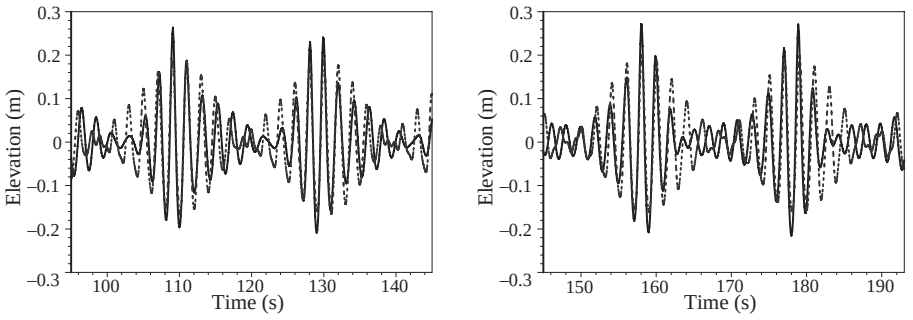

(a) $x = 80$ m (b) $x = 160$ m

Figure 4.9: Numerics (solid line) and the corresponding third order side band approximation (dashed line) for Bichromatic 2.

Before we end this section, we make a remark on the spatial recurrence due to the phase velocity difference between the third order side band bound wave and free wave.

Remark 4.6 *Neglecting the wave number correction in the side band contribution,* $u_{\rm sb}^{(3)}$ *can be written as*

$$u_{\rm sb}^{(3)} = q\left(\frac{q}{\kappa}\right)^2 \left[\begin{array}{l} \beta_{+3}\cos 3[\kappa x-\nu t]\cos[\bar{k}x-\bar{\omega}t]+ \\ \beta_{-3}\sin 3[\kappa x-\nu t]\sin[\bar{k}x-\bar{\omega}t] \end{array} \right].$$

On the other hand, $u_{\rm free}^{(3)}$ *may be approximated in the form*

$$u_{\rm free}^{(3)} = -q\left(\frac{q}{\kappa}\right)^2 \left[\begin{array}{l} \beta_{+3}\cos 3[\kappa x-\nu t]\cos[\bar{k}x-\bar{\omega}t+4K''\nu^2 x]+ \\ \beta_{-3}\sin 3[\kappa x-\nu t]\sin[\bar{k}x-\bar{\omega}t+4K''\nu^2 x] \end{array} \right].$$

Observe the x-dependent shift of the carrier wave that is different from the that of the $u_{\rm sb}^{(3)}$*. The interference of the bound and the free third order carrier waves determines the spatial recurrence length of the solution, given by* $4K''\nu^2 X_{recurr} = 2\pi$*, i.e.*

$$X_{recurr} = \frac{\pi}{2K''\nu^2}. \tag{4.29}$$

In the case of Bichromatic 2 above $X_{recurr} = 63.3$ that corresponds to about 315 m in the laboratory. This recurrence length is found correct compared with numerical calculation.

4.4 Two wave interactions

We have presented the evolution of bichromatic wave groups as a result from the interactions of two modes with the same amplitudes. When dealing with irregular waves, many modes are involved, and in general they have different amplitudes. In this section we discuss two wave interactions in which the amplitudes of wave components are different. To start with, we consider an initial signal given by

$$\begin{aligned} u(0,t) &= 2(q+q_1)\cos(\bar{\omega}-\nu)t + 2q\cos(\bar{\omega}+\nu)t, \\ &= (q+q_1)e^{i(\bar{\omega}-\nu)t} + qe^{i\bar{\omega}+\nu)t} + \text{c.c.} \end{aligned} \tag{4.30}$$

The parameter q_1 is not necessarily small compared to q. This initial signal can be written in the form

$$u(0,t) = 2[2q+q_1]\cos\nu\cos\bar{\omega} - 2q_1\sin\nu\sin\bar{\omega}.$$

Observe that in the preceding sections we restricted our discussion to the case $q_1 = 0$, we only considered an initial signal without an out-of-phase contribution $2q_1\sin\nu\sin\bar{\omega}$.

We now look for the solution $u(x,t)$ of the equation (4.1) with the initial signal (4.30). Since the third order side band contribution is essential for small

difference of wave numbers (frequencies), in this section we consider an approximation for $u(x,t)$ by taking components up to third order side band into account. Following the preceding sections the first order contribution reads

$$\begin{aligned} u^{(1)} &= 2(q+q_1)\cos\theta_{-1} + 2q\cos\theta_{+1}, \\ &= (q+q_1)e^{i\theta_{-1}} + qe^{i\theta_{+1}} + \text{c.c.} \end{aligned} \tag{4.31}$$

where

$$\theta_{\pm 1} = \Theta_{\pm 1} - xK^{\pm}_{\text{corr}}.$$

The wave number correction $K^{\pm}_{\text{corr}}$ is slightly different than in the previous section due to the difference in the component amplitudes. This correction reads

$$K^{\pm}_{\text{corr}} = \frac{9}{4}\frac{K_{\pm 1}}{V_g(K_{\pm 1})}(q^2_{\pm}s_{\pm 1} + q^2_{\mp}(s_0+2s))$$

where

$$q_- = q + q_1 \text{ and } q_+ = q.$$

The term with $s_{\pm 1}$ accounts for the correction of the wave number $k_{\pm}$ from the nonlinear interaction of the wave component $\omega_{\pm}$ with itself, while the term with (s_0+2s) is the contribution in $k_{\pm}$ by the nonlinear interaction of the wave component with frequency $\omega_{\pm}$ and $\omega_{\mp}$.

Writing the first order contribution in a carrier wave modulated by an envelope, we have

$$u^{(1)} = 2[2q+q_1]\cos\Delta\theta\cdot\cos\bar{\theta} - 2q_1\sin\Delta\theta\cdot\sin\bar{\theta}.$$

Observe that it is different than in the preceding sections; i.e. the first order solution already contains a contribution of out-of-phase carrier wave $\sin\bar{\theta}$ modulated by $2q_1\sin\Delta\theta$.

The corresponding second order solution is given by

$$u^{(2)} = u^{(2)}_{\text{bw}} + u^{(2)}_{\text{free}}$$

with

$$u^{(2)}_{\text{bw}} = \frac{3}{2}\left[\begin{array}{l} q^2_- s_{-1}e^{2i\theta_{-1}} + q^2_+ s_{+1}e^{2i\theta_{+1}} + 2q_-q_+ se^{i[\theta_{-1}+\theta_{+1}]} \\ +q_-q_+s_0e^{i[\theta_{+1}-\theta_{-1}]} \end{array}\right] + \text{c.c.} \tag{4.32}$$

and

$$u^{(2)}_{\text{free}} = -\frac{3}{2}\left[\begin{array}{l} q^2_- s_{-1}e^{i\Theta(2\omega_{-1})} + q^2_+ s_{+1}e^{i\Theta(2\omega_{+1})} + \\ 2q_-q_+se^{i\Theta(2\bar{\omega})} + q_-q_+s_0e^{i\Theta(2\nu)} \end{array}\right] + \text{c.c.} \tag{4.33}$$

The third order side band contribution has the form

$$u^{(3)}_{\text{sb}} = u^{(3)}_{\text{bw}} + u^{(3)}_{\text{free}}.$$

The terms $u^{(3)}_{\text{bw}}$ and $u^{(3)}_{\text{free}}$ are given by

$$\begin{aligned} u^{(3)}_{\text{sb}} &= \left[q^2_+q_-a_{+3}e^{i(2\theta_+-\theta_-)} + q_+q^2_-a_{-3}e^{i(2\theta_--\theta_+)}\right] + \text{c.c.} \\ &= 2\left[q^2_+q_-a_{+3}\cos(2\theta_+-\theta_-) + q_+q^2_-a_{-3}\cos(2\theta_--\theta_+)\right] \end{aligned} \tag{4.34}$$

Parameter	Value	Parameter	Value
$\bar{\omega}$	2.2500	q	0.0040
k	5.0692	q_1	0.0120
ν	0.0786	q_-	0.0160
κ	0.3533	q_+	0.0040

Table 4.2: Parameter data for the initial signal in Figure 4.10 (a). These parameters are in normalised variables.

and

$$u^{(3)}_{\text{free}} = -2\left[q_+^2 q_- a_{+3}\cos\Theta(\bar{\omega}+3\nu) + q_+ q_-^2 a_{-3}\cos\Theta(\bar{\omega}-3\nu)\right]. \qquad (4.35)$$

It will be easier to understand the contribution of $u^{(3)}_{\text{bw}}$ by writing it in the form

$$\begin{aligned}
u^{(3)}_{\text{bw}} &= 2qq_1(q+q_1)a_{-3}\cos[2\theta_{-1}-\theta_{+1}] \\
&\quad +2q^2(q+q_1)\left[a_{-3}\cos[2\theta_{-1}-\theta_{+1}] + a_{+3}\cos[2\theta_{+1}-\theta_{-1}]\right], \\
&= 2qq_1(q+q_1)a_{-3}\left[\cos\bar{\theta}\cdot\cos(3\cdot\Delta\theta) + \sin\bar{\theta}\cdot\sin(3\cdot\Delta\theta)\right] \\
&\quad +2\left(\frac{q}{\kappa}\right)^2(q+q_1)\left[\beta_{+3}\cos\bar{\theta}\cdot\cos(3\cdot\Delta\theta) + \beta_{-3}\sin\bar{\theta}\cdot\sin(3\cdot\Delta\theta)\right] \\
&= 2\left[qq_1(q+q_1)a_{-3} + \left(\frac{q}{\kappa}\right)^2(q+q_1)\beta_{+3}\right]\cos\bar{\theta}\cdot\cos(3\cdot\Delta\theta) \\
&\quad +2\left[qq_1(q+q_1)a_{-3} + \left(\frac{q}{\kappa}\right)^2(q+q_1)\beta_{-3}\right]\sin\bar{\theta}\cdot\sin(3\cdot\Delta\theta).
\end{aligned}$$

Hence,

$$\begin{aligned}
u^{(1)} + u^{(3)}_{\text{bw}} &= 2\left[\begin{array}{l}\{2q+q_1\}\cos(\Delta\theta) \quad + \\ \left\{qq_1(q+q_1)a_{-3} + \left(\frac{q}{\kappa}\right)^2(q+q_1)\beta_{+3}\right\}\cos(3\cdot\Delta\theta)\end{array}\right]\cos\bar{\theta} \\
&\quad +2\left[\begin{array}{l}q_1\sin(\Delta\theta) \quad + \\ \left\{qq_1(q+q_1)a_{-3} + \left(\frac{q}{\kappa}\right)^2(q+q_1)\beta_{-3}\right\}\sin(3\cdot\Delta\theta)\end{array}\right]\sin\bar{\theta}.
\end{aligned}$$

As an example, we take an initial signal with parameters (in normalised quantities) given in table 4.2. The initial profile is plotted in Figure 4.10 (a) (on the following page).

The evolution of this wave according to the third order side band approximation is given in Figure 4.10. In this figure we present some signals taken at several positions x equals to 0, 0.13, 0.34, 0.66, 0.87 and 1 times the recurrence length, X_{recurr}. The recurrence length is computed using (4.29) that gives $X_{\text{recurr}} = 125$. At $x = 0.13X_{\text{recurr}}$ we observe that the wave envelope starts growing, showing asymmetry, the wave groups lean forward. The wave height continues to increase and the asymmetry of the envelope is clearly observed at $x = 0.34X_{\text{recurr}}$.

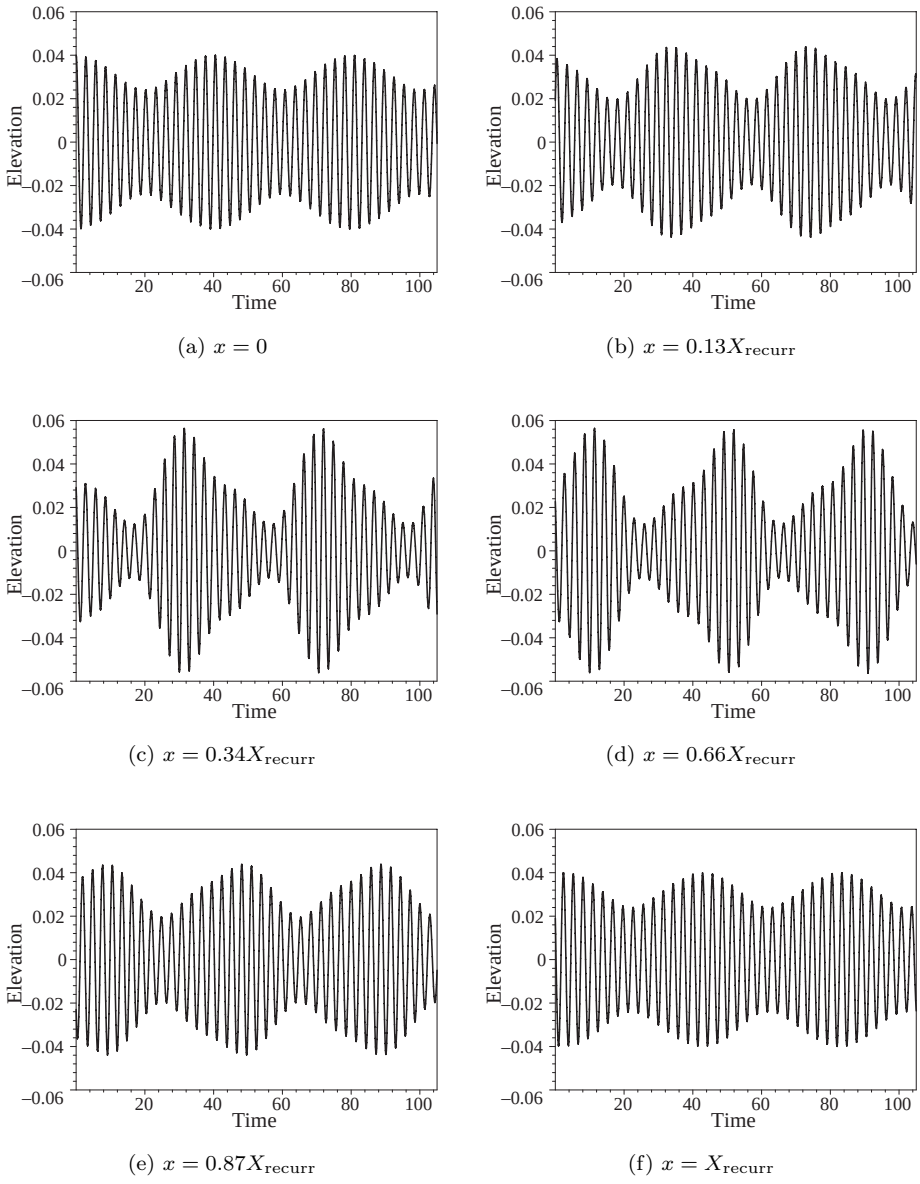

(a) $x = 0$

(b) $x = 0.13X_{\mathrm{recurr}}$

(c) $x = 0.34X_{\mathrm{recurr}}$

(d) $x = 0.66X_{\mathrm{recurr}}$

(e) $x = 0.87X_{\mathrm{recurr}}$

(f) $x = X_{\mathrm{recurr}}$

Figure 4.10: The evolution of two waves of different component amplitudes. For this example, the wave parameters are given in Table 4.2, and the recurrence length is $X_{\mathrm{recurr}} = 125$.

The increase of the wave height at this point is approximately 50 % of the initial signal. The inverse phenomenon of the feature at $x = 0.34X_{\text{recurr}}$ is observed at $x = 0.66X_{\text{recurr}}$. At this point the envelope is asymmetric, but on the opposite side of the envelope in Figure 4.10 (b), the wave groups lean backward. At $x = 0.87X_{\text{recurr}}$ the wave indicates the inverse phenomenon of the signal at $x = 0.13X_{\text{recurr}}$. Finally, the wave group envelope is back to its initial shape at $x = X_{\text{recurr}}$.

4.5 Conclusions

In this chapter we have investigated the evolutions of two classes of bichromatic waves: a class of bichromatic waves that show large envelope deformations and a class of bichromatic waves that do not reveal large envelope deformations. An example of the former is Bichromatic 2, while Bichromatic 1 is an example of the latter.

We have considered wave evolutions in long wave tanks. For such evolutions the linear dispersion relation is not accurate in predicting the propagation speed. This inaccuracy has been significantly reduced by introducing a nonlinear dispersion relation, that is obtained by taking care of the resonance in the third order. The second order approximations, even though with the nonlinear dispersion relation, do not show large envelope deformations as indicated by direct numerical simulations and experiments. Hence, the second order theory with the nonlinear dispersion relation yields a good approximation for bichromatic waves without large envelope deformations.

Based only on Bichromatic 1 and Bichromatic 2 examples, one may come to the conclusion that the amplitude is responsible for the envelope distortion. In this chapter this distortion, however, has been explained from the third order side band contributions. These contributions become essential if the quotient of the amplitude and the wave number difference is large. Hence, the wave number difference turns out to be the additional parameter to the amplitude that are responsible to the large envelope deformations.

The third order contributions contain two components: bound waves and free waves. The free waves propagate with different velocity than the bound waves. At $x = 0$, these components cancel each other, since the presence of the free waves are to make the approximation satisfy the initial signal. Starting from $x = 0$, the velocity difference spatially develops side band contributions to the measured signal causing modulation-demodulation phenomenon.

We have also investigated two wave interactions of different amplitudes. We have shown that large envelope deformations have also been observed when the quotient of the amplitude(s) and the wave number difference is large. When dealing with irregular waves, one actually deals with many wave interactions. In the case that there are exist some wave components that give large quotients of amplitudes and wave number differences, large increment of wave height

can happen at some positions and at certain time. In offshore engineering applications the presence of those very 'large' waves can cause the so-called ringing phenomenon, i.e. the large amplification in few cycles of response of the structure at its natural frequency, see [11, 24]. The ringing phenomenon has been observed both experimentally in the laboratory [10] and in the field situation [33].

Chapter 5

Analytical Wave Codes

In this chapter we present several versions of analytical wave codes (of increasing complexity and accuracy) to predict wave evolutions from one point measurements in a laboratory wave tank. The waves to be predicted are determined by a prescribed signal at a point of measurement somewhere in the tank. In the laboratories, ship or offshore structure models are positioned or sailing for testing their performance in the presence of waves. The prescribed signals resemble the measurements in seas or oceans (on a laboratory scale) where the real ships or offshore structures will be operated.

As a model, we consider the mKdV equation we have used in the previous chapter. For convenience, we write again this equation

$$u_t + i\Omega(-i\partial_x)u + \frac{3}{4}\partial_x u^2 = 0. \tag{5.1}$$

5.1 Mathematical interpretations of signals obtained from measurements

In this section we recall Remark 3.1 and discuss how we will proceed for given signals in the laboratories. In a practical situation, we deal with signals that were measured, 'given' only for a finite time interval, say

$$s(t), \text{ for } t \in [0, T].$$

Then, in principle there are two ways to continue the mathematical reasoning. First, extend the signal by zero outside the given time-interval. This leads to a square integrable function

$$s_0 = \begin{cases} s(t), & t \in [0, T] \\ 0, & t \notin [0, T]. \end{cases}$$

Second, make a T-periodic continuation of the signal, and use Fourier series:

$$s(t) = \sum_m \hat{s}_m e^{-i\omega_m t}, \tag{5.2}$$

where

$$\omega_m = \frac{2\pi}{T} \cdot m \quad \text{and} \quad \hat{s}_m = \frac{1}{T} \int_0^T s(t) e^{i\omega_m t} dt. \tag{5.3}$$

Theoretically, the sum should be taken for $m = -\infty$ to ∞. In practice, however, the signal is evaluated at a finite number of points, say $2M$. In this chapter we merely consider the periodic case, and the sum in (5.2) is only taken for $m = -M, \cdots, M$ by assuming that $\omega_m = 0$ for all m where $|m| > M$. Moreover, since $s(t)$ is a real function, we have

$$\hat{s}_{-m} = \overline{\hat{s}_m},$$

where the over-line denotes the complex conjugate. Taking the still water level to be zero, we have $\hat{s}_0 = 0$. From now on the amplitude coefficient with subscript 0 will be left out.

5.2 Direct second order approximations

In this section we look for an approximate solution of the mKdV equation (5.1) up to second order in amplitude somewhat similar to what we have discussed in the previous chapter. However, there will be some differences that will become clear throughout the discussion below. We start with applying a perturbation method and write u as a series expansion in the form

$$u = u^{(1)} + u^{(2)} + u^{(3)} + \cdots. \tag{5.4}$$

The superscripts denote the order in amplitude. On substituting (5.4) into (5.1) the equations for $u^{(1)}$ and $u^{(2)}$ read

$$u_t^{(1)} + i\Omega(-i\partial_x)u^{(1)} = 0, \tag{5.5}$$

and

$$u_t^{(2)} + i\Omega(-i\partial_x)u^{(2)} + \frac{3}{4}\partial_x \left[u^{(1)}\right]^2 = 0. \tag{5.6}$$

In this section we consider a direct second order approximation

$$u(x,t) = u^{(1)} + u^{(2)}, \tag{5.7}$$

where $u^{(1)}$ and $u^{(2)}$ are to be computed from (5.5) and (5.6), respectively.

5.2.1 Solution for wave interactions

The aim is to find a solution of (5.5) that consists of many discrete frequencies. This lowest order solution reads

$$u^{(1)} = \sum_m a_m e^{i[K_m x - \omega_m t]}, \tag{5.8}$$

with $K_m = K(\omega_m)$ that satisfies the dispersion relation. The complex amplitudes a_m's should be determined later. Note that even though $u^{(1)}$ is a linear solution, the presence of modes composed of many frequencies may cause a complex interference phenomenon during the evolution. Such waves are often called, in laboratory vocabulary, *irregular*.

On substituting (5.8) into (5.6), and solving for $u^{(2)}$, we have the corresponding second order contribution in the form

$$u^{(2)} = \frac{3}{4} \sum_{m,n,m+n\neq 0} a_m a_n \Gamma_2(\omega_m + \omega_n, \omega_n) e^{i[\{K_m+K_n\}x - \{\omega_m+\omega_n\}t]}, \tag{5.9}$$

where

$$\Gamma_2(\omega, \sigma) = \frac{K(\sigma) + K(\omega - \sigma)}{\omega - \Omega(K(\sigma) + K(\omega - \sigma))}. \tag{5.10}$$

This second order transfer function $\Gamma_2(\omega, \sigma)$, mathematically speaking, is the multiplication factor from nonlinear interactions of modes σ and $\omega - \sigma$ that produce a wave with frequency ω. From the concavity of Ω (or the convexity of K), $\Gamma_2(\omega, \sigma)$ is not singular for $\sigma \neq 0$ and $\sigma \neq \omega$. This means that there is no resonance in second order.

The second order contribution (5.9) is real, provided that the lowest order component $u^{(1)}$ is real. This can be easily proved by using the fact that

$$\Gamma_2(-\omega, -\sigma) = \Gamma_2(\omega, \sigma), \text{ and } \Gamma_2(\omega, \omega - \sigma) = \Gamma_2(\omega, \sigma),$$

and then, showing that

$$B(-m, -n) = \overline{B(m, n)},$$

where

$$B(m, n) = a_m a_n \Gamma_2(\omega_m + \omega_n, \omega_n) e^{i[\{K_m+K_n\}x - \{\omega_m+\omega_n\}t]}.$$

Observe that terms $e^{i[\{K_m+K_n\}x - \{\omega_m+\omega_n\}t]}$ with $m + n = 0$ are not present in (5.9). This means that $u^{(2)}$ does not contain a non-zero constant term (the equilibrium level is unchanged).

We remark that there is no restriction in the spectra for the solutions obtained using the perturbation technique above. This means that these solutions are applicable for narrow-banded as well as for broad-banded spectra. Hence, these are more general than the solutions of the NLS equation that are only valid for narrow-banded spectra, see chapter 3 for the details of this restriction for the NLS equation.

5.2.2 Determination of free and bound wave contributions from one point measurement

When waves, being generated in the laboratory, evolve freely, nonlinear interactions will take place. At any position away from the generators, the wave field is composed of free and bound waves. With the expression given above, it is possible to determine these separate contributions in the following way. Let at a certain point in the tank, without restriction of generality, say at $x = 0$, the wave be described by a signal $s(t)$. At this point the wave elevation u should satisfy $s(t) = u(x = 0, t)$. This leads in second order to

$$a_m + \frac{3}{4} \sum_{p+n=m} a_p a_n \Gamma_2(\omega_p + \omega_n, \omega_n) = \hat{s}_m, \text{ for } |m| = 1, \cdots, M. \tag{5.11}$$

Solving up to the relevant second order for a_m, we get the following explicit result

$$a_m = \hat{s}_m - \frac{3}{4} \sum_{p+n=m} \hat{s}_p \hat{s}_n \Gamma_2(\omega_p + \omega_n, \omega_n), \text{ for } |m| = 1, \cdots, M. \tag{5.12}$$

It should be remarked that this explicit solution avoids the use of an iteration procedure applied in [48, 63].

Observe that $u(x = 0, t)$ contains terms $e^{-i[\omega_p + \omega_n]t}$ with $\omega_p + \omega_n > \omega_M$, the highest frequency of $s(t)$. The presence of these terms cause the so-called *aliasing phenomenon*, i.e. a phenomenon of falsely translating spectral components outside the frequency range $[-\omega_M, \omega_M]$ into that range. The largest frequency, ω_M, is called the *Nyquist* critical frequency. The details can be found in standard text books on signal analysis, for examples [42, 60], or in some books on numerical recipes by Press et al., for example [44]. To avoid this, one can consider large value for ω_M such that all relevant wave components, including second order interactions, fall into the frequency range $[-\omega_M, \omega_M]$. By doing this, all bound wave components with frequencies larger than ω_M are not substantial, and left out. Hence, the second order contribution $u^{(2)}$, given by (5.9), is replaced by

$$u^{(2)} = \frac{3}{4} \sum_{\substack{m,\, n,\, m+n \neq 0, \\ |m+n| \leq M}} a_m a_n \Gamma_2(\omega_m + \omega_n, \omega_n) e^{i[\{K_m + K_n\}x - \{\omega_m + \omega_n\}t]}. \tag{5.13}$$

We end this section with a remark below, but we note that in this chapter we do NOT use the technique given in this remark.

Remark 5.1 *A different point of view in solving this signaling problem has been introduced in the previous chapter for the bichromatic waves. For the case of irregular waves we are able to proceed in a similar way;* $u^{(1)}$ *and* $u^{(2)}$ *should be found from*

$$u_t^{(1)} + i\Omega(-i\partial_x)u^{(1)} = 0$$

with

$$u^{(1)}(0,t) = s(t) = \sum_m \hat{s}_m e^{-i\omega_m t},$$

and

$$u_t^{(2)} + i\Omega(-i\partial_x)u^{(2)} + \frac{3}{4}\partial_x\left[u^{(1)}\right]^2 = 0$$

with $u^{(2)}(0,t) \equiv 0$, *respectively.*

This gives

$$u^{(1)} = \sum_m \hat{s}_m e^{i[K_m x - \omega_m t]},$$

and

$$u^{(2)} = u_{bw}^{(2)} + u_{free}^{(2)},$$

where

$$u_{bw}^{(2)} = \frac{3}{4} \sum_{m,n,m+n\neq 0} \hat{s}_m \hat{s}_n \Gamma_2(\omega_m + \omega_n, \omega_n) e^{i[\{K_m + K_n\}x - \{\omega_m + \omega_n\}t]},$$

and

$$u_{free}^{(2)} = -\frac{3}{4} \sum_{m,n,m+n\neq 0} \hat{s}_m \hat{s}_n \Gamma_2(\omega_m + \omega_n, \omega_n) e^{i[K(\omega_m + \omega_n)x - \{\omega_m + \omega_n\}t]}.$$

This method does not require determination of the amplitude as given by (5.12), since the component amplitudes have been already given by $\hat{s}_m$. *Stated differently, the 'free waves' are chosen to cancel the second order bound waves at the point of measuring the signal.*

5.3 AWC1 based on the direct second order approximation

The algorithm of the analytical wave code (AWC) based on the direct second order approximation is given in Figure 5.1. From now on we call the AWC based on the direct second order approximation as AWC1, to distinguish it from other AWC's that we will introduce later on. AWC1 starts with the given periodic signal $s(t)$ with period T. The frequency ω_m and the Fourier coefficient $\hat{s}_m$ are computed using (5.3). The wave number K_m is found from the dispersion relation $K_m = K(\omega_m)$, and the second order transfer function Γ_2 is computed using (5.10). The amplitude components a_m's are determined using (5.12). Hence, we can compute the direct second order approximation at any point x and for any time t given by $u(x,t) = u^{(1)} + u^{(2)}$.

In the following we present the performance of AWC1 by comparing the results with wave evolutions obtained using direct numerical computation from the basic equations for surface waves done by Westhuis, see [58] and from experiments as well, see [56]. The computations of the predicted waves using AWC1 were run on a moderate PC (700 MHz, Pentium III processor).

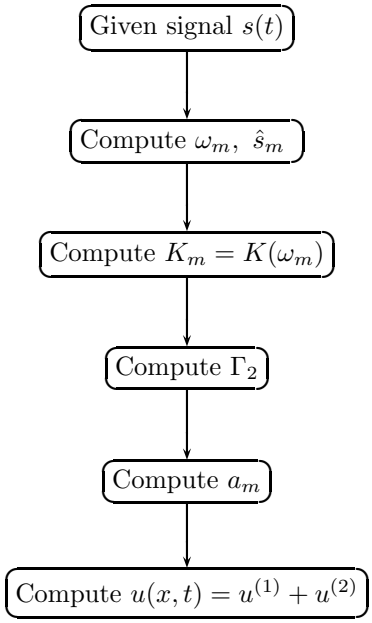

Figure 5.1: The algorithm of the analytical wave code based on the direct second order approximation (AWC1).

Predictions of AWC1 compared to numerical results

To evaluate the performance of AWC1, we will first apply AWC1 to predict the evolutions of the Bichromatic 1 and Bichromatic 2 we have discussed in the previous chapter. Figure 5.2 shows the numerical results and the corresponding predictions at several positions. For both cases the length of the time interval of the signal, $[0, T]$, is $T = 200$ s, and the signals were evaluated at 2000 equally distant points, $M = 1000$. For these examples each computation at any position took only few seconds. Bichromatic 1 and Bichromatic 2 are not purely bichromatic waves, but 'pseudo' bichromatic waves. This is because the start-up effects in generating these waves, see Remark 4.4 in the previous chapter for the start-up effects. Therefore, their amplitude spectra are not delta-Dirac functions, but are given in Figure 5.3. For Figure 5.2 we make the following observations.

- At $x = 0$ m the numerical results and the predictions can hardly be distinguished. This fact indicates the following. First, the spectral amplitudes a_m's are significantly well determined using the formula (5.12). Second, the small discrepancy as observed in the previous chapter, see Remark 4.4, has been substantially reduced by introducing wave modes composed of many frequencies.

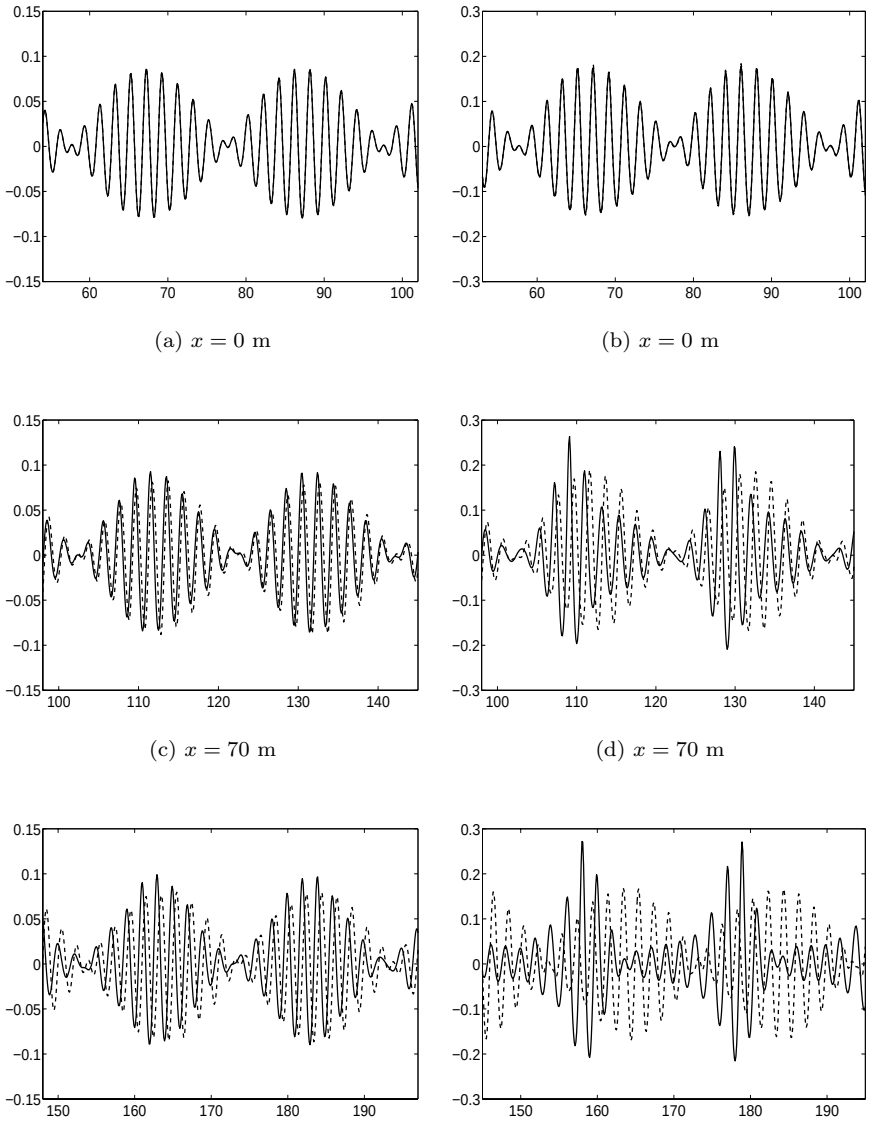

(a) $x = 0$ m (b) $x = 0$ m

(c) $x = 70$ m (d) $x = 70$ m

(e) $x = 150$ m (f) $x = 150$ m

Figure 5.2: Numerical results (solid lined) and predictions using AWC1 (dashed line). In this figure (a), (c) and (e) are Bichromatic 1, and (b), (d) and (f) are Bichromatic 2. The axes are elevation in m (vertical) and time in s (horizontal).

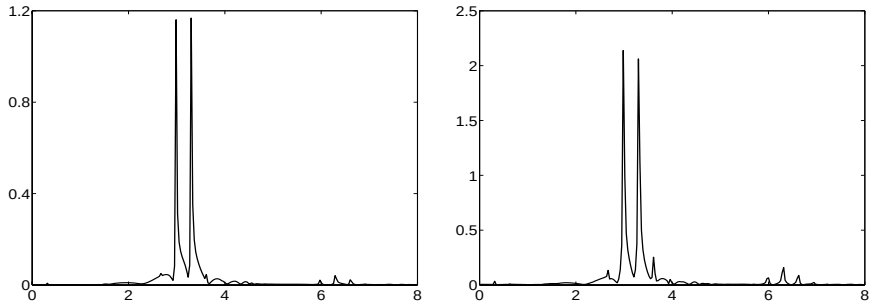

(a) Bichromatic 1 (b) Bichromatic 2

Figure 5.3: Raw spectral amplitudes of Bichromatic 1 and Bichromatic2 at $x = 0$. The horizontal and vertical axes are angular frequency, ω_m, in rad·s^{-1} and raw spectral amplitude, $2|\hat{s}_m|/\Delta\omega$, in m/$\left(\text{rad} \cdot \text{s}^{-1}\right)$, respectively.

- At $x = 70$ and 150 m there is a phase shift between the numerical results and the predictions for both Bichromatic 1 and Bichromatic 2. This phase shift depends on the positions where the signals are measured, indicating that, even though modes of many frequencies have been taken into account, the inaccuracy of the direct second order approximation in predicting the propagation speed still remains. The phase shift is larger for the larger amplitude wave.

Predictions of AWC1 compared to experimental results

The experiments that we consider were performed in the Seakeeping and Manoeuvring Basin (SMB) of MARIN [64]. The geometry of this basin is 170 m long and 5 m deep. There are two types of experiments that will be discussed: irregular waves and a bichromatic wave. This bichromatic wave, however, has parameters that are different than Bichromatic 1 and Bichromatic 2. This experimental bichromatic wave is generated by two modes of equal amplitudes 12 cm, but different (angular) frequencies: $\omega_1 = 2.86$ and $\omega_2 = 3.49$ rad/s (see experiment no. 636901 in [56] for the details). This experimental bichromatic is named Bichromatic 3. Observations in predicting Bichromatic 3 are qualitatively the same as Bichromatic 1, therefore, we do not give more discussions than just plotting the experiments and the predictions, see Figure 5.4. The computations have been done for $T = 200$, and the signals were evaluated at 1696 equally distant points or $M = 848$. These computations took few seconds for each position.

Figure 5.5 shows the experiment and the prediction at several positions for irregular waves. In this case, we only plot for comparisons in a fixed time-

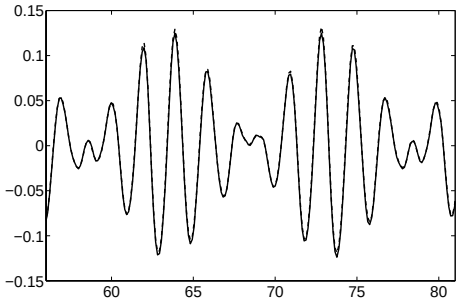

(a) $x = 0$ m

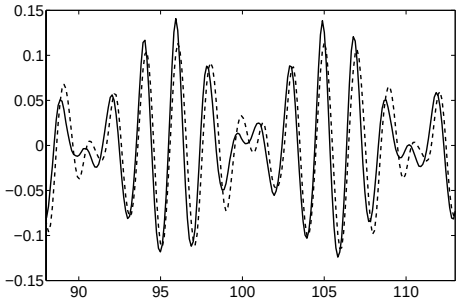

(b) $x = 50$ m

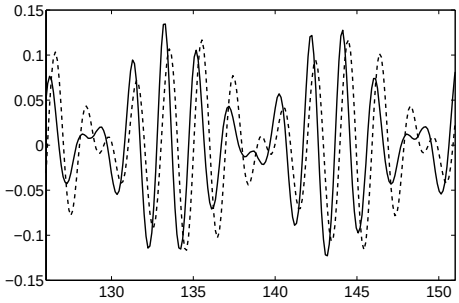

(c) $x = 110$ m

Figure 5.4: Experiments (solid lined) and predictions using AWC1 (dashed line) for Bichromatic 3.

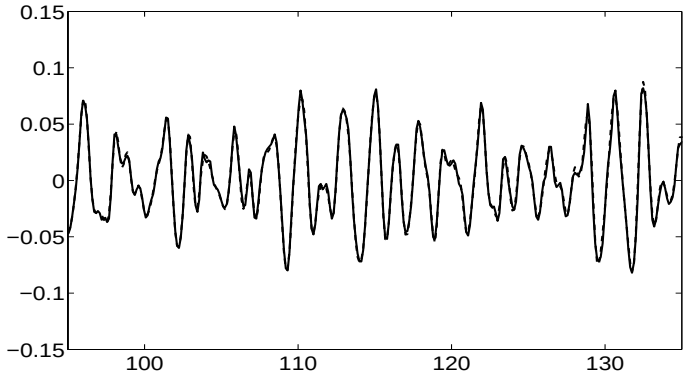

(a) $x = 0$ m

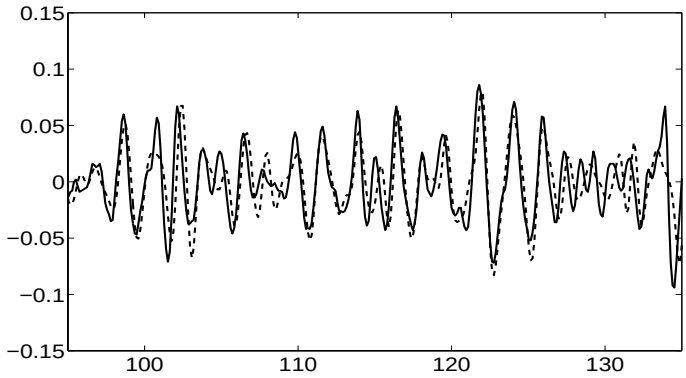

(b) $x = 50$ m

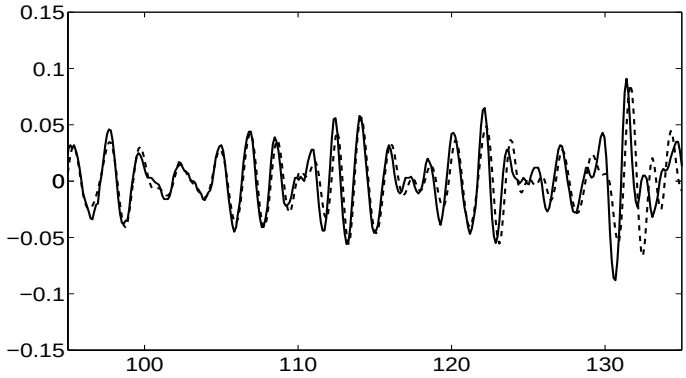

(c) $x = 80$ m

Figure 5.5: Experiments (solid lined) and predictions using AWC1 (dashed line) for irregular waves.

interval; [95,135] s, since we cannot follow the wave with a well-defined group velocity as in the bichromatic case. In this figure we observe the following. First, at $x = 0$ m the difference between the experiment and the prediction (or the corresponding direct second order approximation) is hardly noticed. This shows that formula (5.12) is capable to determine the spectral amplitudes a_m's. Second, at $x = 50$ m and 80 m there is a small phase shift between the experiments and the predictions. Moreover, AWC1 is not accurate to predict large waves as observed between $t = 100$ and 120 Figure 5.5 (b). Poor prediction for large waves is also observed in Figure 5.5 (c) at t around 130 s. For offshore engineering applications large waves may cause serious damage to ships and offshore structures. Therefore, a good prediction of the large waves is very important and is the interest here. For the computations of this irregular wave, we have used $T = 200$ and the signals were evaluated at 1666 equally distant points, $M = 833$. This computation also took few seconds.

Figure 5.6 shows the spectral amplitudes of these experimental bichromatic and irregular waves at $x = 0$. Since from Figure 5.5 it is not clear to make any observations as in the predictions of the Bichromatic 1 and Bichromatic 2, some analyses of the spectral amplitude and the phase shift difference for this irregular waves are needed. These will be given in the next section, together with taking the so-called nonlinear dispersion relation for irregular waves into account.

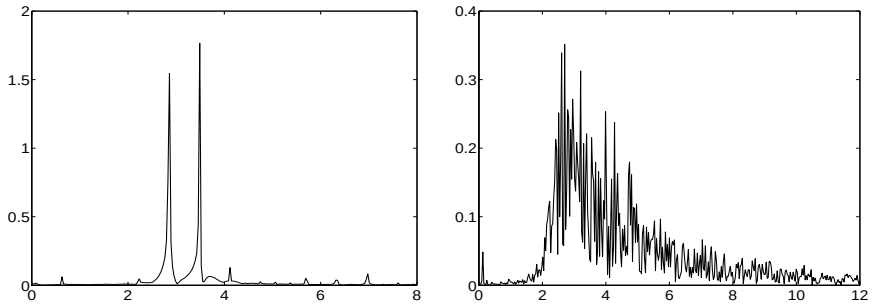

(a) Experimental bichromatic (b) Irregular waves

Figure 5.6: Raw spectral amplitudes of the experimental bichromatic and irregular waves at $x = 0$. The horizontal and vertical axes are angular frequency, ω_m, in rad·s^{-1} and raw spectral amplitude, $2|\hat{s}_m|/\Delta\omega$, in m/$\left(\text{rad} \cdot \text{s}^{-1}\right)$, respectively.

5.4 Nonlinear dispersion relation

It is already observed, also for the pure bichromatic case in the previous chapter, that the linear dispersion relation causes error in propagation speed that is

too large for the distances and times in the laboratories. This error has been explained from the resonance in the third order for the pure bichromatic case. For the case of waves composed of many frequencies, we generalise the discussion given in section 4.2. Substituting (5.4) into (5.1) gives an equation for $u^{(3)}$ in the form

$$u_t^{(3)} + i\Omega(-i\partial_x)u^{(3)} + \frac{3}{2}\partial_x\left[u^{(1)}u^{(2)}\right] = 0.$$

Write

$$\frac{3}{2}\partial_x\left[u^{(1)}u^{(2)}\right] = F_{\rm res} + F_{\rm nonres}.$$

The resonant forcing $F_{\rm res}$ at frequency ω_m is obtained from the interactions between components of $u^{(1)}$ and $u^{(2)}$:

i) $a_n e^{-i[K_n x-\omega_n t]}$ and $\frac{3}{4}a_m a_n \Gamma_2(\omega_m+\omega_n,\omega_n)e^{i[\{K_m+K_n\}x-\{\omega_m+\omega_n\}t]}$,

ii) $a_n e^{i[K_n x-\omega_n t]}$ and $\frac{3}{4}a_m a_n \Gamma_2(\omega_m-\omega_n,-\omega_n)e^{i[\{K_m-K_n\}x-\{\omega_m-\omega_n\}t]}$.

Hence, $F_{\rm res}$ has the form

$$\begin{aligned} F_{\rm res} &= \frac{9}{8}a_m K_m \left[\sum_{n\neq -m}|a_n|^2\Gamma_2(\omega_m+\omega_n,\omega_n) + \sum_{n\neq m}|a_n|^2\Gamma_2(\omega_m-\omega_n,-\omega_n)\right] \\ &\quad \times e^{i[K_m x-\omega_m t]} \\ &= \frac{9}{4}a_m K_m \left[\sum_{n\neq -m}|a_n|^2\Gamma_2(\omega_m+\omega_n,\omega_n)\right] e^{i[K_m x-\omega_m t]}. \end{aligned}$$

The resonant terms of $\frac{3}{2}\partial_x u^{(1)}u^{(2)}$, $F_{\rm res}$, lead to the third order contribution in the form

$$-\frac{9}{4}a_m t K_m \left[\sum_{n\neq -m}|a_n|^2\Gamma_2(\omega_m+\omega_n,\omega_n)\right] e^{i[K_m x-\omega_m t]}.$$

As already observed in the previous chapter for purely bichromatic waves, this third order resonant contribution linearly grows in time, then for large t this will dominate the second order contribution.

To prevent this growth, we need to take care of the resonance. To do that, we consider the following Ansatz:

$$u(x,t) = u^{(1)} + u^{(2)} + u^{(3)}, \tag{5.14}$$

where

$$u^{(1)} = \sum_m a_m e^{i[k_m x-\omega_m t]}$$

with

$$k_m = k_m^{(0)} + k_m^{(1)} + k_m^{(2)} + \cdots .$$

Observe that even though we use the same notation $u^{(1)}$, it is different than in the preceding sections; the wave number k_m is now given as a series expansion in amplitude. This technique is known as Lindstedt-Poincaré method. In chapter 3 we have discussed this method to find an approximate solution of an ordinary differential equation, see also cited references in that chapter. For a partial differential equation, a simple example of this method was given by Whitham in [59].

We now proceed like in the previous chapter. The differences will be on the one hand, that now we consider waves of many frequencies, and on the other hand, we do not have any condition yet for u at $x = 0$. In this case, the *homogeneous* solution for $u^{(2)}$ (and $u^{(3)}$) will simply be taken to be zero. Substituting (5.14) into the left hand side of (5.1), and collecting the first, second and third order residues into $A^{(1)},\ A^{(2)},\ A^{(3)}$ respectively, we have

$$A^{(1)} + A^{(2)} + A^{(3)} + \text{h.o.t.}, \tag{5.15}$$

where h.o.t. means higher order terms. The residue (5.15) has to be made as small as possible. Writing

$$\theta_m = k_m x - \omega_m t,$$

$A^{(j)}$ for $j = 1, 2, 3$ are given as follows

$$A^{(1)} = \sum_m a_m \left[\Omega(k_m^{(0)}) - \omega_m\right] e^{i\theta_m}, \tag{5.16}$$

$$A^{(2)} = u_t^{(2)} + i\Omega(-i\partial_x)u^{(2)} + F^{(2)}, \tag{5.17}$$

$$A^{(3)} = u_t^{(3)} + i\Omega(-i\partial_x)u^{(3)} + F^{(3)}. \tag{5.18}$$

Before we write the expressions for $F^{(2)}$ and $F^{(3)}$, we make $A^{(1)} = 0$ which gives

$$\Omega(k_m^{(0)}) = \omega_m \text{ or } k_m^{(0)} = K(\omega_m) = K_m, \tag{5.19}$$

meaning that in lowest order the linear dispersion relation has to be satisfied.

The function $F^{(j)}$, for $j = 2, 3$, contains resonant and non-resonant terms:

$$F^{(j)} = F_{\text{res}}^{(j)} + F_{\text{nonres}}^{(j)}.$$

Using $k_m^{(0)} = K_m$, $F_{\text{res}}^{(2)}$ and $F_{\text{nonres}}^{(2)}$ are given by

$$F_{\text{res}}^{(2)} = \sum_m a_m k_m^{(1)} \Omega'(K_m) e^{i\theta_m}$$

and

$$F_{\text{nonres}}^{(2)} = \frac{3}{4} \sum_{m,n,m+n\neq 0} a_m a_n (K_m + K_n) e^{i[\theta_m + \theta_n]},$$

respectively. Making the resonant and non-resonant terms of $A^{(2)}$ separately to vanish leads to the condition

$$k_m^{(1)} \equiv 0$$

and to the equation

$$u_t^{(2)} + i\Omega(-i\partial_x)u^{(2)} + F_{\text{nonres}}^{(2)} = 0.$$

Taking the homogeneous solution be zero, the last equation gives

$$u^{(2)} = \frac{3}{4} \sum_{m,n,m+n\neq 0} a_m a_n \Gamma_2(\omega_m + \omega_n, \omega_n) e^{i[\theta_m + \theta_n]}. \tag{5.20}$$

In the third order residue, we now merely consider the resonant term which is $F_{\text{res}}^{(3)}$. This is given by

$$F_{\text{res}}^{(3)} = \sum_m \left[a_m k_m^{(2)} \Omega'(K_m) + \frac{9}{4} a_m K_m \sum_{n\neq -m} |a_n|^2 \Gamma_2(\omega_m + \omega_n, \omega_n) \right] e^{i\theta_m}.$$

Making the resonance in the third order to vanish, we come to the so-called Nonlinear Dispersion Relation (NDR) for waves composed of many frequencies:

$$k_m = K_m - K_{\text{corr}}^{(m)},$$

where

$$K_{\text{corr}}^{(m)} = -k_m^{(2)} = \frac{9}{4} \frac{K_m}{\Omega'(K_m)} \left[\sum_{n\neq -m} |a_n|^2 \Gamma_2(\omega_m + \omega_n, \omega_n) \right]. \tag{5.21}$$

The nonlinear dispersion relation is well-known by applying frequency corrections (see for examples [59] for monochromatic waves, and [63] for irregular waves). However, we use wave number corrections that is more convenient for the signaling problem we deal with.

Observe that this wave number correction is of second order in amplitude. The wave number correction can be written as

$$K_{\text{corr}}^{(m)} = \frac{9}{4} \frac{K_m}{\Omega'(K_m)} \left[|a_m|^2 \Gamma_2(2\omega_m, \omega_m) + \sum_{\substack{n\neq m \\ n\neq -m}} |a_n|^2 \Gamma_2(\omega_n + \omega_m, \omega_m) \right].$$

The term with $\Gamma_2(2\omega_m, \omega_m)$ accounts for the correction of the wave number k_m from the nonlinear interaction of the wave component ω_m with itself, while the term with $\Gamma_2(\omega_n + \omega_m, \omega_m)$ is the contribution to the correction in k_m by the nonlinear interaction of the wave components with ω_n.

Summarising so far, the second order approximation with the nonlinear dispersion relation,

$$u = u^{(1)} + u^{(2)},$$

is given as follows. The phase with frequency ω_m is denoted by θ_m and can be written as

$$\theta_m = K_m x - \omega_m t - K_{\text{corr}}^{(m)} x. \tag{5.22}$$

The lowest order contribution is then given by

$$u^{(1)} = \sum_m a_m e^{i\theta_m}.$$

Taking only significant mode contributions that fall in the frequency range $[-\omega_M, \omega_M]$, the second order contribution reads

$$u^{(2)} = \frac{3}{4} \sum_{m,n,m+n\neq 0} a_m a_n \Gamma_2(\omega_m + \omega_n, \omega_n) e^{i[\theta_m + \theta_n]}.$$

At $x = 0$ the equation $u(0,t) = s(t)$ should be satisfied up to second order. The amplitude components a_m's are determined using (5.12), since the wave number corrections do not influence the solution at $x = 0$.

5.5 AWC2 based on the direct second order approximation with NDR

To incorporate the nonlinear dispersion relation in the AWC, the algorithm of AWC1 given by Figure 5.1 needs to be improved. The improvement is merely in determining the improved wave number by taking the nonlinear dispersion relation into account. This requires that the 'linear' wave numbers, the second order transfer functions and the amplitude components should be computed first. Then, we are able to compute the wave number corrections. This new AWC, based on the second order approximation with NDR, will be called AWC2. The complete algorithm of AWC2 is given in Figure 5.7.

In the following we evaluate the performance of AWC2 in predicting numerical and experimental results in section 5.3. In this evaluation we do not plot the comparisons between the predictions and the numerical or experimental results at $x = 0$. These comparisons, however, give the same results as in section 5.3, since the amplitude components are determined in the same way for AWC1 and AWC2.

We note that the computations were done for the same length of time-interval and number of points. The additional computation time is only needed once for determining the wave number corrections, but not for computing the wave elevation $u(x,t)$ at any position x. For the examples above, this additional computation was very fast and took only a few seconds.

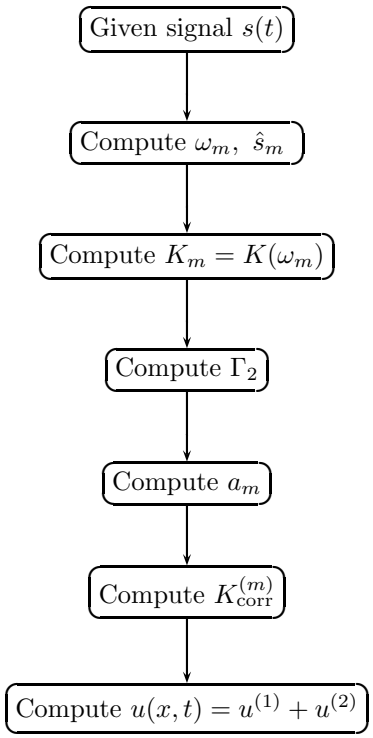

Figure 5.7: The algorithm of the analytical wave code based on the second order approximation with nonlinear dispersion relation (AWC2).

Predictions of AWC2 compared to numerical results

Figure 5.8 shows the numerical results and the predictions of AWC2 for Bichromatic 1 and Bichromatic 2 at $x = 70$ and 150 m. In this figure we have qualitatively the same observations as Figure 4.5 in the previous chapter. First, the phase shift has significantly reduced. However, this is achieved after multiplying the wave number corrections with constants, 5 for Bichromatic 1 and 3 for Bichromatic 2. This will be clear in the discussion about *near-resonant interactions* in section 5.6.2. Second, the prediction of Bichromatic 2 does not reveal large envelope deformations. Hence, we come to the stronger conclusions than already presented in the previous chapter: the nonlinear dispersion has significantly reduced the error in the wave propagation, but the second approximation, even though many frequencies have been taken into account, is still not capable to reveal the large envelope deformation as shown by the experiments and the direct numerical simulations for Bichromatic 2. We conclude that AWC2 is significantly capable in predicting bichromatic waves that do not reveal large envelope deformations.

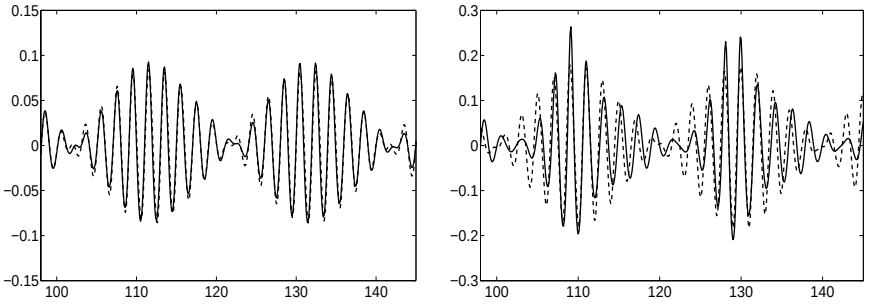

(a) $x = 70$ m (b) $x = 70$ m

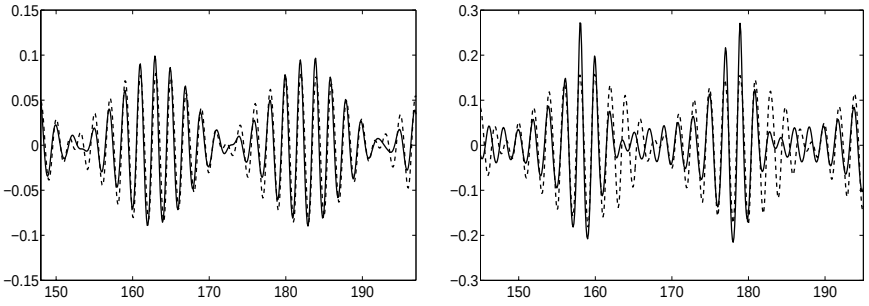

(c) $x = 150$ m (d) $x = 150$ m

Figure 5.8: Numerical results (solid lined) and predictions using AWC2 (dashed line). In this figure (a) and (c) are Bichromatic 1, and (b) and (d) are Bichromatic 2.

Predictions of AWC2 compared to experimental results

The performance of AWC2 in predicting Bichromatic 3 is given in Figure 5.9. Qualitatively similar observations as the case of Bichromatic 1 are noticed. For this experimental bichromatic wave, the wave number corrections have been multiplied by 3 such that the phases of the experiments and the predictions are in a good agreement.

For the case of irregular waves the comparisons between the experiments and the predictions are given in Figure 5.10. In this figure we observe that for large waves, the most important part of these evolutions, the predictions of AWC2 are better than the predictions of AWC1 given in Figure 5.5, the inaccuracy in predicting the large waves has significantly been reduced.

To investigate this performance in more detail, we will investigate the spectral amplitude and phase errors of the predictions. This is done as follows. Let there

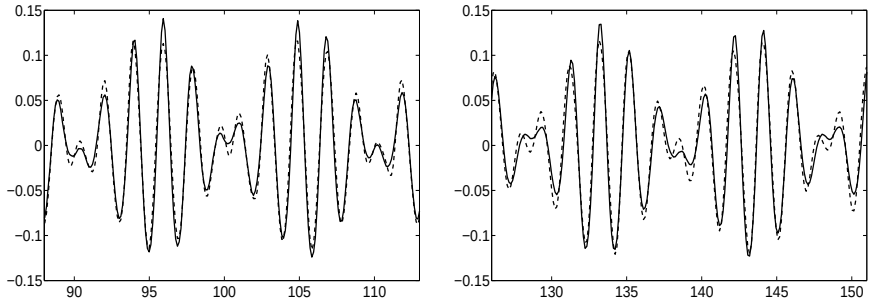

(a) $x = 50$ m (b) $x = 110$ m

Figure 5.9: Experiments (solid lined) and predictions using AWC2 (dashed line) for Bichromatic 3.

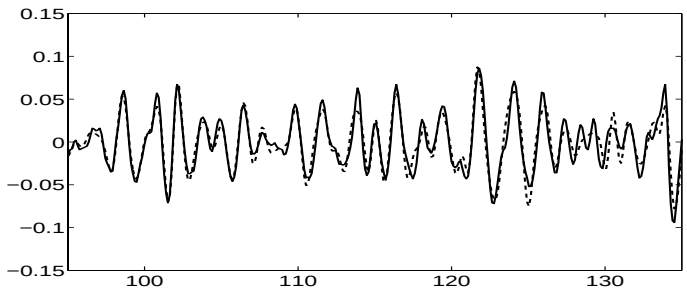

(a) $x = 50$ m

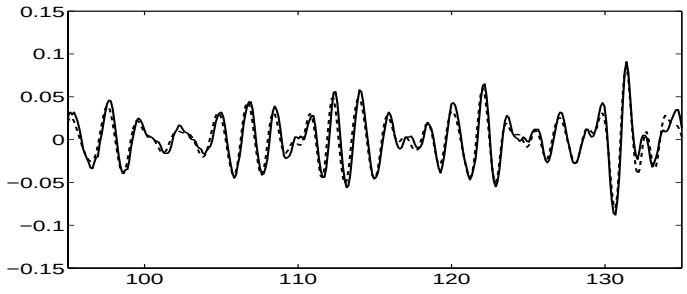

(b) $x = 80$ m

Figure 5.10: Experiments (solid lined) and predictions using AWC2 (dashed line) for irregular waves.

be given a time-signal $f(t)$ that is evaluated at equally distant points $2M$ in a finite time-interval $[0, T]$. Assuming that the signal is periodic, see section 5.1, we write f in the Fourier series

$$f(t) = \sum_{m=-M}^{M} b(\omega_m) e^{-i\omega_m t}, \tag{5.23}$$

where

$$b(\omega_m) = \frac{1}{T} \int_0^T f(t) e^{i\omega_m t} dt.$$

The expression (5.23) can be written in the form

$$f(t) = \sum_{m=1}^{M} 2 \left| b(\omega_m) \right| \cos\left(\omega_m t - \bar{\theta}^{(m)} \right), \tag{5.24}$$

where $0 \leq \bar{\theta}^{(m)} < 2\pi$ that satisfies

$$\cos\theta^{(m)} = \mathrm{Re}(b(\omega_m)), \qquad \sin\bar{\theta}^{(m)} = \mathrm{Im}(b(\omega_m)).$$

$\mathrm{Re}(b)$ means the real part of b, and $\mathrm{Im}(b)$ means the imaginary part of b. This determination of the spectral amplitudes and the phases are applied for the signals obtained from the experiments, the predictions of AWC1 and AWC2 at $x = x_0$. These signals are written in the forms

$$\sum_{m=1}^{M} 2 \left| b_{\mathrm{exper}}(\omega_m) \right| \cos\left(\omega_m t - \bar{\theta}^{(m)}_{\mathrm{exper}} \right),$$

$$\sum_{m=1}^{M} 2 \left| b_{\mathrm{AWC1}}(\omega_m) \right| \cos\left(\omega_m t - \bar{\theta}^{(m)}_{\mathrm{AWC1}} \right),$$

and

$$\sum_{m=1}^{M} 2 \left| b_{\mathrm{AWC2}}(\omega_m) \right| \cos\left(\omega_m t - \bar{\theta}^{(m)}_{\mathrm{AWC2}} \right),$$

respectively.

The spectral amplitude of these irregular waves at $x = 0$ is already given in Figure 5.6. In the following, we will present spectral amplitude and phase errors only in the frequency range [2,6] rad/s, the most substantial frequency range of these irregular waves. Figure 5.11 shows the spectral amplitude errors of the predictions using AWC1 and AWC2, $2\left|b_{\mathrm{exper}} - b_{\mathrm{AWC1}}\right| / \Delta\omega$ and $2\left|b_{\mathrm{exper}} - b_{\mathrm{AWC2}}\right| / \Delta\omega$ respectively, at positions $x = 50$ and 80 m. In this figure we observe that there is no significant difference between the spectral amplitude errors of the predictions using AWC1 and AWC2. This is due to the component amplitudes a_m's for both AWC's have been determined in the same way.

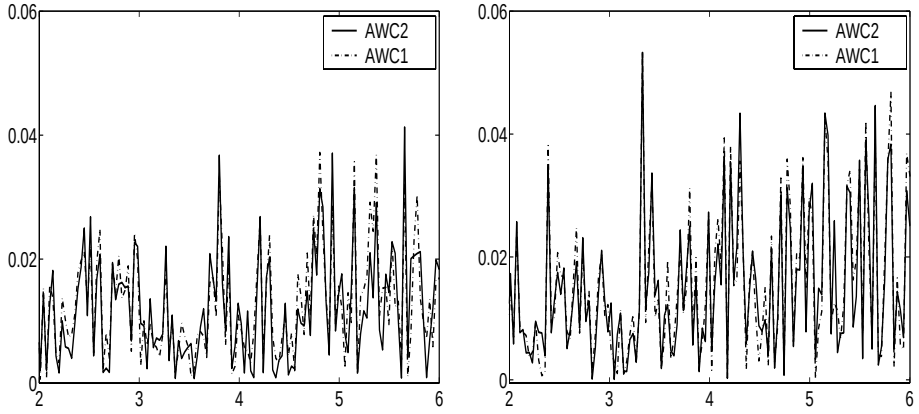

(a) $x = 50$ m (b) $x = 80$ m

Figure 5.11: Raw spectral amplitude errors of the predictions using AWC1 and AWC2 at positions $x = 50$ and 80 m. The axes are angular frequency in rad·s^{-1} (horizontal) and raw spectral amplitude error in m/$\left(\text{rad} \cdot \text{s}^{-1}\right)$ (vertical).

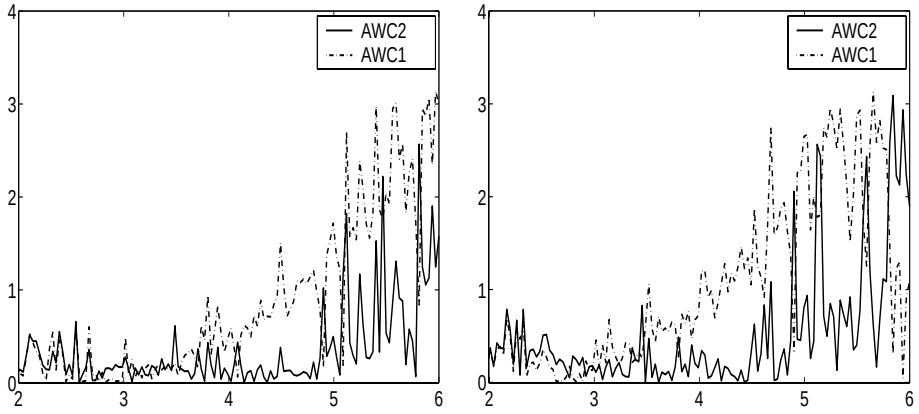

(a) $x = 50$ m (b) $x = 80$ m

Figure 5.12: Phase error of the predictions using AWC1 and AWC2 at positions $x = 50$ and 80 m. The axes are angular frequency in rad·s^{-1} (horizontal) and phase error (vertical).

The phase errors of the predictions of AWC1 $\left|\bar{\theta}_{\text{exper}} - \bar{\theta}_{\text{AWC1}}\right|$ and the predictions of AWC2 $\left|\bar{\theta}_{\text{exper}} - \bar{\theta}_{\text{AWC2}}\right|$ are presented in Figure 5.12. In this figure we observe that the phase error of the predictions using AWC2 is much less than the phase error of the predictions using AWC1 in this substantial frequency region, especially in the most essential low-frequency region. Some large phase errors in the angular frequency range [5,6] of the predictions using AWC2 are observed. These errors correspond to small amplitude components of the Fourier series of the signals. Hence, the contribution of these error in the inaccuracy of the predictions is not substantial. These show that the wave number correction has substantially reduced the phase error.

5.6 Third order contribution

In the preceding sections we have observed that the AWC's based on the second order approximations, even though modes and wave number corrections for many frequencies have been taken into account, are not capable in predicting large envelope deformation of Bichromatic 2. In the previous chapter we have investigated that the third order side band contributions have become substantial if the quotient of amplitude and frequency difference is small. Moreover, we showed that the approximation is in a good agreement with the numerical result for Bichromatic 2 in revealing large envelope deformations. Based on this investigation, we also consider third order contributions for waves that consist of many frequencies. These contributions should be computed from the equation that is obtained by making the non-resonant terms of $A^{(3)}$ in (5.18) to vanish. This equation reads

$$u_t^{(3)} + i\Omega(-i\partial_x)u^{(3)} + F_{\text{nonres}}^{(3)} = 0. \tag{5.25}$$

The forcing function $F_{\text{nonres}}^{(3)}$ is non-resonant and given by a triple sum (in m, n and p)

$$F_{\text{nonres}}^{(3)} = \frac{9}{8} \sum_{\substack{m \neq -n \\ m \neq -p \\ n \neq -p}} \left[\begin{array}{l} a_m a_n a_p \cdot \{K_m + K_n + K_p\} \times \\ \\ \Gamma_2(\omega_n + \omega_p, \omega_p) e^{i\{\theta_m + \theta_n + \theta_p\}} \end{array} \right]. \tag{5.26}$$

5.6.1 Third order side band contributions

Solving (5.25) leads to the solution for $u^{(3)}$ that is given in a triple sum of the form

$$u^{(3)} = \frac{9}{8} \sum_{\substack{m \neq -n \\ m \neq -p \\ n \neq -p}} \left[\begin{array}{l} \Gamma_3(\omega_m + \omega_n + \omega_p, \omega_n + \omega_p, \omega_p) \times \\ \\ a_m a_n a_p \times e^{i\{\theta_m + \theta_n + \theta_p\}} \end{array} \right], \tag{5.27}$$

where

$$\Gamma_3(\omega,\mu,\sigma)=\Gamma_2(\mu,\sigma)\frac{K(\sigma)+K(\mu-\sigma)+K(\omega-\mu)}{\omega-\Omega(K(\sigma)+K(\mu-\sigma)+K(\omega-\mu))}.$$

The third order transfer function $\Gamma_3(\omega,\mu,\sigma)$ is, mathematically speaking, the multiplication factor from third order interactions that produce a wave with frequency ω. These interactions are of the mode $\omega-\mu$ and the second order bound wave μ, where this bound wave is the second order interaction of two modes σ and $\mu-\sigma$, see Figure 5.13 for this interaction in frequency domain.

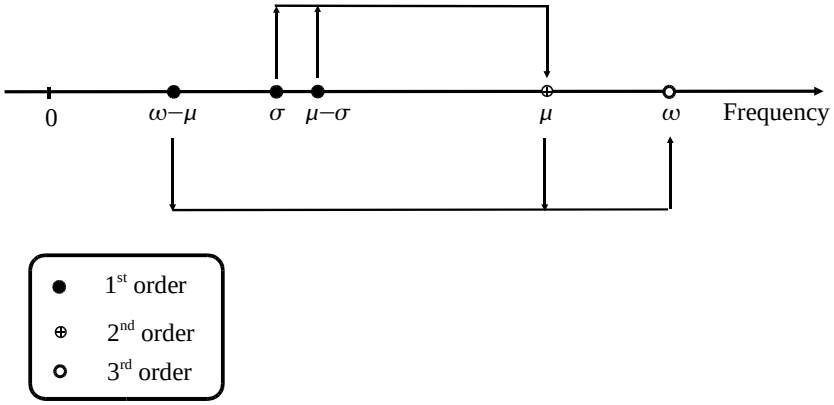

Figure 5.13: Third order interaction in the frequency domain.

Observe that if conditions $\mu=0$, $\sigma=\omega$ or $\mu=\sigma+\omega$ are satisfied, this transfer function is singular, meaning that there is resonance. We introduce the notation $\mathcal{C}_0$ defined by

$$\mathcal{C}_0(\omega)=\{(\sigma,\mu)|\sigma=\omega \text{ or } \mu=0 \text{ or } \mu=\sigma+\omega\} \tag{5.28}$$

to denote the set of points in σ,μ-plane where the resonance conditions at frequency ω are satisfied, see Figure 5.14.

Note that $\Gamma_3(\omega_m+\omega_n+\omega_p,\omega_n+\omega_p,\omega_p)$ is simply equal to

$$\Gamma_2(\omega_n+\omega_p,\omega_p)\frac{K_m+K_n+K_p}{\omega_m+\omega_n+\omega_p-\Omega(K_m+K_n+K_p)}.$$

It is already observed in the previous chapter that third order side band contributions become essential if the frequency difference is small. We now investigate

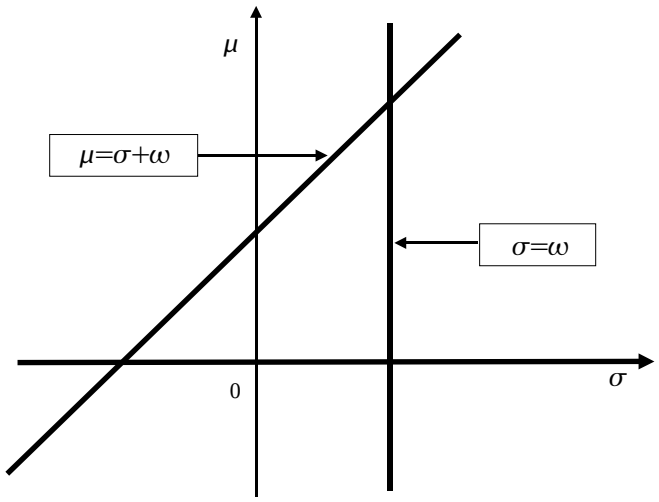

Figure 5.14: $\mathcal{C}_0$ in σ, μ-plane.

the third order side band contribution of frequency ω_q at frequency $\omega = \omega_q + \epsilon$. Hence, one of the following three conditions $\omega_m = \omega_q$, $\omega_n = \omega_q$ or $\omega_p = \omega_q$ should be satisfied. The sign of ϵ determines which side band is considered, positive is for the upper side band, while negative is for the lower side band. For $\epsilon = 0$ we have resonance that has been taken care of. We introduce the notation Δ given by

$$\Delta = K(\omega_{m_1}) + K(\omega_{M_2}), \text{ where } \omega_{m_1} + \omega_{m_2} = \epsilon.$$

Rewriting the three conditions above in more detail we have the following

i) $\omega_m = \omega_q$ $(K_m = K_q)$ and $\omega_n + \omega_p = \epsilon$ $(K_n + K_p = \Delta)$,

ii) $\omega_n = \omega_q$ $(K_n = K_q)$ and $\omega_m + \omega_p = \epsilon$ $(K_m + K_p = \Delta)$,

iii) $\omega_p = \omega_q$ $(K_p = K_q)$ and $\omega_m + \omega_n = \epsilon$ $(K_m + K_n = \Delta)$.

This is given in Figure 5.15. The difference between cases ii) and iii) that look similar in this figure can clearly be seen in Figure 5.16. Observe that cases i), ii) and iii) are side band contributions near the resonance lines $\mu = 0$, $\mu = \sigma + \omega_q + \epsilon$ and $\sigma = \omega_q + \epsilon$, respectively. For these cases, we have

$$\Gamma_3^{\pm} = \Gamma_3(\omega_q \pm \epsilon, \omega_n + \omega_p, \omega_p) \sim \frac{1}{\frac{1}{2}\Delta^2\Omega'' \pm \frac{1}{6}\Delta^3\Omega'''},$$

where the second and third derivatives of Ω should be evaluated at K_q. Obviously, $\Gamma_3^{\pm}$ tends to infinity as Δ tends to zero. Moreover, we also have

$$\Gamma_3^{+} + \Gamma_3^{-} \sim \frac{1}{\Delta^2\Omega''} \tag{5.29}$$

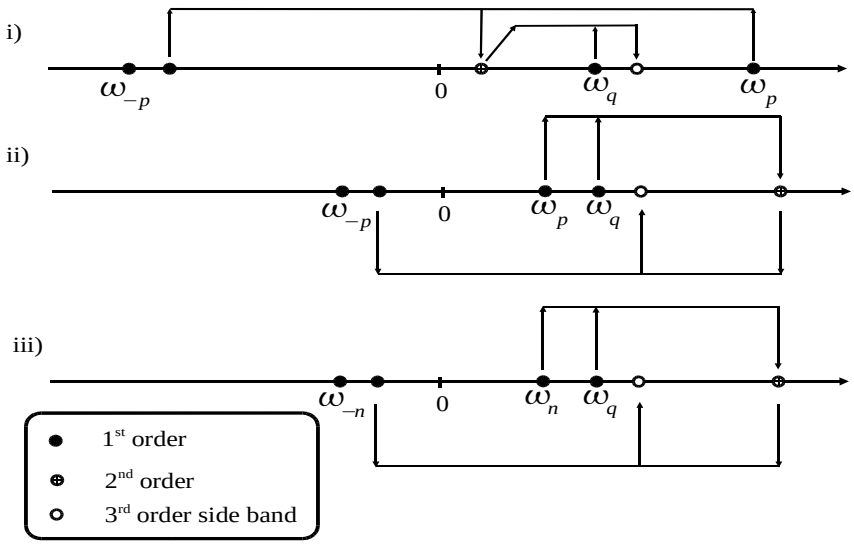

Figure 5.15: Side band contribution of frequency ω_q at frequency $\omega_q + \epsilon$.

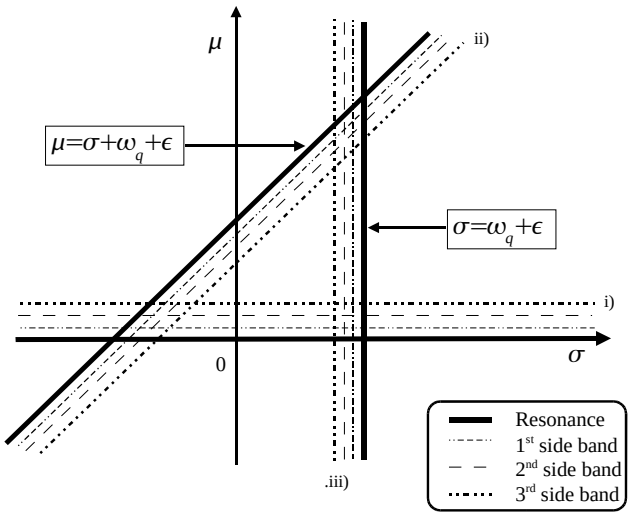

Figure 5.16: Side band contribution of frequency ω_q at frequency $\omega_q + \epsilon$ in σ, μ-plane.

and

$$\Gamma_3^+ - \Gamma_3^- \sim \frac{\Omega'''}{\Delta \cdot [\Omega'']^2}. \tag{5.30}$$

The difference between lower and upper side band contributions, as shown by $\Gamma_3^+ - \Gamma_3^-$, yields an out-of phase contribution.

For discrete frequencies (due to periodic continuation of the signal $s(t)$) $\epsilon = j \cdot \Delta\omega$, where j is an integer. From now on we only consider non-zero j, which does not yield resonance.

Before we proceed, we note that

$$\omega_{p_1} + \omega_{p_2} = \omega_{p_1+p_2},$$

and since $\Gamma_2(\omega_{p_2+p_3}, \omega_{p_2}) = \Gamma_2(\omega_{p_2+p_3}, \omega_{p_3})$, we also have

$$\Gamma_3(\omega_{p_1}, \omega_{p_2+p_3}, \omega_{p_2}) = \Gamma_3(\omega_{p_1}, \omega_{p_2+p_3}, \omega_{p_3}).$$

Let M_0 be a positive integer. We define third order, M_0^{th} side band, contribution by third order interactions between mode ω_q and any modes that produce side band contributions at frequencies $\omega_q - (M_0 \cdot \Delta\omega)$ and $\omega_q + (M_0 \cdot \Delta\omega)$. These are upper and lower side band contributions, respectively. The third order, M_0^{th} side band, contribution reads

$$\begin{aligned}
u_{sb}^{(3)} &= \frac{9}{8} \sum_{\substack{q \neq -p \\ q \neq p-j \\ j = \pm M_0}} a_q a_{-p+j} a_p \Gamma_3(\omega_{q+j}, \omega_j, \omega_p) e^{i\{\theta_q + \theta_p + \theta_{-p+j}\}} \\
&\quad + \frac{9}{8} \sum_{\substack{q \neq -p \\ q \neq p-j \\ j = \pm M_0}} a_q a_{-p+j} a_p \Gamma_3(\omega_{q+j}, \omega_{p+q}, \omega_p) e^{i\{\theta_q + \theta_p + \theta_{-p+j}\}} \\
&\quad + \frac{9}{8} \sum_{\substack{q \neq -n \\ q \neq n-j \\ j = \pm M_0}} a_q a_{-n+j} a_n \Gamma_3(\omega_{q+j}, \omega_{n+q}, \omega_q) e^{i\{\theta_q + \theta_n + \theta_{-n+j}\}} \\
&= \frac{9}{8} \sum_{\substack{q \neq -p \\ q \neq p-j \\ j = \pm M_0}} a_q a_{-p+j} a_n \left[\begin{array}{l} \Gamma_3(\omega_{q+j}, \omega_j, \omega_p) + \\ 2\Gamma_3(\omega_{q+j}, \omega_{p+q}, \omega_p) \end{array} \right] e^{i\{\theta_q + \theta_p + \theta_{-p+j}\}}.
\end{aligned} \tag{5.31}$$

Even though this is still a triple sum in q, p and j, the index j is only taken for $j = \pm M_0$. Observe that $u_{sb}^{(3)}$ given by formula (5.31) contains much less terms compared to $u^{(3)}$ in formula (5.27).

5.6.2 Near-resonant interactions

The third order side band interactions may yield contributions that are substantially large, even larger than the first order contribution. These interactions are

called *near-resonant interactions*. If this happens the series expansion for the approximate solution is no longer valid, and the perturbation technique breaks down. We note that this does not happen for ordinary differential equations nor if we only consider a single frequency solution for a partial differential equation, see [59].

Near-resonant interactions are observed in Bichromatic 2. Figure 5.17 shows amplitude spectra of the lowest order contribution and the third order side band contributions for several values of M_0. At the first side band, $M_0 = 1$, the

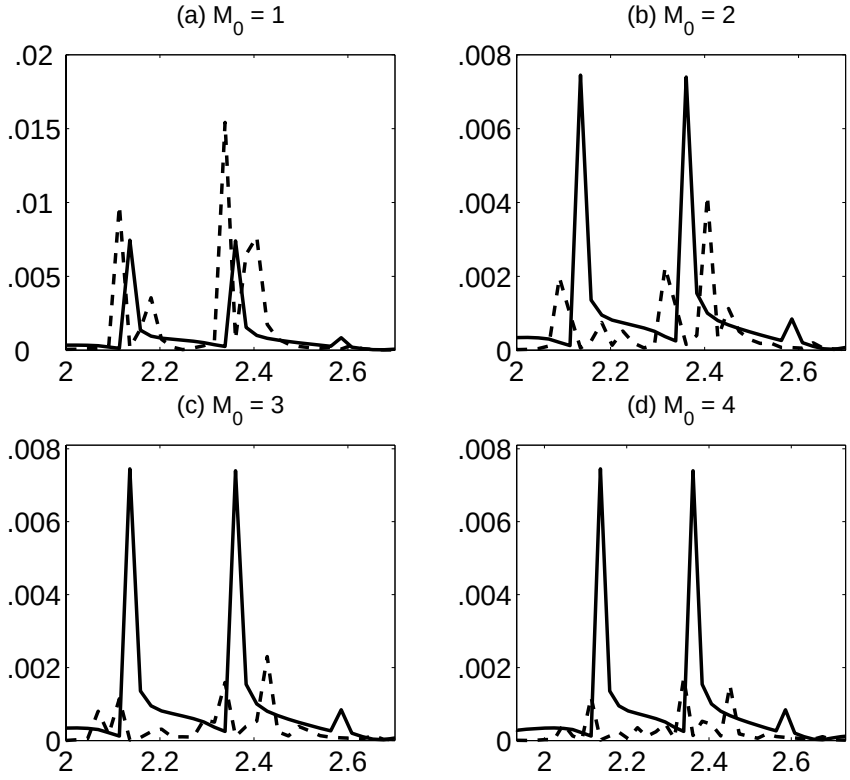

Figure 5.17: Amplitude spectra of the lowest order contribution (solid line) and the third order side band contributions (dashed line) for several values of M_0. For this Bichromatic 2, all quantities are in normalised forms.

amplitude spectrum of the third order contribution is larger than the spectrum of the lowest order contribution. Hence, this first side band interaction is near-resonant, and should be taken care of. For $M_0 \geq 2$ the amplitude spectra of the third order contributions are less dominant than the amplitude spectrum of the lowest order contribution.

Before we discuss how M_0 should be determined, we will present how we deal

with the near-resonant interactions. Let the third order contributions in the side band(s) less than M_0 be near-resonant. These contributions are due to the forcing

$$F^{(3)}_{\text{nearres}} = \frac{9}{8} \sum_{\substack{q \neq -p \\ q \neq p-j \\ |j| < M_0}} \left[\begin{array}{l} a_q a_{-p+j} a_p \left[K_q + K_p + K_{-p+j} \right] \\ \\ \times \{ \Gamma_2(\omega_j, \omega_p) + 2\Gamma_2(\omega_{p+q}, \omega_p) \} \end{array} \right] e^{i\{\theta_q + \theta_p + \theta_{-p+j}\}}.$$

Observe that for $|j| < M_0$, we have

$$\omega_q + \omega_p + \omega_{-p+j} = \omega_q + \omega_j = \omega_q + \epsilon,$$

$$K_q + K_p + K_{-p+j} = K_q + K_j = K_q + \Delta.$$

Hence, $\theta_q + \theta_p + \theta_{-p+j} \approx \theta_q$, and the forcing can be approximated by

$$F^{(3)}_{\text{nearres}} \approx \frac{9}{8} \sum_{\substack{q \neq \pm p \\ |j| < M_0}} \left[\begin{array}{l} a_q a_{-p} a_p K_q \times \\ \\ \{ \Gamma_2(0, \omega_p) + 2\Gamma_2(\omega_{p+q}, \omega_p) \} \end{array} \right] e^{i\theta_q}.$$

The second order transfer function for $\Gamma_2(0, \sigma)$ the very long wave interaction should be interpreted by its limiting case as follow.

$$\begin{aligned} \Gamma_2(0,\sigma) &= \lim_{\omega \to 0} \Gamma_2(\omega, \sigma) = \lim_{\omega \to 0} \frac{K(\sigma) + K(\omega - \sigma)}{\omega - \Omega(K(\sigma) + K(\omega - \sigma))} \\ &= \lim_{\omega \to 0} \frac{K'(\sigma) \cdot \omega}{\omega - \Omega(K'(\sigma) \cdot \omega)} = \lim_{\omega \to 0} \frac{K'(\sigma) \cdot \omega}{\omega - \Omega'(0) \cdot K'(\sigma) \cdot \omega} \\ &= \frac{1}{V(\sigma) - \Omega'(0)} = -\frac{1}{1 - V(\sigma)} \end{aligned}$$

where $V(\sigma)$ is the group velocity at frequency σ defined by $V(\sigma) = 1/K'(\sigma)$.

Taking care of this approximate near-resonant forcing, we have additional terms to the wave number correction (5.21). These terms read

$$\frac{9}{4} \frac{K_m}{\Omega'(K_m)} (M_0 - 1) \sum_{p \neq -m} \left[\begin{array}{ll} \Gamma_2(0, \omega_p) & + \\ 2\Gamma_2(\omega_{p+m}, \omega_p) & \end{array} \right] |a_p|^2.$$

Without the presence of term $\Gamma_2(0, \omega_p)$, this additional wave number correction is equal to $2(M_0 - 1)K^{(m)}_{\text{Corr}}$. Factor $2(M_0 - 1)$ comes from the total number of near-resonant interactions in the lower and upper side bands, at each side there are $M_0 - 1$ bands.

Hence, $K^{(m)}_{\text{Corr}}$ in θ_m given by formula (5.22) should be replaced by $K^{(m)}_{\text{CorrSb}}$, where

$$\begin{aligned} K^{(m)}_{\text{CorrSb}} &= K^{(m)}_{\text{Corr}} + \frac{9}{4} \frac{K_m}{\Omega'(K_m)} (M_0 - 1) \sum_{p \neq -m} \left[\begin{array}{ll} \Gamma_2(0, \omega_p) & + \\ 2\Gamma_3(\omega_{p+m}, \omega_p) & \end{array} \right] |a_p|^2 \\ &= \frac{9}{4} \frac{K_m}{\Omega'(K_m)} \sum_{p \neq -m} \left[\begin{array}{ll} \{M_0 - 1\}\Gamma_2(0, \omega_p) & + \\ \{2M_0 - 1\}\Gamma_3(\omega_{p+m}, \omega_p) & \end{array} \right] |a_p|^2. \end{aligned} \tag{5.32}$$

Note that the condition $M_0 = 1$ means that there is no near-resonant interaction, therefore $K^{(m)}_{\text{CorrSb}} = K^{(m)}_{\text{Corr}}$.

Determining M_0 is not easy and probably there is no standard way. However, there are two conditions that should be considered for this purpose. First, M_0 should be determined such that the third order contribution at the side band M_0 should be less dominant than the lowest order contribution, but not necessarily than the second order contribution. Second, the choice for M_0 should give the best approximation for the propagation speed compared to the experiments or direct numerical simulations.

The following is one technique to determine M_0. Let $\bar{a}$ be the maximum of the amplitude spectrum of the lowest order contribution, in the example above $\bar{a} = 0.007$. Denote $\bar{\omega}$ be the frequency which gives the largest amplitude $\bar{a}$, or to be less strict a frequency nearby the frequency which gives the largest amplitude $\bar{a}$. Since the third order side band contribution should be less dominant than the lowest order contribution, we have a condition

$$\frac{9}{8}\bar{a}^3 \begin{bmatrix} \Gamma_3(\bar{\omega}+\epsilon,\epsilon,\bar{\omega})+ \\ 2\Gamma_3(\bar{\omega}+\epsilon,2\bar{\omega}+\epsilon,\bar{\omega}) \end{bmatrix} < \bar{a}, \tag{5.33}$$

see formula (5.31) by taking $\omega_p = \omega_q = \bar{\omega}$ and $\epsilon = M_0 \cdot \Delta\omega$. Note that $\Delta\omega$ is determined from the initial signal, see section 5.1. Observe that

$$\begin{aligned} \begin{bmatrix} \Gamma_3(\bar{\omega}+\epsilon,\epsilon,\bar{\omega})+ \\ 2\Gamma_3(\bar{\omega}+\epsilon,2\bar{\omega}+\epsilon,\bar{\omega}) \end{bmatrix} &= \begin{bmatrix} \Gamma_2(\epsilon,\bar{\omega})+ \\ 2\Gamma_2(2\bar{\omega}+\epsilon,\bar{\omega}) \end{bmatrix} \frac{K(\bar{\omega})+\Delta}{\bar{\omega}+\epsilon-\Omega(K(\bar{\omega})+\Delta)} \\ &\approx \begin{bmatrix} \Gamma_2(0,\bar{\omega})+ \\ 2\Gamma_2(2\bar{\omega},\bar{\omega}) \end{bmatrix} \frac{K(\bar{\omega})}{-\frac{1}{2}\Delta^2 \cdot \Omega''}. \end{aligned}$$

The wave number difference Δ is given by

$$\Delta = K(\bar{\omega} + \{M_0 \cdot \Delta\omega\}) - K(\bar{\omega}),$$

which can be approximated by

$$\Delta \approx M_0 \cdot K'(\bar{\omega}) \cdot \Delta\omega = \frac{M_0 \cdot \Delta\omega}{\Omega'}.$$

Using this approximation, the condition (5.33) gives

$$M_0 > \frac{\bar{a}}{\Delta\omega} \cdot \Omega' \cdot \sqrt{\frac{9}{4}\frac{K(\bar{\omega})}{-\Omega''}\,[\Gamma_2(0,\bar{\omega}) + 2\Gamma_3(2\bar{\omega},\bar{\omega})]}.$$

M_0 may be different for different waves. For waves we have discussed, these values can be found in Table 5.1. Observe that a wave with larger quotient $\frac{\bar{a}}{\Delta\omega}$ need less side bands than one with smaller $\frac{\bar{a}}{\Delta\omega}$. This is because the side bands 1 to $M_0 - 1$ should be taken care of using NDR. For those waves, we have $\bar{\omega} \approx 2.1$,

which comes from the laboratory interest in waves of length about 7 m in the 5 m deep basin. In this case, we also have

$$\Omega' \cdot \sqrt{\frac{9}{4}\frac{K(\bar{\omega})}{-\Omega''}\left[\Gamma_2(0,\bar{\omega}) + 2\Gamma_3(2\bar{\omega},\bar{\omega})\right]} \approx 16$$

We note that in this criterion, the restriction is only due to the lowest order contribution, but not the second order contribution.

	$\bar{a}$	$\Delta\omega$	M_0	$2M_0 - 1$
Bichromatic 1	0.0035	0.0225	3	5
Bichromatic 2	0.007	0.0225	5	9
Bichromatic 3	0.004	0.0281	2	3
Irregular	0.0012	0.0281	1	1

Table 5.1: M_0 for considered Bichromatic and irregular waves.

From this table M_0's agree with the multiplication factors that have been taken into account for the adjustment of the propagation speeds of Bichromatic 1 and Bichromatic 3 in section 5.5. The wave number correction of Bichromatic 1 was multiplied by 5, of Bichromatic 3 by 3.

However, to get the propagation speed correct, the wave number correction of Bichromatic 2 was multiplied by the factor 3, instead of 9. The explanation is that the third order contribution at the side band 2 is already needed for the large envelope deformations for Bichromatic 2 . This side band contribution is less dominant than the lowest order contribution as shown in Figure 5.17, therefore, taking that contribution into account does not make the perturbation method break down.

5.6.3 Third order contribution at the outer side bands

We have shown that some side band contributions are needed to be taken care of, because their presence makes the perturbation technique fail. In the following we will show that side band contributions outside M_0^{th} side band may be substantial, and therefore they should be taken into account. Figure 5.18 shows amplitude spectra of the lowest order contribution and third order contributions only at the side band M_0 and at the side bands M_0 to M_1. In this figure we observe that the main difference between the amplitude spectra of the third order contributions at the side band M_0 and at the side bands M_0 to M_1 is at the frequency 2.57. At this frequency the spectrum of the former contribution is small, but the spectrum of the latter is indeed substantial, about one third of the largest amplitude spectrum of the lowest order contribution. The contribution is due to the interaction between two main frequencies 2.13 and 2.35.

As already observed, the contributions at outer side bands may be substantial. But, how many outer side bands should be considered? Or stated differently,

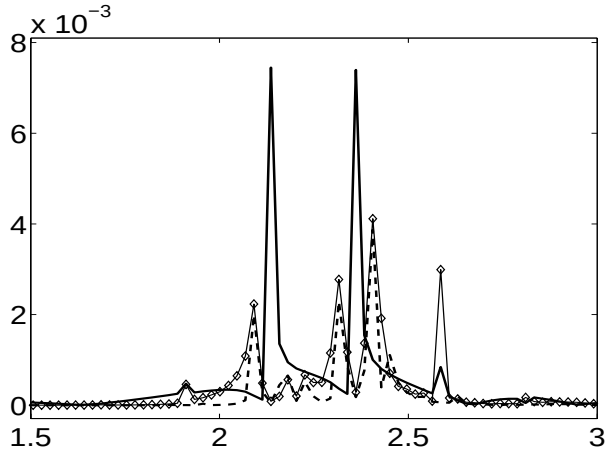

Figure 5.18: Amplitude spectra of the lowest order contribution (thick, solid line), the third order contributions merely at the side band $M_0 = 2$ (dashed line) and at side bands $M_0 = 2$ to $M_1 = 47$ (thin line with diamonds).

how can we determine M_1? This will be done as follows. Two cosine signals of the same amplitude around frequency $\bar{\omega}$ with the side band ν can be written as

$$\frac{1}{2}\cos\left(\{\bar{\omega}-\nu\}t\right)+\frac{1}{2}\cos\left(\{\bar{\omega}+\nu\}t\right)=\cos(\nu t)\cos(\bar{\omega}t).$$

For small ν, there are many waves in an envelope. As ν increases, the number of waves within an envelope decreases, see Figure 5.19. For $\nu = \frac{1}{2}\bar{\omega}$, there is only one crest or one trough within an envelope, this allows a wave to appear individually as a single crest (or trough). We will use this to determine M_1, i.e. from the condition

$$M_1 \cdot \Delta\omega = \frac{1}{2}\bar{\omega},$$

or

$$M_1 = \frac{\bar{\omega}}{2\cdot\Delta\omega}.$$

For Bichromatic 2, this condition gives $M_1 = 47$.

The third order contributions at the side bands M_0 to M_1 read

$$u_{sb}^{(3)} = \frac{9}{8}\sum_{\substack{q\neq -p\\ q\neq p-j\\ M_0\leq|j|\leq M_1}} a_q a_{-p+j} a_n \left[\begin{array}{l}\Gamma_3(\omega_{q+j},\omega_j,\omega_p)+\\ 2\Gamma_3(\omega_{q+j},\omega_{p+q},\omega_p)\end{array}\right] e^{i\{\theta_q+\theta_p+\theta_{-p+j}\}}. \quad (5.34)$$

Taking also the outer side band contributions into account gives very substantial improvement to the approximate solution as we will see in next section.

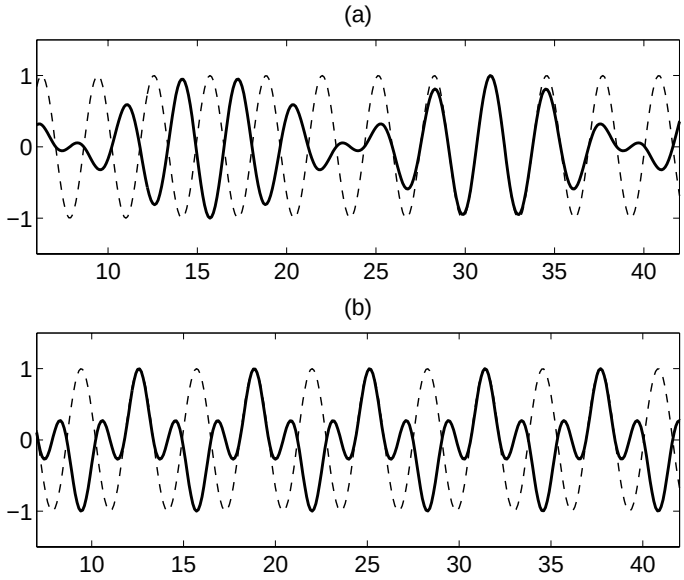

Figure 5.19: Solid line: $\cos(\nu t)\cos(\bar{\omega}t)$, dashed line: $\cos(\bar{\omega}t)$. In this example, $\bar{\omega} = 2$, (a) $\nu = 0.2$ which gives 4 waves within an envelope, and (b) $\nu = 1$ which yields one wave in an envelope.

5.6.4 Determination of free wave, second order and third order side band bound wave contributions from one point measurement

At $x = 0$ the approximation $u(0,t)$ should be equal to the prescribed signal $s(t)$, up to higher order. Hence, it is possible to obtain the lowest order, second order and third order side band contributions separately. Up to second order, this has been discussed in section 5.2. We will improve the technique to incorporate the third order side band contributions. The condition $u(0,t) = s(t)$ gives the equation

$$\begin{aligned} & a_m + \tfrac{3}{4} \sum_{p+n=m} a_p a_n \Gamma_2(\omega_p + \omega_n, \omega_n) \\ & + \tfrac{9}{8} \left[\sum_{\substack{q \neq -p \\ q \neq p-j \\ M_0 \leq |j| \leq M_1 \\ q+j=m}} a_q a_{-p+j} a_p \left[\begin{array}{l} \Gamma_3(\omega_{q+j}, \omega_j, \omega_p) + \\ 2\Gamma_3(\omega_{q+j}, \omega_{p+q}, \omega_p) \end{array} \right] \right] = \hat{s}_m. \end{aligned} \tag{5.35}$$

The amplitude a_m is approximated using an iterative method as follows. Take $a_m^{(0)} = \hat{s}_m$, for any m, and $a_m^{(r)}$ for $r \geq 1$ should be determined from the following

explicit equation

$$a_m^{(r)} = \hat{s}_m - \tfrac{3}{4} \sum_{p+n=m} a_p^{(r-1)} a_n^{(r-1)} \Gamma_2(\omega_p + \omega_n, \omega_n)$$
$$-\tfrac{9}{8} \left[\sum_{\substack{q \neq -p \\ q \neq p-j \\ M_0 \leq |j| \leq M_1 \\ q+j=m}} a_q^{(r-1)} a_{-p+j}^{(r-1)} a_p^{(r-1)} \left[\begin{array}{l} \Gamma_3(\omega_{q+j}, \omega_j, \omega_p) + \\ 2\Gamma_3(\omega_{q+j}, \omega_{p+q}, \omega_p) \end{array} \right] \right] . \quad (5.36)$$

In the following we will show that this iteration converges. To do that, for simplicity of the notations, we write

$$\sum_{p,n}^{m} a_p^{(r)} a_n^{(r)} \Gamma_2^{p,n} = \sum_{p+n=m} a_p^{(r)} a_n^{(r)} \Gamma_2(\omega_p + \omega_n, \omega_n)$$

and

$$\sum_{p,q,j}^{m} a_q^{(r)} a_{-p+j}^{(r)} a_p^{(r)} \Gamma_3^{p,q,j} = \sum_{\substack{q \neq -p \\ q \neq p-j \\ M_0 \leq |j| \leq M_1 \\ q+j=m}} a_q^{(r)} a_{-p+j}^{(r)} a_p^{(r)} \left[\begin{array}{l} \Gamma_3(\omega_{q+j}, \omega_j, \omega_p) + \\ 2\Gamma_3(\omega_{q+j}, \omega_{p+q}, \omega_p) \end{array} \right] .$$

Observe that in the first iteration

$$\begin{aligned}
a_m^{(1)} \quad & + \frac{3}{4} \sum_{p,n}^{m} a_p^{(1)} a_n^{(1)} \Gamma_2^{p,n} + \frac{9}{8} \sum_{p,q,j}^{m} a_q^{(1)} a_{-p+j}^{(1)} a_p^{(1)} \Gamma_3^{p,q,j} \\
= \quad & \hat{s}_m - \frac{3}{4} \sum_{p,n}^{m} \hat{s}_p \hat{s}_n \Gamma_2^{p,n} - \frac{9}{8} \sum_{p,q,j}^{m} \hat{s}_q \hat{s}_{-p+j} \hat{s}_p \Gamma_3^{p,q,j} \\
& + \frac{3}{4} \sum_{p,n}^{m} \hat{s}_p \hat{s}_n \Gamma_2^{p,n} + \frac{3}{4} \sum_{p,n}^{m} \hat{s}_p \Gamma_2^{p,n} \left[\frac{3}{4} \sum_{p_1,n_1}^{n} \hat{s}_{p_1} \hat{s}_{n_1} \Gamma_2^{p,n} \right] \\
& + \frac{3}{4} \sum_{p,n}^{m} \hat{s}_n \Gamma_2^{p,n} \left[\frac{3}{4} \sum_{p_1,n_1}^{p} \hat{s}_{p_1} \hat{s}_{n_1} \Gamma_2^{p,n} \right] + h.o.t \\
& + \frac{9}{8} \sum_{p,q,j}^{m} \hat{s}_q \hat{s}_{-p+j} \hat{s}_p \Gamma_3^{p,q,j} \\
& + \frac{9}{8} \sum_{p,q,j}^{m} \hat{s}_q \hat{s}_{-p+j} \Gamma_3^{p,q,j} \left[\frac{9}{8} \sum_{p_1,q_1,j_1}^{p} \hat{s}_{q_1} \hat{s}_{-p_1+j_1} \hat{s}_{p_1} \Gamma_3^{p_1,q_1,j_1} \right] \\
& + \frac{9}{8} \sum_{p,q,j}^{m} \hat{s}_q \hat{s}_p \Gamma_3^{p,q,j} \left[\frac{9}{8} \sum_{p_1,q_1,j_1}^{-p+j} \hat{s}_{q_1} \hat{s}_{-p_1+j_1} \hat{s}_{p_1} \Gamma_3^{p_1,q_1,j_1} \right] \\
& + \frac{9}{8} \sum_{p,q,j}^{m} \hat{s}_{-p+j} \hat{s}_p \Gamma_3^{p,q,j} \left[\frac{9}{8} \sum_{p_1,q_1,j_1}^{q} \hat{s}_{q_1} \hat{s}_{-p_1+j_1} \hat{s}_{p_1} \Gamma_3^{p_1,q_1,j_1} \right] + h.o.t.
\end{aligned}$$

$$
\begin{aligned}
= \quad & \hat{s}_m + \frac{3}{4}\sum_{p,n}^{m} \hat{s}_p \Gamma_2^{p,n} \left[\frac{3}{4} \sum_{p_1,n_1}^{n} \hat{s}_{p_1} \hat{s}_{n_1} \Gamma_2^{p,n} \right] + \frac{3}{4}\sum_{p,n}^{m} \hat{s}_n \Gamma_2^{p,n} \left[\frac{3}{4} \sum_{p_1,n_1}^{p} \hat{s}_{p_1} \hat{s}_{n_1} \Gamma_2^{p,n} \right] \\
& + \frac{9}{8}\sum_{p,q,j}^{m} \hat{s}_q \hat{s}_{-p+j} \Gamma_3^{p,q,j} \left[\frac{9}{8} \sum_{p_1,q_1,j_1}^{p} \hat{s}_{q_1} \hat{s}_{-p_1+j_1} \hat{s}_{p_1} \Gamma_3^{p_1,q_1,j_1} \right] \\
& + \frac{9}{8}\sum_{p,q,j}^{m} \hat{s}_q \hat{s}_p \Gamma_3^{p,q,j} \left[\frac{9}{8} \sum_{p_1,q_1,j_1}^{-p+j} \hat{s}_{q_1} \hat{s}_{-p_1+j_1} \hat{s}_{p_1} \Gamma_3^{p_1,q_1,j_1} \right] \\
& + \frac{9}{8}\sum_{p,q,j}^{m} \hat{s}_{-p+j} \hat{s}_p \Gamma_3^{p,q,j} \left[\frac{9}{8} \sum_{p_1,q_1,j_1}^{q} \hat{s}_{q_1} \hat{s}_{-p_1+j_1} \hat{s}_{p_1} \Gamma_3^{p_1,q_1,j_1} \right] + h.o.t.
\end{aligned}
$$

We write this result as

$$s_m + s\left[s\Gamma_2\right]^2 + s\left[s^2\Gamma_3\right]^2.$$

The second term contains third order in s and second order in Γ_2. Since Γ_2 is bounded, the contribution of this term is small, see determination of amplitude spectrum up to second order in section 5.2. The last term contains fifth order in s and second order in Γ_3. Even though Γ_3 may be large, the third order contributions have a restriction that the absolute value of $s^2\Gamma_3$ less than 1, otherwise we have near-resonant interactions.

This process can be continues and we have

$$
\begin{aligned}
a_m^{(2)} \quad & + \frac{3}{4}\sum_{p,n}^{m} a_p^{(2)} a_n^{(2)} \Gamma_2^{p,n} + \frac{9}{8}\sum_{p,q,j}^{m} a_q^{(2)} a_{-p+j}^{(2)} a_p^{(2)} \Gamma_3^{p,q,j} \\
& = s_m + s\left[s\Gamma_2\right]^3 + s\left[s^2\Gamma_3\right]^3.
\end{aligned}
$$

And for up to r iteration, this gives

$$
\begin{aligned}
a_m^{(r)} \quad & + \frac{3}{4}\sum_{p,n}^{m} a_p^{(r)} a_n^{(r)} \Gamma_2^{p,n} + \frac{9}{8}\sum_{p,q,j}^{m} a_q^{(r)} a_{-p+j}^{(r)} a_p^{(r)} \Gamma_3^{p,q,j} \\
& = s_m + s\left[s\Gamma_2\right]^{r+1} + s\left[s^2\Gamma_3\right]^{r+1}.
\end{aligned}
$$

This shows that the iterative method (5.36) up to r iteration give an approximate solution that has error in order $s\left[s\Gamma_2\right]^{r+1} + s\left[s^2\Gamma_3\right]^{r+1}$ to equation (5.35).

We note that the near-resonant interactions have been taken care of, therefore their contribution excluded in formula (5.36).

5.7 AWC3 based on the third order side band approximation

The AWC based on the third order side band approximation will be called AWC3. The complete algorithm of this AWC3 is presented in Figure 5.20.

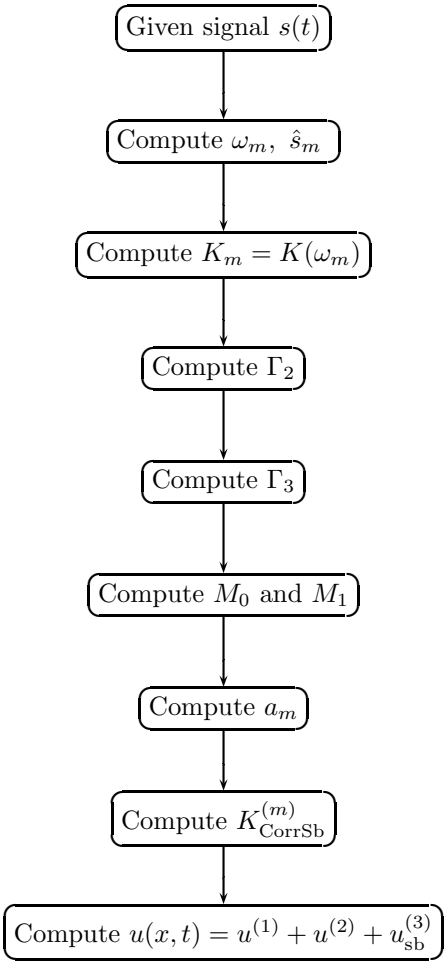

Figure 5.20: The algorithm of the analytical wave code based on the third order side band approximation (AWC3).

Compared to AWC2, AWC3 has several modifications. These modifications are as follows. First, the need to compute the third order transfer function Γ_3 at

the side band frequencies, and determine the side bands that will be considered, from M_0 to M_1. Second, the amplitudes a_m's should be computed by taking the third order side band contribution into account. Hence, we apply formula (5.36), instead of formula (5.12). Next, the wave number correction should be computed from the formula (5.32) after taking care of the near-resonant interactions. Finally, the third order contributions at the side bands M_0 to M_1 have to be taken into account to the predicted surface elevation $u(x,t)$.

In the following we present the performance of AWC3 to predict the evolution of Bichromatic 2. For this bichromatic wave, the first side band interaction is considered as near-resonant, therefore $M_0 = 2$ and $M_1 = 47$. Figure 5.21 shows the direct numerical results and the predictions using AWC3. In this figure we observe that the amplitude spectrum of the prediction has well been determined using the iterative method (5.36). This is indicated by Figure 5.21, where the prediction and the direct numerical result are in a good agreement. At the position $x = 70$ m, the prediction deforms, shows an amplitude increase as the numerical result. The largest amplitude increment is about 8 cm, from 16 cm at $x = 0$ m to about 24 cm. The prediction show an asymmetry of the envelope, especially in the region where the slope of the envelope is not steep, behind the 'centre' of wave groups. However, in front of wave groups where the envelope has steep slope, there is amplitude difference between the predicted waves and the numerical result. We also notice that there is no phase shift between them. At the position $x = 150$ m the prediction and the simulation are in good agreement, especially in the region of large waves, the main important part of the evolution and also in front of wave groups where the envelope slope is not steep. Behind the centre of wave groups, where the slope of the envelope are steep there is amplitude difference between the prediction and the numerical result.

Even though the predictions of waves without large envelope deformations; Bichromatic 1, Bichromatic 3 and irregular waves have also been done, the comparisons are not presented here. For these waves, the performance of AWC3 are qualitatively not different compared to AWC2. This is because, on the one hand, the propagation speed has been similarly improved. And, on the other hand, the third order side band for these waves are small and insignificant.

5.8 Conclusions

We have presented the construction of three different Analytical Wave Codes based on, respectively, the direct second order approximation (AWC1), the second order approximation with the nonlinear dispersion relation (AWC2) and the third order side band approximation (AWC3). These AWC's have been constructed to predict the wave evolutions from a given wave signal at one point. This signal is given on a finite-time interval. For the need of methods to find those approximations, the prescribed signal has been assumed to be peri-

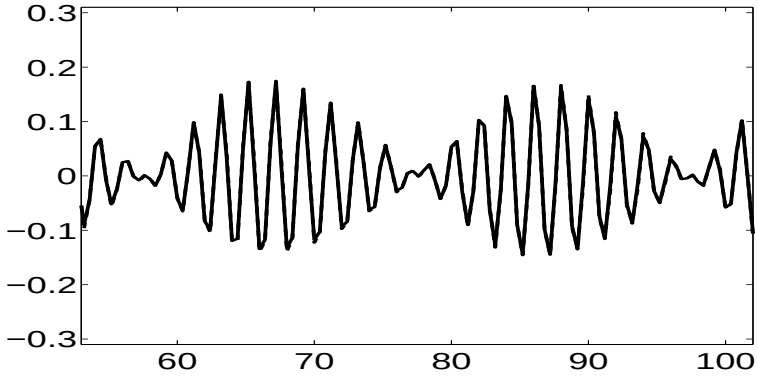

(a) $x = 0$ m

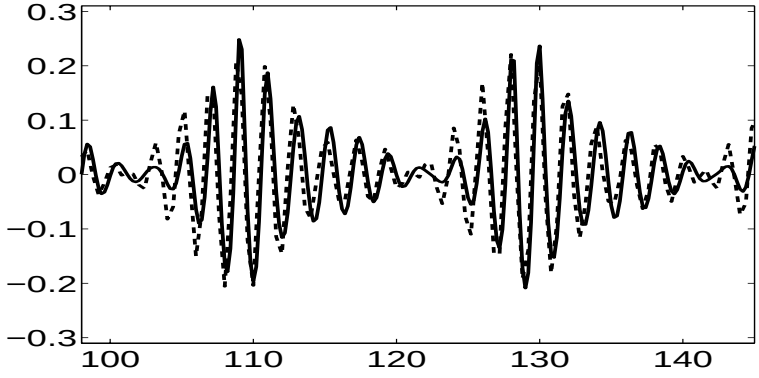

(b) $x = 70$ m

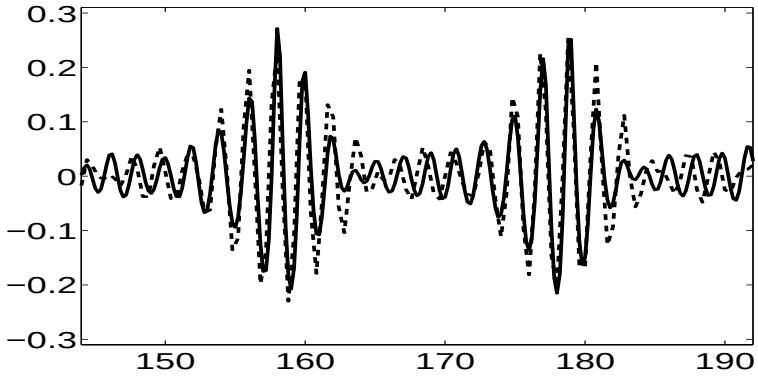

(c) $x = 150$ m

Figure 5.21: Numerics (solid line) and predictions using AWC3 (dashed line) of Bichromatic 2.

odic with the period of the time-interval as length of the signal, therefore it can be expressed as a Fourier series.

AWC1 and AWC2 are based on the second order approximations. Hence, for a given prescribed signal at $x = 0$, the approximation at this point should be equal, up to second order, to this signal. By taking the approximation up to second order in the amplitude causes two major problems that have been taken care of: the determination of the spectral amplitudes and the presence of the second order contributions which have frequencies larger than the Nyquist critical frequency of the prescribed signal. The spectral amplitudes are directly determined up to the relevant second order (in amplitude) using the explicit formula (5.12). On the other hand, the Nyquist frequency has been taken to be large enough to allow all substantial second order contributions fall into the frequency range below the Nyquist frequency. By doing this, the second order contributions at the higher frequencies are small, therefore, neglecting them does not substantially cause the aliasing phenomenon.

We have considered the direct second order approximation and the second order approximation with the nonlinear dispersion relation. The difference between them is the relation between the frequencies and the wave numbers. In lowest order, the frequencies and the wave numbers of the direct second order approximation satisfy the (linear) dispersion relation, where in the discussion above the wave number has been expressed as a function of the frequency. For the second order approximation with the nonlinear dispersion relation, however, the wave number is a function of both the frequency and the amplitude as well.

The performance of AWC1 and AWC2 in predicting wave evolutions has been presented. AWC1 is not capable in predicting wave evolutions in long wave tanks. This is observed, on the one hand, from the presence of a phase error and on the other hand, the incapability of revealing large envelope deformations, for example of Bichromatic 2, as shown by the experiments and the direct numerical simulations. We showed that AWC2 has significantly reduced the phase error. To reduce this phase error, however, we have multiplied the wave number corrections with a positive integer that has been explained from near-resonant interactions in the third order. We also applied AWC1 and AWC2 to predict the evolution of experimental irregular waves. For predicting these irregular waves, AWC2 performs significantly better than AWC1 in the sense of the laboratory interest to have a good prediction for large amplitude waves.

We have also investigated the performance of AWC3 by applying this code to predict Bichromatic 1, Bichromatic 2, Bichromatic 3 and the irregular waves. For this AWC, we take care of not only the resonant interactions, but also the near-resonant interactions. This explains why an adjustment of the wave number corrections for AWC2 may be needed to achieve good agreement with the numerical or experimental results. We have considered third order contributions at several side bands, including outer side bands, in the approximation. The outer side band contributions allow a single wave to be present individually. AWC3 that is based on this approximation predicts the envelope increase of

Bichromatic 2 as the the numerical simulation. Asymmetry of the envelope is also predicted, especially in the region where the slope of the envelope is not steep the prediction is in good agreement with the direct numerical result. In the region where the envelope has a steep slope, however, the wave amplitudes of the prediction and the simulation are different. For waves that do not reveal large envelope deformations; Bichromatic 1, Bichromatic 3 and the irregular waves, the predictions of AWC3 are similar as the predictions of AWC2. This is because the third order side band contributions of these waves are small.

Chapter 6

Conclusions and remarks

We have presented several models for surface waves including the mKdV equation, which is used as a model to study surface wave evolution. This model is chosen for its simplicity to understand the theory which is applied, yet still gives approximate analytical solutions that are in good agreement with the direct numerical simulations and experiments.

The approximate solutions of mKdV equation have been obtained by applying perturbation methods. To understand the methods, we started with illustrating the methods to solve an ordinary differential equation. We considered several different methods of increasing complexity and better approximation to the solutions. Those methods are direct second order approximation and third order approximation by taking care of the resonant interaction(s). In the former method, the period of the solution is independent of the amplitude, but the latter method exhibits a solution with period that depends on the amplitude, known as the Lindstedt-Poincaré method.

The same methods have been applied to solve mKdV equation, which is a partial differential equation. First, we applied the methods for a simple case, to study an evolution of bichromatic waves. In lowest order, this method introduce (linear) dispersion relation, the wave number is a function of frequency. This dispersion relation determines the wave propagation speed. Direct second order solution, which has linear dispersion properties, is not an accurate approximation, since it underestimates the propagation speed of the direct numerical results and it does not reveal large envelope deformations as the numerical simulation does for a specific class of bichromatic waves. Applying the Lindstedt-Poincaré method by taking care of the resonant interaction in the third order, we come to the nonlinear dispersion relation, the wave number is a function of both frequency and amplitude. The second order approximation with the nonlinear dispersion properties gives a good prediction for the wave propagation speed. However, this still does not show large envelope deformations. Third order side band contributions are shown to be responsible for the

envelope deformations. These contributions are found to quadratically depend on the quotient of amplitude and wave number difference. Hence, if this quotient is large the deformation is also large. However, if this quotient is too large, the method breaks down. We note that these third order side band contributions do not appear in an ordinary differential equation nor if one only considers a single frequency solution of a partial differential equation. This third order side band approximation does not show strong asymmetric envelope of wave groups during the evolution, while the direct numerical simulations and also the experiments really do. The asymmetric envelope is due to the wave generations numerically or experimentally which lose periodicity, and give a pseudo-bichromatic wave which is different than a purely bichromatic wave, as indicated by small discrepancy of the initial signal.

The same methods are also applied to obtain approximate solutions with many frequencies. Based on these methods we constructed three different Analytical Wave Codes (of increasing complexity and accuracy) to predict wave evolutions. Hence, the AWC's are capable for predicting irregular waves. AWC1, which is based on the direct second order approximation, is not accurate to predict experiments nor simulations. The inaccuracy is due to its poor prediction of the propagation speed and its incapability in predicting large envelope deformations observed numerically and experimentally for a class of waves. AWC2, which is based on the second order approximation with the nonlinear dispersion relation, has significantly reduced the error of propagation speed, but it does not reveal large envelope deformations. To achieve a good prediction for the propagation speed, the wave number corrections have been multiplied with some factors that may be different for different waves. These multiplication factors have been explained from near-resonant interactions in third order. In addition, we note that AWC2 is still not capable to predict large envelope deformations.

AWC3, which is based on the third order side band approximation, is capable to predict large envelope deformations. The predictions show large amplitude increase as the direct numerical simulation does. Moreover, it also predict asymmetry of the envelope of the wave groups during the evolution. Several remarks are made to apply the third order side approximation in AWC3. First, the third order side band contribution to be considered should be less dominant than the lowest order contribution. Some third order contributions, however, may be more dominant than the lowest order contribution, and their presence will make the perturbation methods break down. To proceed, they have been considered as near-resonant interactions and taken care of which give a modification to the nonlinear dispersion relation. This explains why for AWC2 we need to multiply the wave number corrections with some factors to get a good prediction of the propagation speed. Second, third order contributions at several side bands have been taken into account. Even though the outer side band contributions may be small, they may give a single wave to be present individually that can be responsible for the asymmetry of the envelope of wave groups.

Table 6.1 shows performance of the approximations based on considered perturbation methods compared to the numerical results for Bichromatic 2. The

interests for the comparisons are mainly in the small discrepancy at $x = 0$ (where the approximations should coincide with the prescribed signal), phase shift and large envelope deformations. Second order approximations with only two frequencies, with or without the nonlinear dispersion relation, show small discrepancy at $x = 0$ compared to the direct numerical simulations. This discrepancy is not observed if one considers solutions with many frequencies. Second order approximations are not capable to predict large envelope deformations, even though many frequencies and nonlinear dispersion properties are taken into account. Phase shift has been reduced by applying the nonlinear dispersion, which is used in the second order approximation with the nonlinear dispersion relation (NDR) and the third order side band approximation. And, the large envelope deformations can be explained from the third order side band contribution, but not from the first order and second order interactions.

		Discrepancy at $x = 0$	Phase shift	Incapability to show large envelope deformations
Two frequencies	Direct 2nd order	+	+	+
	2nd order with NDR	+	-	+
	Third order side band	+	-	-
Many frequencies	Direct 2nd order	-	+	+
	2nd order NDR	-	-	+
	Third order side band	-	-	-

Table 6.1: Performance of approximate solutions with two and many frequencies in predicting properties of a pseudo-bichromatic wave. The sign + indicates that the property is observed, while the sign - shows that the property is not observed.

Understanding the large envelope deformations will facilitate a better understanding of extreme wave evolutions, waves which reveal large amplitudes at some positions for some period of time. Extreme waves which are also called *freak waves* or *rogue waves* are interesting research topics in the last few years. The presence of extreme waves has been observed in seas, see [34, 45], and also in shallow water, see [7, 43]. Extreme waves are important for offshore engineering applications. It has been mentioned in [11] that the presence of extreme

waves can lead to dangerous ringing phenomenon, i.e. the large amplification in few cycles of response of the offshore structure at its natural frequency. The ringing phenomenon has been observed in the laboratory [10] and also in field application [33]. In [24] it is shown that this phenomenon is also caused by second order bound waves.

Bibliography

[1] M. J. Ablowitz, B. M. Herbst and C. M. Schober. The nonlinear Schödinger equation: Asymmetric perturbations, traveling waves and chaotic structures. Mathematics and Computers in Simulation 1997;43:3-12.

[2] M. J. Ablowitz, J. Hammack, D. Henderson and C. M. Schober. Long-time dynamics of the modulational instability of deep water waves. Physica D 2001;152-153:416-433.

[3] Y. Agnon, P. A. Madsen and H. A. Schäffer. A new approach to high-order Boussinesq models. J. Fluid Mech. 1999;399:319-333.

[4] F. P. H. van Beckum. Hamiltonian-consistent discretisation of wave equations. PhD thesis, Univervity of Twente, 1995.

[5] T. Benjamin and Feir. The disintegration of wave trains in deep water. part 1. theory. J. Fluid Mech. 1967;27:417-430.

[6] J. P. Boyd and G-Y. Chen. Weakly nonlinear wavepackets in the Korteweg-de Vries equation: the KdV/NLS connection. Mathematics and Computers in Simulation 2001;55:317-328.

[7] T. E. Baldock and C. Swan. Extreme waves in shallow water and intermediate water depth. Coastal Engng. 1996;27:21-46.

[8] E. Cahyono, E. van Groesen and Andonowati. Predicting wave field evolutions in towing tanks. Proc. ITB Suplemen 1999;31-2:331-339.

[9] E. Cahyono, E. van Groesen and Andonowati. An analytical investigation on the nonlinear evolution of bichromatic wave groups. Submitted.

[10] J. R. Chaplin, R. C. T. Rainey and R. W. Yemm. Ringing of a vertical cylinder in waves. J. Fluid Mech. 1997;350:119-147.

[11] G. Conteno, R. Codiglia and F. D'Este. Nonlinear effects in 2D transient nonbreaking waves in a closed flume. Applied Ocean Research 2001;23:3-13.

[12] E. F. G. van Daalen. Studies of water waves and floating bodies. PhD thesis, University of Twente. 1993.

[13] L. Debnath. Nonlinear water waves. Academic Press, cop. Boston. 1994: pp. 544.

[14] F. Dias and C. Kharif Nonlinear gravity and capilary-gravity waves. Annu. Rev. Fluid Mech. 1999;31:301-346.

[15] K. B. Dysthe. Note on a modification to the nonlinear Schrödinger equation for application to deep water waves. Proc. R. Soc. London A 1979;369:105-114.

[16] K. B. Dysthe and K. Trulsen. Note on breather type solutions of the NLS as models for freak waves. Phys. Scripta T82 1999:48-52.

[17] E. van Groesen and S. R. Pudjaprasetya. Uni-directional waves over slowly varying bottom. Part I: Derivation of a KdV-type of equation. Wave Motion 1993;18: 345-370.

[18] E. van Groesen and E.M. de Jager. Mathematical structures in continuous dynamical systems. Studies in Mathematical Physics, North-Holland, Amsterdam 1994.

[19] E. van Groesen, Andonowati and E. Soewono. Non-linear effects in bichromatic surface waves Proc. Estonian Acad. Sci. Phys. Math. **48**, 3/4. Tallinn, Estonia, 1999. p. 206-228.

[20] E. van Groesen. Wave groups in uni-directional surface-wave models. J. Eng. Math. 1998;34: 215-226.

[21] E. van Groesen, F. S. Widoyono and T. Nusantara. Modeling waves in towing tank Int. J. Indonesian Math Soc. 1998;4: 55-68.

[22] E. van Groesen, E. Cahyono and A. Suryanto. Uni-directional models for narrow and broad pulse propagation in second order nonlinear media, accepted in Optical and Quantum Electronics.

[23] E. van Groesen. Lectures on Free Surface Waves, Lecture notes for course LABMATH: Mathematical support for Hydrodynamic Laboratories, P4M, ITB, Indonesia, August-Sepetmber 2001.

[24] K. R. Gurley and A. Kareem. Simulation of ringing in offshore systems under viscous loads. J. Engineering Mechanics, ASCEE, 1998;124(5):182-586.

[25] P. C. A. de Haas. Numerical simulation of nnlinear water waves using a panel method: decomposition and applications. PhD thesis, University of Twente. 1997.

[26] J. L. Hammack and D. M. Henderson. Resonant interactions among surface water waves. Ann. Rev. Fluid Mech. 1993;25:55-97.

[27] M. H. Holmes. Introducton to perturbation methods. Texts in Applied Mathematics 20. Springer-Verlag, New York, 1995: pp. 337.

[28] R. S. Johnson. A modern introduction to the mathematical theory of water waves. Cambridge texts in applied mathematics. Cambridge university press. Cambridge, 1997: pp. 445.

[29] J. Kevorkian and J. D. Cole. Perturbation methods in applied mathematics. Springer-Verlag, New York. 1981 pp. 558.

[30] J. Kevorkian and J. D. Cole. Multiple scale and singular perturbation methods. Applied Mathematical Sciences 114. Springer-Verlag, New York. 1996, pp. 632.

[31] C. H. Kim, A. H. Clément and K. Tanizawa. Recent research and development of numerical wave tanks-a review. Int. J. of Offshore and Polar Eng. 1999;9:241-256.

[32] E. Kit, L. Shemer, E. Pelinovsky, T. Talipova, O. Eitan and Hiying Jiao. Nonlinear wave group evolution in shallow water. Journal of Waterway, Port, Coastal and Ocean Engineering, September/October 2000:221-228.

[33] I. Langen, O. Skjastad and S. Haver. Measured and predicted dynamic behaviour of an offshore gravity platform. Applied Ocean Research 1998; 20:15-26.

[34] I. Lavrenov. The wave energy concentration at the Agulhas current of South Africa. Nat. Hazards 1998;17:117-127.

[35] E. Lo and C. C. Mei. A numerical study of water-wave modulation based on a higher order Nonlinear Schrödinger equation. J. Fluid Mech. 1985;150:395-416.

[36] P. A. Madsen, R. Murray and O. R. Sorensen. A new form of the Boussinesq equations with improved linear dispersion characteristics. Part 1. Coastal Eng. 1991;15:371-388.

[37] P. A. Madsen and O. R. Sorensen. A new form of the Boussinesq equations with improved linear dispersion characteristics. Part 2. A slowly-varying bathimetry. Coastal Eng. 1992;18:183-204.

[38] P. A. Madsen and H. A. Schäffer. A review of Boussinesq-type equations for gravity waves." In Advances in Coastal and Ocean Engineering, Volume 5, pp 1-94. World Scientific Publishing Co. Pte. Ltd., edited by Philip L.-F. Liu.

[39] M. Mizuguchi and H. Toita. Generation of second order long waves by a wave group in a laboratory flume and its control. Proc., 25th ICCE 1996:493-501.

[40] A. H. Nayfeh. Introduction to perturbation techniques. Wiley, New York. 1993 pp. 519.

[41] O. Nwogu. Alternative form of Boussinesq equations for nearshore wave propagation. Journal Waterway, Port, Coastal and Ocean Engineering. ASCE, 1999;6:618-638.

[42] A. V. Oppenheim and R. W. Schafer. Discrete-time signal processing. London: Prentice-Hall, Inc., 2nd ed. 1999. p. 879.

[43] E. Pelinovsky, T. Talipova and C. Kharif. Nonlinear-dispersive mechanisme of the freak wave formation in shallow water. Physica D 2000;147:83-94.

[44] W. H. Press, S. A. Teukolsky, W. T. Vettering and B. P. Flannery. Numerical recipes in Fortran. Cambridge: Cmbridge Univ. Press, 1992, p. 490-529.

[45] S. E. Sand, N. E. O. Hansen, P. Klinting, O. T. Gudmestad and M. J. Sterndorf. Freak wave kinematics, in O. Torum, O. T. Gudmestad (Eds), Water Wave Kinematics, Kluwer Academic Publishers, Dorddrecht, 1990, pp.535-549.

[46] H. A. Schäffer and P. A. Madsen. Further enhancements of Boussinesq equations. Coastal Engineering 1995;26:1-14.

[47] H. A. Schäffer. Second order wavemaker theory for irregular waves. Ocean Engineering 1996;23:47-88.

[48] C. A. Spell, J. Zhang and R. E. Randall. Hybrid wave model for unidirectional irregular waves-Part II. Comparison with laboratory measurements. Applied Ocean Research 1996;18:93-110.

[49] C. T. Stansberg. On the nonlinear behaviour of ocean wave groups In: B. L. Edge and J. M. Hemsley (eds), Ocean Wave Measurement and Analysis, Reston, VA, USA: American Society of Civil Engineers (ASCE) 2 1997: 1227-1241.

[50] A. Suryanto. Model for reflection properties of hydrodynamic beaches. Master's thesis, University of Twente, 1999.

[51] A. Suryanto, E. van Groesen and J.W.M. Hoekstra. Deformation of modulated wave groups in third-order nonlinear media. Optical and Quantum Electronics 2001;33:513-525.

[52] K. Trulsen and K. B. Dysthe. A modified nonlinear Schrödinger equation for broader bandwith gravity waves on deep water. Wave Motion 1996;24:281-289.

[53] M. P. Tulin and T. Waseda. Laboratory observations of wave group evolution, including breaking effects. J. Fluid Mech. 1999;378:197-232.

[54] J. Westhuis and Andonowati. Applying FEM in numerically solving the two dimensional free surface water wave equations. 13th IWWW & FB. Alphen a/d Rijn, The Netherlands, 1998: 171-174.

[55] J. Westhuis, E. van Groesen and R. H. M. Huijsmans. Long time evolution of unstable bichromatic waves. Proc. 15th IWWW & FB. Caesarea, Israel, 2000: 184-187.

[56] J. Westhuis and R. H. M. Huijsmans. Unstable bichromatic wavegroups. MARIN Report No. 15309.152. Wageningen, the Netherlands, 2000.

[57] J. Westhuis, E. van Groesen and R. H. M. Huijsmans. Experiments and Numerics of Bichromatic Wave Groups. Journal of Waterway, Port, Coastal & Ocean Engineering 2001;127(6):334-342.

[58] J. Westhuis. The numerical simulation of nonlinear waves in a hydrodynamic model test basin. PhD thesis University of Twente, 2001. pp. 252.

[59] G. B. Whitham. Linear and nonlinear waves. New York: J. Wiley 1974. p. 471-473.

[60] D. Williamson. Discrete signal processing: an algebraic approach. London: Springer, cop. 1999. p. 421.

[61] H. C. Yuen and B. M. Lake. Instabilities of waves on deep water. Annu. Rev. Fluid Mech. 1980;12:303-334.

[62] H. C. Yuen and B. M. Lake. Nonlinear dynamics of deep-water gravity waves. Advances in Applied Mechanics. vol 22 by Academic press 1982 ISBN 0-12-002022-X

[63] J. Zhang, L. Chen, M. Ye and R. E. Randall. Hybrid wave model for unidirectional irregular waves-part I. Theory and numerical scheme. Appl Ocean Res 1996;18: 77-92.

[64] website of MARIN, www.marin.nl.